Characterization of mineral parageneses and metamorphic textures in eclogite- to high-pressure granulite-facies marble at Allmenningen, Roan, western Norway

Stylianos Karastergios

Dissertations in Geology at Lund University,
Master's thesis, no 609
(45 hp/ECTS credits)

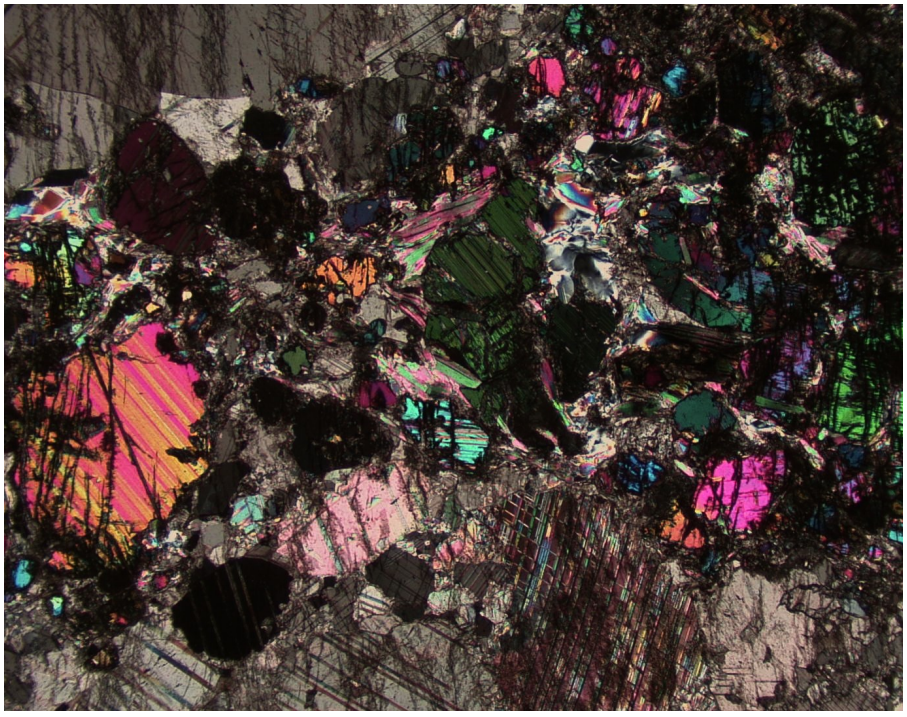

Department of Geology
Lund University
2020

Characterization of mineral parageneses and metamorphic textures in eclogite- to high-pressure granulite-facies marble at Allmenningen, Roan, western Norway

Master's thesis

Stylianos Karastergios

Department of Geology
Lund University

2020

Contents

Cover Picture: XPL photo of sample CM16R-09f1 (photo taken by Stylianos Karastergios)

Contents, continuation

Characterization of mineral parageneses and metamorphic textures in eclogite- to high-pressure granulite-facies marble at Allmenningen, Roan, western Norway

STYLIANOS KARASTERGIOS

Karastergios, S., 2020: Characterization of mineral parageneses and metamorphic textures in eclogite- to high-pressure granulite-facies marble at Allmenningen, Roan, western Norway. *Dissertations in Geology at Lund University*, No 609, 83 pp. 45 ECTS credits.

Abstract: The Roan peninsula in western Norway, Vestranden, is known for exposing one of the deepest parts of the Scandinavian Caledonian orogen, similar to the Western Gneiss Region. Throughout the Roan area, eclogites and high-pressure granulite- and amphibolite-facies gneisses occur, associated with supracrustal rocks including marbles, calc-silicate rocks and amphibolites. Although extensive research has been conducted regarding Western Gneiss Region and Vestranden, the mineralogical and petrographical data from marbles and calc-silicate rocks are limited.

The study materials are from Allmenningen, an island located 9 km west of Roan. The studied rocks belong to the Einarsdalen Supracrustal Unit, which is composed of paragneisses, marbles, calc-silicate rocks with mafic lenses and amphibolites. The aim of this study is to determine the petrography, textural characteristics, and mineral chemistry of the marbles, calc-silicate and associated mafic rocks, and how they are connected to the metamorphic conditions in Roan. Furthermore, calcareous rocks are of environmental importance because they emit significant amounts of CO2 into the atmosphere during metamorphism.

Twelve samples collected from Allmenningen have been analysed under petrographic microscope and five further studied in SEM-EDS. Based on the EDS analyses, one sample was used for P–T mineral equilibria calculation using TWQ geothermobarometry.

The petrographic data show that the mineral assemblage in the marbles is calcite + dolomite + clinopyroxene + scapolite ± epidote + phlogopite + amphibole + quartz. Calc-silicate rocks are composed of calcite + dolomite + clinopyroxene ± amphibole + scapolite + phlogopite + garnet + quartz. Mafic rocks contain garnet + clinopyroxene + zoisite + plagioclase ± amphibole + calcite. Accessory minerals include titanite, apatite, zircon, and opaques. All three rock types have mineral assemblages that indicate high-pressure granulite-facies metamorphism. P–T estimates using TWQ suggest temperatures ~875°C and pressures ~14 kbar for the formation of garnet rims in a garnet-rich mafic calc-silicate rock in the presence of a fluid phase composed of 75% CO2 and 25% H2O.

Diopside and grossular-rich garnet formed by heating and devolatilization in both carbonate and mafic rocks. The dominant minerals that were consumed are zoisite, calcite, plagioclase and quartz. Fluorine is present mainly in apatite, and in minor amounts in phlogopite and amphibole, suggesting that the CO2-rich fluid phase contained minor amounts of dissolved halogens during metamorphism.

Keywords: Western Gneiss Region, Vestranden, Roan, Caledonides, marble, calc-silicate, metabasic, petrography, SEM-EDS, mineral chemistry, mineral equilibrium, P–T estimate, devolatilization

Supervisor: Charlotte Möller

Subject: Bedrock Geology

Stylianos Karastergios, Department of Geology, Lund University, Sölvegatan 12, SE-223 62 Lund, Sweden. E-mail: st6776ka-s@student.lu.se

Karakterisering av mineralparageneser och metamorfa texturer i eklogit- till högtrycksgranulit-facies marmor från Allmenningen, Roan, västra Norge

STYLIANOS KARASTERGIOS

Karastergios, S., 2020: Karakterisering av mineralparageneser och metamorfa texturer i eklogit- till högtrycksgranulit-facies marmor från Allmenningen, Roan, västra Norge. *Examensarbeten i geologi vid Lunds universitet.* Nr. 609, 83 pp. 45 ECTS poäng.

Abstrakt: Roanhalvön i västra Norge, Vestranden, är känd för att exponera en av de djupaste delarna av de skandinaviska Kaledoniderna, i likhet med den Västra gnejsregionen i Norge. I Roan-området förekommer eklogiter och granulit- till amfibolit-facies ortognejser, tillsammans med suprakrustalbergarter som paragnejser, marmor, kalksilikat och amfibolit. Även om omfattande undersökningar har gjorts i Västra gnejsregionen och Vestranden, har det gjorts få mineralogiska och petrografiska undersökningar av marmor och kalksilikatbergarter.

Studiematerialet kommer från ön Allmenningen 7 km väster om Roan. De studerade bergarterna tillhör Einarsdalen Supracrustal Unit, som består av paragnejser, marmor, kalksilikat, samt mafiska linser och amfibolit. Syftet med denna studie är att bestämma petrografi, texturer och mineralkemi för marmor, kalksilikat och associerade mafiska bergarter, och hur de är kopplade till de metamorfa förhållandena i Roan. Metamorfos av karbonatbergarter är dessutom av betydelse eftersom de avger mängder koldioxid till atmosfären som bidrar till klimatförändringar.

Tolv prov från Allmenningen har analyserats med petrografisk mikroskopi och fem studerades vidare med SEM-EDS. Baserat på EDS-analyserna valdes ett prov ut för P–T-beräkning med hjälp av TWQ-geotermobarometri.

Petrografidata visar att paragenesen i marmor är kalcit + dolomit + klinopyroxen + skapolit ± epidot + flogopit + amfibol + kvarts. Kalksilikatbergarter består av kalcit + dolomit + klinopyroxen ± amfibol + skapolit + flogopit + granat + kvarts. Mafiska bergarter innehåller granat + klinopyroxen + zoisit + plagioklas ± amfibol + kalcit. Accessoriska mineral är titanit, apatit, zirkon och opakmineral. Alla tre bergartstyper har parageneser som motsvarar högtrycksgranulit-facies. P–T-estimat beräknade med TWQ indikerar temperaturer ~875°C och tryck ~14 kbar för bildning av granatkanter i en granatrik mafisk kalksilikatbergart, i närvaro av en fluid fas bestående av 75% CO_2 och 25% H_2O.

Diopsid och grossular-rik granat bildades under metamorfosen genom upphettning och devolatilisering av både karbonatbergarter och mafiska bergarter De mineral som konsumerades är zoisit, kalcit, plagioklas och kvarts. Närvaro av fluor, huvudsakligen i apatit men även i mindre mängder i flogopit och amfibol, antyder att den CO_2-rika vätskefasen innehöll mindre mängder upplösta halogener.

Nyckelord: Västra gnejsregionen, Vestranden, Roan, Kaledoniderna, marmor, kalksilikat, metabasit, petrografi, SEM-EDS, mineralkemi, mineraljämvikt, P–T-bestämning, devolatilisering

Handledare: Charlotte Möller

Ämnesinriktning: Berggrundsgeologi

Stylianos Karastergios, Geologiska institutionen, Lunds Universitet, Sölvegatan 12, 223 62 Lund, Sverige. E-post: st6776ka-s@student.lu.se

1 Introduction

Norway is a country with very interesting geology because it hosts rocks from a broad variety of metamorphic terranes from the Caledonian orogeny. The Western Gneiss Region (WGR, Fig. 1) is a Precambrian basement area located in the southwestern part of the country and it is famous for hosting spectacular eclogite formed during the Caledonian orogeny (Brueckner 2018, and references therein). However, the Caledonian orogen is well imprinted on northerly parts as well. Vestranden is a Precambrian basement area that is considered a northern analogue of the WGR, and the tectonic history and the P–T–t metamorphic path show similarities with the WGR (Johansson & Möller 1986; Möller 1988; Dallmeyer et al. 1992; Gordon et al. 2016).

Although the P–T–t evolutions of the WGR and Vestranden have been investigated previously, mineralogical and petrographical studies of marbles and associated rocks are few. Ramberg (1943), documented mineralogical assemblages of eight marble occurrences along the coasts of Vestranden. For at least one of these occurrences, Allmenningen, variations are considerable amongst the marbles and associated rocks.

High pressure granulite -and eclogite- facies assemblages have been documented in mafic rocks in the Roan peninsula and nearby areas in Vestranden (Johansson & Möller 1986; Möller 1988). However, the marbles in the same area have received little attention since the study of Ramberg (1943). These rocks are of interest due to the metamorphism that they have been subjected to, at high pressure granulite- and eclogite-facies. Furthermore, their mineralogy is interesting due to interference of silicate material and mafic rocks. Pure white marbles have been quarried from Allmenningen in Roan and used as pillars in the Nidaros Cathedral in Trondheim (e.g., Heldal 2012), so this study provides some cultural interest as well.

In this study, the petrography, textural characteristics and mineral chemistry of marble and associated mafic rocks at Allmenningen, Roan, Vestranden, are analysed and connected to the metamorphic conditions. What is remarkable about this succession of rocks are the metamorphic conditions during Caledonian times. Möller (1988) estimated that the metamorphic conditions in Roan reached temperatures of 870 ± 50°C and pressures around 14.5 ± 2 kbar, which can be translated to the equivalent of a 50 km overburden in the crust (Johansson & Möller 1986). The metamorphic evolution is subdivided in many stages and will be described later.

Roan exposes one of the deepest structural units of the Caledonian orogen, and thus as an area, constitutes one of the best examples that provides evidence on the tectono-metamorphic history of the Caledonian orogen in central Norway. The aim of this study is to provide insights into the complex mineralogy of the marbles, calc-silicates and mafic rocks, collected from Allmenningen, Roan, their mineral assemblages, textures, and mineral chemistries.

2 Geological Setting

The Western Gneiss Region (WGR) and Vestranden in Norway represent the deepest parts of the basement in the Scandinavian Caledonides. These regions cover a large part of the central Norwegian coastline and extend approximately from Bergen northwards to the Foldereid-Vikna area (Fig. 1).

2.1 Western Gneiss Region

The dominant rock types in the Western Gneiss Region are high-grade metamorphic gneisses with occurrences of eclogite and garnet peridotite (e.g., Eskola 1921; Tveten et al. 1998). Other rock types are orthogneisses, high-pressure granulites, paragneisses, marbles, amphibolitized eclogites and granulites, and late pegmatitic dykes (Engvik et al. 2018, and references therein).

Eclogite and other high-pressure parageneses formed in the Western Gneiss Region during Caledonian orogenesis, specifically, during Silurodevonian continental collision between Baltica and Laurentia (Cuthbert et al. 1983; Griffin et al. 1985). As a result of this collision, extensive tectonic burial of the bedrock formed eclogites and high-pressure granulites (Mørk 1985; Griffin et al. 1985). The metamorphic conditions in the WGR fall within the eclogite field and increase towards the northwest (Krogh 1977); in the region of Kristiansund, estimated pressures range between 18 and 20 kbar and temperature reaches 800°C (Griffin et al. 1985). In southern WGR, ultra high-pressure (UHP) conditions (coesite stability field) have been recorded in three domains: Nordfjord, Sørøyane, and Nordøyane (Fig. 1; e.g., Wain 1997; Root et al. 2005; Vrijmoed et al. 2006; Hacker et al. 2010). Between these three domains, peak metamorphic conditions increase from 700°C and 28 kbar in Nordfjord to 850°C and 32-36 kbar in Nordøyane (Krogh 1977; Cuthbert et al. 2000; Krogh Ravna & Terry 2004; Hacker 2006; Young et al. 2007).

The crystalline bedrock of the WGR is considered to represent the parautochthonous shortened margin of Baltica (Fig. 1; Gee et al. 1985). The metamorphic basement is composed of orthogneisses of mainly granitic bulk composition, which are mixed with amphibolites, metamafic bodies, and rocks of supracrustal origin and unknown age.

Caledonian metamorphism in the Western Gneiss Region is dated at the Silurian–Devonian, ca. 400–425 Ma, based on Sm-Nd mineral ages and U-Pb zircon ages from eclogites (Krogh et al. 1974; Griffin & Brueckner 1980; Mearns & Lappin 1982; Kullerud et al. 1986; Mørk & Mearns 1986). This event is termed the Scandian event (Gee et al. 2008). The protoliths of the orthogneisses throughout the WGR have been estimated by Kullerud et al. (1986) using U–Pb ages from zircon crystals. Also, Mørk and Mearns (1986), using Sm–Nd ages, proved that the crystallization of the mafic protoliths of some metagabbros and metadolerites occurred at around 1250 Ma. Recent zircon U–Pb data date the main magmatism in the proto-WGR at the Paleoproterozoic, ca. 1686–1594 Ma (Røhr et al. 2013).

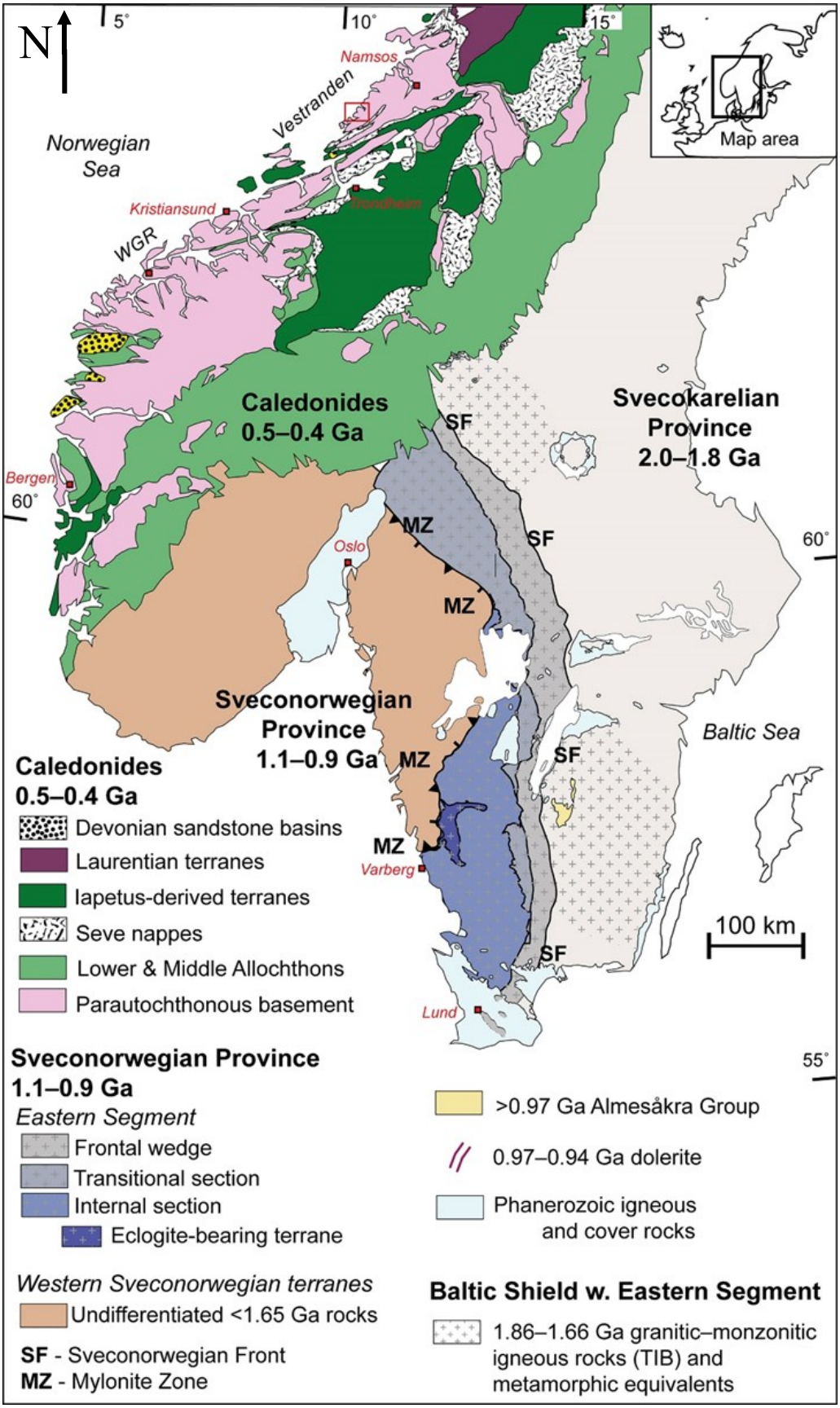

Figure 1. Simplified tectonic map of southern Scandinavia, based on Geological Survey databases of Sweden and Norway. The small red rectangle in the upper part of the map is the Roan area. Subdivision of the Scandinavian Caledonides after Gee et al. 1985. Subdivision of the Eastern Segment of the Sveconorwegian orogen after Möller et al. 2015. Illustration provided by C. Möller.

2.2 Vestranden and the Roan area

The name Vestranden is used for the strip of metamorphosed Precambrian bedrock, and young intrusive plutonic rocks (e.g. in the islands of Smøla and Hitra), along the Norwegian coast from Kristiansund to Namsos (Fig. 1; Kjerulf 1871; Ramberg 1943). Vestranden is commonly considered to be the northern extension of the WGR (Ramberg et al. 2008). The peak metamorphic event in Vestranden coincides with the main phase of Caledonian orogeny.

Similar to the WGR, Precambrian rocks dominate large parts of Vestranden (Solli et al. 1997). The Precambrian rocks range in age between ca. 1830 and 1630 Ma (Johansson 1986a; Schouenborg et al. 1991; Gordon et al. 2016). These gneisses are intercalated and folded together with amphibolite complexes and metasupracrustal rocks of hitherto unknown ages and origins (Birkeland 1958; Ramberg 1943, 1966; Johansson et al. 1987a; Möller 1988; Schouenborg 1989).

The Roan peninsula is part of Vestranden (Fig. 2), and its bedrock is composed of many different rock types. Möller (1988) distinguished three main complexes in the Roan area: The Roan Igneous Complex (RIC), the Banded Gneiss Complex (BGC), and the Einarsdalen Supracrustal Unit (ESU; Fig. 2). Younger penetrative pegmatite dykes are found throughout these complexes. The BGC and equivalents can be found under other names in literature, for example, Basal Gneiss Complex in Cuthbert et al. (1983) and Vestranden Gneiss Complex in Dallmeyer et al. (1992), respectively. This paper, though, will use the term Banded Gneiss Complex.

The island of Allmenningen is part of the Roan area (Fig. 2) and is located approximately 9 kilometres west of the Roan peninsula. The rock samples that are analysed in this study are from this island and were collected by C. Möller and L. Johansson in 2016 and 2019.

The major rock types in the Roan area are orthogneisses which vary in composition from granitic to quartz-monzodioritic (Möller 1988, 1990). The protolith ages of the orthogneisses have been determined using U-Pb dating of zircon crystals and yield ages around 1640-1650 Ma (Johansson and

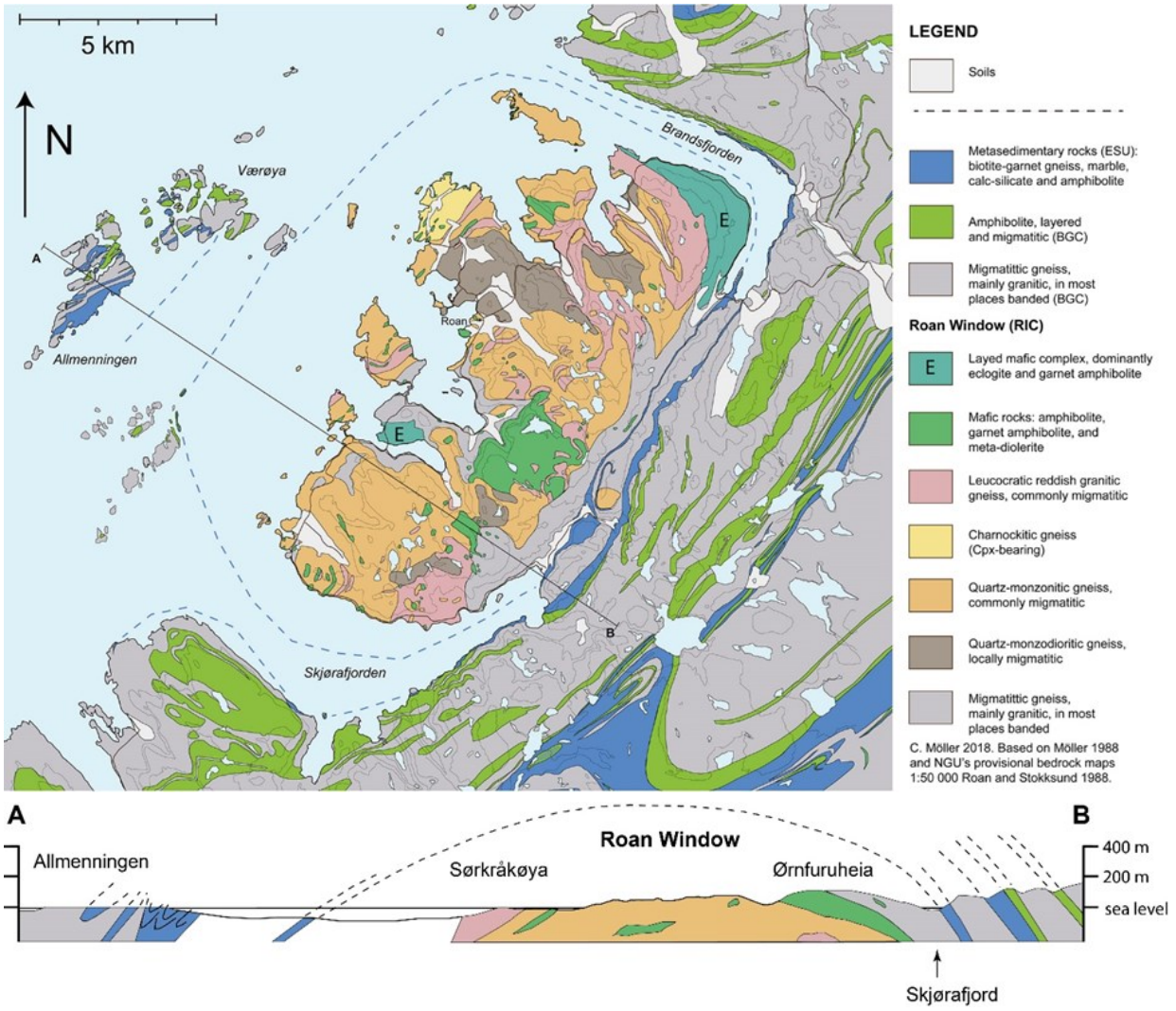

Figure 2. Bedrock map of the Roan area, with the marble-bearing supracrustal unit (Einarsdalen Supracrustal Unit, ESU) in blue. Note the location of Allmenningen in NW and the cross section beneath the map (marked A–B in the map). The blue hatched lines in the map, correspond with the hatched lines in the cross section that follow the folding of the rocks. Illustration provided by C. Möller.

Möller unpublished data; Gordon et al. 2016). The Einarsdalen Supracrustal Unit (Möller 1988, 1990) forms sheets that contain paragneisses and mafic rocks together with marbles and calc-silicate rocks and is commonly associated with up to 1 km thick banded amphibolite sheets. Supracrustal rocks and banded amphibolites are intercalated with and multiply folded together with the orthogneisses.

Petrographic and petrologic studies (Ramberg 1943; Johansson & Möller 1986; Möller 1988, 1990) suggest that the metamorphic peak conditions in Vestranden were lower in terms of pressure and higher in terms of temperature than of the WGR. An estimate based on garnet and two pyroxenes for a garnet pyroxenite yielded 870 ± 50 °C and 14.5 ±2 kbar (Johansson & Möller 1986).

The metamorphic P–T path of the rocks in Roan records a prograde part with metamorphic peak conditions in the high-pressure granulite field, at ca. 870°C and 14.5 kbar, and a later near-isothermal decompression (Johansson & Möller 1986; Möller 1988; Dallmeyer et al. 1992). Sm–Nd ages (Opx-Cpx-wr-Grt) dated the high-pressure metamorphism at the Silurian 432 ± 6 Ma (Dallmeyer et al. 1992), following broadly the general pattern of the Scandian metamorphism in WGR. Cooling ages that correspond to the near-isothermal decompression were dated with the 40Ar–39Ar method on hornblende and provided results of 400 ± 16 Ma (Dallmeyer et al. 1992), i.e., younger than the peak metamorphic event, confirming the P–T–t path proposed by Johansson and Möller (1986). Recent U–Pb zircon ages date the crystallization of migmatite veins in orthogneiss at ca. 400 Ma (late Silurian – early Devonian; Gordon et al. 2016).

New and unpublished U–Pb zircon ages (C. Möller and D. Williams SIMS and LA-ICP-MS dates, respectively, presented in abstract by Möller et al. 2020) date the peak metamorphism at ca. 420 Ma. These new data also demonstrate that the origins of eclogite and banded amphibolites are Ordovician in age and thus originated somewhere west of Baltica's margin.

2.2.1 Roan Igneous Complex (RIC)

The Roan Igneous Complex (RIC) was interpreted by Möller (1988) as the deepest structural unit in Vestranden. The main rock types of the RIC are orthogneisses which vary in composition from granite to quartz monzonite and quartz monzodiorite, with lesser amounts of charnockite and mafic rocks (Möller 1988). It has been observed that some rocks have preserved igneous textures and parageneses partly surviving the main Caledonian metamorphic episode. The contact between the Roan Igneous Complex and the overlying Banded Gneiss Complex is a ductile highly strained zone, which contains two thin layers of metasedimentary rocks (Einarsdalen Supracrustal Unit) intercalated with layers of orthogneisses (Möller 1988).

2.2.2 Banded Gneiss Complex (BGC)

The Banded Gneiss Complex overlies the Roan Igneous Complex. The BGC is composed of migmatitic orthogneisses, which vary in composition from felsic to intermediate, as well as amphibolites, supracrustal rocks, and meta-mafic lenses and bodies of amphibolite, metagabbro and metadolerite that can be found in the orthogneisses (Möller 1988). Rocks in the RIC are better preserved in comparison to the more deformed BGC. Extensive folding is observed in BGC, where refolded isoclinal folds, including sheets of migmatitic orthogneisses, are present at several locations (Möller 1988). Möller (1988, 1990) suggested that BGC has been thrust onto the RIC either as recumbent fold nappes, or as an imbricated sequence. Locally observed granulite-facies parageneses in rocks of the RIC and BGC, suggest that both units were subjected to the main high-pressure granulite facies metamorphism.

2.2.3 Einarsdalen Supracrustal Unit (ESU)

The marble sequence at Allmenningen, which this study is focused on, is part of the Einarsdalen Supracrustal Unit. East of the RIC, the ESU forms two thin layers that are separated by a layer of orthogneisses (Möller 1988; Fig. 2). ESU is mainly composed of metasedimentary rocks such as garnet-kyanite-bearing paragneisses, marbles and calc-silicates incorporated with lenses of mafic rocks, and amphibolites (Möller 1988, 1990). Occurrences of ESU include the islands west of Roan (Allmenningen, Farmannsøya, Klokkarholmen and Vaerøya), west of the Roan peninsula, as well as towards the east, north and south interfolded with the orthogneisses of the BGC (Möller 1990; Fig. 2).

Individual rock groups of ESU vary in thickness between less than a metre and 200 metres. Despite its relative thinness, it can be traced for several kilometres in the field (Möller 1990). The different rock layers within ESU vary from centimetres to several tens of metres (Möller 1990). These rocks are locally isoclinally folded and have a penetrative fabric subparallel to the compositional layering (Möller 1990). Locally, the ESU rocks are cross-cut by late intrusive granitic pegmatite. Field observations of migmatitic structures in metasedimentary rocks of the ESU (Möller 1988) suggest that ESU was subjected to high-temperature metamorphism.

The most diagnostic rocks in ESU are paragneisses which are composed of reddish-brown biotite, pinkish garnet, quartz, feldspar, and aluminium-silicates (Möller 1990). However, there are also some biotite-poor, quartz-rich layers which are alternating with the biotite-rich layers. The quartz-rich paragneisses contain pink garnet, kyanite, quartz, feldspar, and/or graphite, with a significant abundance in heavy minerals such as rutile, ilmenite, iron-sulphides, apatite, zircon, and monazite (Möller 1988; 1990).

The mafic rocks form either layers or lenses. Generally, they are dominated either by hornblende or biotite, and contain variable amounts of garnet, biotite, and plagioclase ± titanite ± quartz. The metabasic rocks vary in thickness: layers can be several metres thick, while the lenses vary from very small (20 cm long) up to some metres (Möller 1990). Mafic lenses occur in the marbles, too.

This paper focusses on the occurrence of marbles, calc-silicates, and their associated mafic pods on the

island of Allmenningen. Previous studies have given insights to the mineralogy of this occurrence. Ramberg (1943), referred to the calc-silicates as 'Lime Silicate Schists' defining also the mineral parageneses containing andesine, quartz, biotite, almandine ± hornblende ± muscovite. Moreover, he categorized the marbles in Vestranden based on the metamorphic grade. Marbles from Allmenningen were considered to belong to the highest-grade metamorphic marbles, based on the migmatitic state of the associated rocks. Rare metamorphic minerals were observed in the marbles and nearby skarn formations, (e.g. vesuvianite) and metamorphic varieties of specific amphiboles (e.g. cummingtonite; Ramberg 1943).

Möller (1988, 1990) reported that calc-silicate rocks of the ESU generally form thin layers up to several decimetres thick. The parageneses observed include variable amounts of diopside, garnet, scapolite, zoisite, titanite, plagioclase and/or calcite. The marbles vary in colour and mineralogy, and thickness ranges between a few centimetres up to 40 metres. The white marble at Allmenningen has been quarried and used for pillar construction for the Nidaros Cathedral in Trondheim (Fig. 3). According to Ramberg (1943) the white marble contains dolomite, diopside, scapolite and cummingtonite. Other varieties of marble are pinkish or yellowish.

Mafic rocks in the ESU are present as layers between calc-silicate and marble layers, or inside these rocks as lenses and pods. This study investigates mafic lenses in marble, which are macroscopically dark green–brown in colour and relatively heavy. Möller (1990) categorized this kind of rocks as 'rusty weathering mafic granulites' and reported garnet, clinopyroxene, plagioclase, quartz, and lesser amounts of amphibole, zoisite, biotite, white mica, chlorite and pyrrhotite.

The amphibole-free varieties of these rocks were used by Möller (1990) to calculate a P-T estimate for the Einarsdalen Supracrustal Unit. The temperature estimation was obtained by applying the garnet-clinopyroxene geothermometer calibration by Ellis and Green (1979), and the pressure estimation from the garnet-clinopyroxene-plagioclase-quartz (Mg-endmembers) geobarometer of Moecher et al. (1988). Results from this study provided a temperature estimate from the mineral cores of 860 ± 12 °C and pressure of 14.2 ± 0.25 kbar. Data from the rims of the same mineral parageneses were also studied but provided results with lower values (780 ± 25 °C and 10.6 – 12.6 kbar). These numbers are in concordance with the P-T estimate previously reported for a garnet pyroxenite on the mainland (Kråkfjord, Roan; Johansson & Möller 1986).

Dallmeyer et al. (1992) extracted 13 hornblende and 6 muscovite concentrates from rocks in Vestranden, including the supracrustal units similar to those of Einarsdalen Supracrustal Unit. The concentrates were analysed with the ^{40}Ar–^{39}Ar method and their plateau ages range between 396 ± 3 and 406

Figure 3. Columns made of marble from Allmenningen, in the Nidaros Cathedral in Trondheim. Photo from Tom Heldal, NGU.

± 4 Ma for hornblende and 392 ± 1 and 393 ± 1 Ma for muscovite.

2.3 Metamorphic evolution of meta-supracrustal rocks in Roan

Möller (1988, 1990), interpreted the metamorphic evolution of Roan, including RIC, ESU and BGC, based on the mineral assemblages that were formed during each metamorphic stage and coupled them to structural observations of deformation in the bedrock. Seven metamorphic stages were defined:

1) Prograde metamorphism defined by garnet growth and inclusions in the garnet grains.

2) Peak metamorphic episode at high-pressure granulite-facies forming the main garnet-bearing mineral assemblages in e.g. eclogites, mafic granulites and garnet-kyanite paragneisses.

3) Formation of disequilibrium textures in the rocks during decompression. In some mafic and intermediate rocks, garnet rims were replaced by symplectites (e.g., of orthopyroxene and plagioclase), and clinopyroxene and kyanite reacted to form plagioclase-clinopyroxene intergrowths and orthopyroxene, corundum, sapphirine and anorthite.

4) Hydration of the assemblages described above, and associated deformation. The main mineral parageneses in orthogneisses comprise amphibole, feldspar ± biotite ± quartz.

5) Formation of the second generation of migmatite veins in the gneisses while the hydrous minerals from the paragenesis in stage 4, define the penetrative foliation.

6) Second retrograde ductile deformation phase of the metamorphic evolution. During this time, the migmatite veins and foliation from stage 5 are extensively deformed and refolded at solid state conditions. The mineral paragenesis that defines the foliation in the felsic gneisses was still amphibolite-facies, however below the granite solidus.

7) During the last stage, pegmatite dykes intruded the metamorphic bedrock. Late localized shear also affected the pegmatites after their solidification.

2.4 Marbles and associated rocks in Allmenningen

This chapter contains field photos of the study area. All illustrations used in this work have been taken and provided by C. Möller. The photos below show a variety of outcrops in Allmenningen featuring mostly the main rock types that are investigated and described in this work.

On Allmenningen, the main rock types of ESU are blended and alternate with each other in several beddings (Fig. 4a). The beddings incorporate meta-supracrustal rocks (e.g. marbles, calc-silicate rocks and mafic rocks).

Generally, marbles are white in colour (Fig. 4), but unusual colours may appear as well, such as yellow and pink. Marbles appear either weathered or unaffected, based on their mineralogy. Weathered surfaces of the marbles are coloured greyish-blueish, while pure, unaffected marble horizons are white (Fig. 4d, 4e, 4h).

Mafic rocks in Allmenningen are greenish-grey with white domains (Fig. 4b, 4c). Mafic rocks are found as knobs inside calc-silicate beds and/or thicker

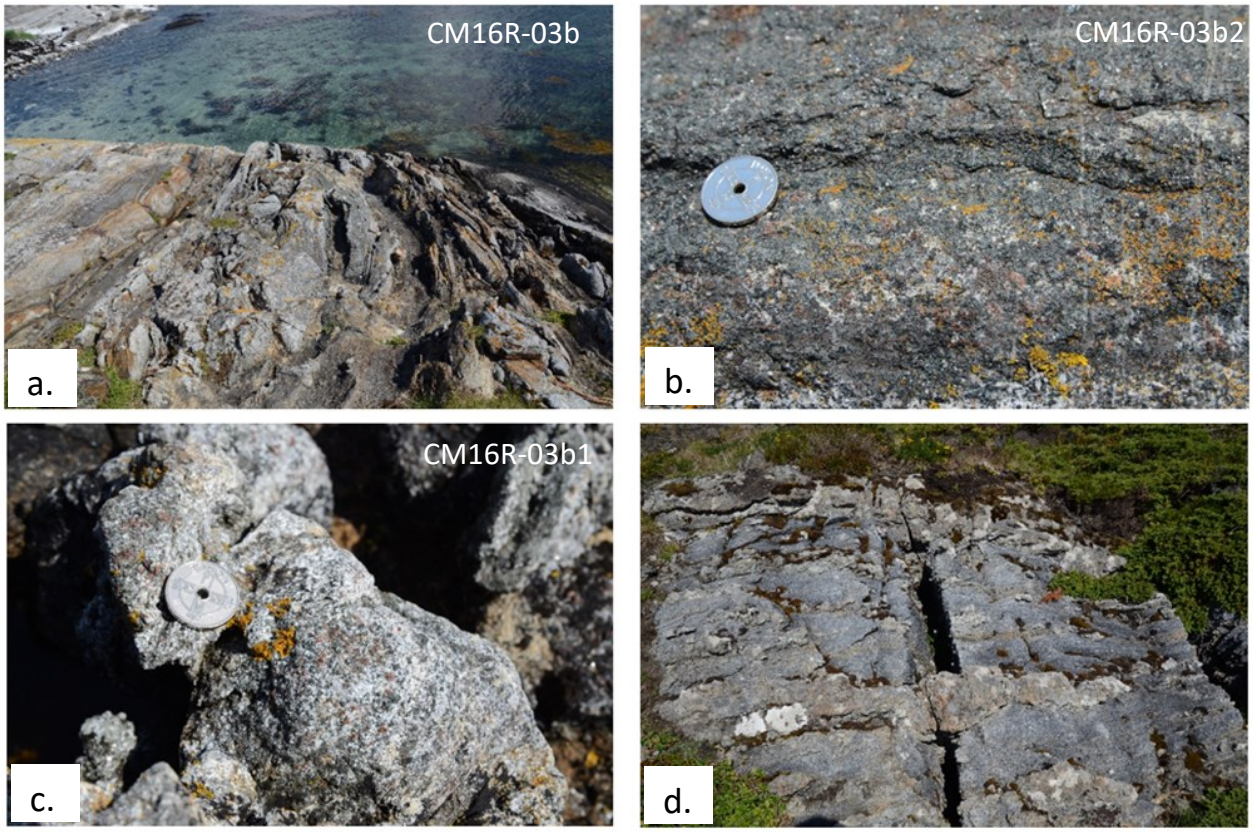

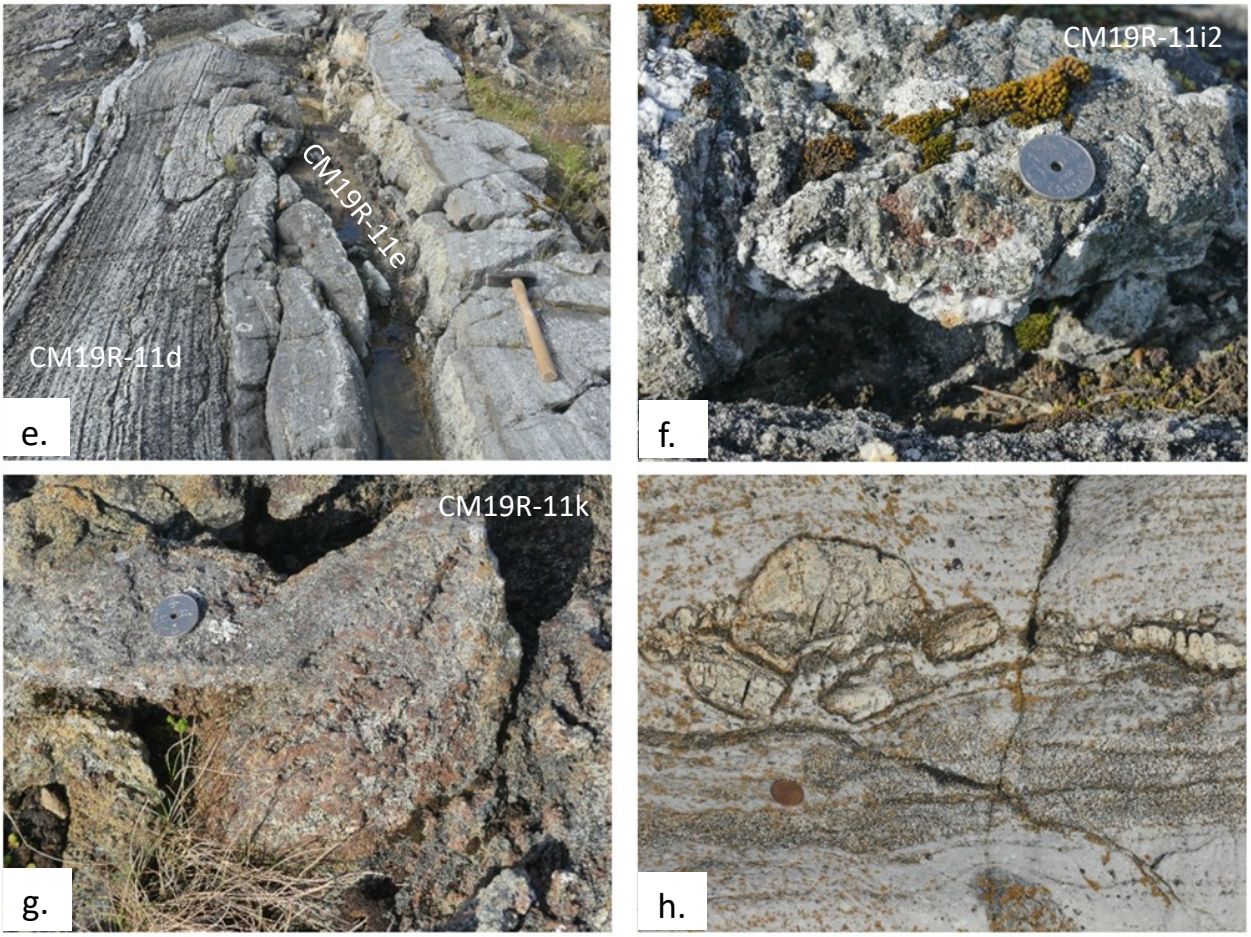

Figure 4. Field photos from Allmenningen. All illustrations have been taken and provided by C. Möller. a): Overview of outcrop (about 2 m wide) with banded marble, calc-silicates and mafic rocks. Carbonate and mafic rocks have been collected from this outcrop (samples CM16R-03b1, CM16R-03b2, CM16R-03b3). b): Close-up photograph of mafic rock (sample CM16R-03b2) interbedded with marble and calc-silicate rocks. 20 mm coin (1 Norwegian krone), for scale. c): Close-up of mafic, calc-silicate rock (sample CM16R-03b1) interbedded with marble and mafic rocks. 20 mm coin (1 Norwegian krone), for scale. d): Blueish grey weathering in white marble with pinch-and-swell boudinaged calc-silicate layers. Outcrop width ca. 2 m. e): Deeply weathered (right) and weathering-resistant (left) marble layers next to one another. Yellowish white marble with silicates (sample CM19R-11e) and weathering-resistant marble layer (sample CM19R-11d) were collected from this outcrop. Hammer, 55 cm, for scale. f): Garnet-bearing calc-silicate knob (sample CM16R-11i2) in white marble. 20 mm coin (1 Norwegian krone), for scale. g): Garnet-clinopyroxene-rich knob (sample CM16R-11k) at the contact between marble and metabasite. 20 mm coin (1 Norwegian krone), for scale. h): Sea-washed outcrop of white marble with boudinaged calc-silicate layers. 19 mm coin (1 Swedish krona) for scale.

marble horizons (Fig. 4f, 4g). Their mineralogy is close to a mafic granulite and they present similar textural characteristic of such rocks. Some of these rock types contain calcite and scapolite. For this reason, they may be confused with calc-silicate rocks but in fact they are mafic rocks.

Calc-silicate layers are embedded between marble horizons and have been deformed by tectonic processes during the metamorphic episodes. These rocks form characteristic boudinage structures. Their color varies compared to the host marble, depending on the type and amount of silicate minerals they contain (Fig. 4d, 4h). They usually have white color, but black amphiboles, green diopside and white zoisite or yellowish epidote are sometimes observed.

3 Methods

3.1 Sample Preparation

Twenty-one samples were selected, together with supervisor C. Möller, for thin section preparation. After rock sawing, samples were sent for thin section manufacturing. Sample IDs, with coordinates and notes about colour and petrography, are given in Table 1. Figure 5 provides a map of the study area with localities plotted from the coordinates given in Table 1.

3.2 Microscopy

3.2.1 Optical Microscopy and Photomicrographs

All 21 thin sections were investigated in a polarized light microscope. Twelve samples were selected for petrographic documentation in this thesis. The selection process was mainly based on petrographic criteria such as: peculiar metamorphic texture, or minerals that could not be recognized in the optical microscope. Photomicrographs were captured using HD-digital camera connected to a polarized transmitted light Olympus BX53 microscope at the

Department of Geology, Lund University. The objectives used for photo capturing are 2X and 4X. In every photo taken there is a scale bar on the lower right corner and description in the figure caption. Mineral abbreviations on photomicrographs, text, reactions and tables, follow Siivola and Schmid (2007).

3.2.2 Scanning Electron Microscopy (SEM) and Energy Dispersive X-ray Spectroscopy (EDS)

Five of the samples were selected to be studied with scanning electron microscopy (SEM) for further mineral identification and mineral chemical analysis using Energy Dispersive X-ray Spectroscopy (EDS). In this way, mineral grains that could not be correctly identified by optical microscopy were identified using EDS spectra. All analyses were performed at the SEM-laboratory of the Department of Geology, Lund University. The machine is a Tescan Mira 3 Field Emission Scanning Electron Microscope (FE-SEM), linked to an EDS analysis system Aztec by Oxford Instruments.

The SEM uses an electron beam under vacuum conditions which is formed in high voltage and passes through a tungsten filament. The sample, in this case the thin section, is mounted on a metal holder and placed on the stage which can move in x and y directions inside the vacuumed chamber while the electron beam is located under a fixed position. The electron beam must be focused several times using the magnification tools on the machine. The focusing is conducted for a better image acquisition of the thin section. The focusing of the beam is performed progressively every time, by decreasing the distance of the stage from the electron beam (e.g. 45, 30 and 15 mm).

When the fired electron beam hits the carbon-coated surface of the sample it generates four main products: (a) secondary electrons (SE), (b) back-scattered electrons (BSE), (c) cathodoluminescence (CL), and (d) X-rays. Secondary electrons are produced from the electrons of the sample that are dislocated when they interact with the beam. BSE are electrons from the beam which are formed by the reflection of the beam from hitting the sample. The CL is the emission of photons with predefined wavelength from a material which is subjected under high-energy electron bombardment. X-rays are emitted when the outer electrons are changing atomic orbitals. These X-rays are unique for every element of the periodic table (Egerton 2005).

The selected thin sections were coated with a

Sample name	Coordinates (ETRS89 zone 32N)		Rock type
	North	East	
CM16R-02b2	7118094	549945	Calc-silicate layer
CM16R-03b1	7117417	550120	Scapolitic mafic granulite
CM16R-03b2	7117417	550120	Mafic granulite
CM16R-03b3	7117417	550120	Carbonate rock
CM16R-03e1	7117242	550035	Rusty weathering Grt-Cpx mafic rock
CM16R-03e2*	7117242	550035	Rusty weathering Grt-Cpx mafic rock
CM16R-09c*	7117398	549816	Pink marble with a green mineral
CM16R-09d	7117409	549813	Mafic rock with 2-3 cm white layers
CM16R-09f1*	7117322	549825	White marble
CM16R-09f2	7117322	549825	White carbonate layer with black minerals
CM19R-11	Block, not in situ		Pure white marble, quarried rock
CM19R-11b*	7117443	550136	White marble with 1 cm silicate layers
CM19R-11d	7117232	550036	Weathering-resistant (dolomitic?) marble layer
CM19R-11e	7117187	549976	Yellowish white marble layer with silicates
CM19R-11f	7117187	549963	White marble with coarse white knobs
CM19R-11g2	7116985	549810	Thin calc-silicate layers in marble
CM19R-11g3	7116985	549792	Coarse knob in marble
CM19R-11h2	7116950	549767	Rusty weathering Grt-Cpx mafic rock
CM19R-11i1	7116863	549663	Calc-silicate layer
CM19R-11i2	7116863	549663	Grt-bearing knob in calc-silicate
CM19R-11k*	7116938	549735	Grt-Cpx-rich knob in contact zone marble-amphibolite

*Table 1. List of samples with locations. Samples selected for petrographic illustrations are in bold; * = selected samples for EDS analyses of minerals.*

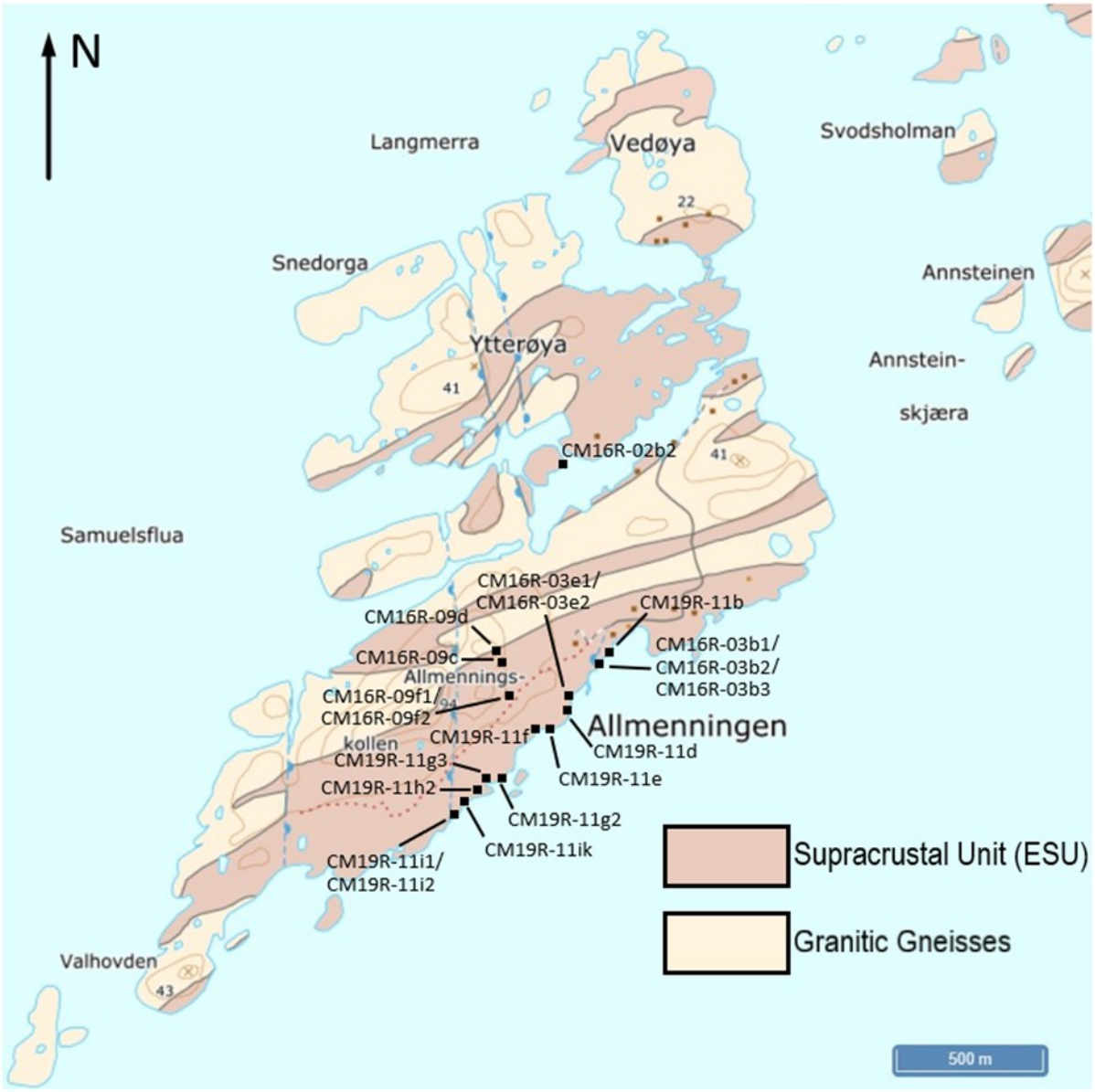

Figure 5. Geological map of Allmenningen and localities of the samples. Map acquired from the database of Norway's Geological Survey.

carbon layer ca. 20 nm thick. Before coating, the edges of the thin sections were covered with aluminium tape in order to ensure electric current conductivity. Furthermore, three pieces of slim carbon tape were attached to connect the thin section with the sample holder. The analyses were performed under an acceleration voltage of 15 kV, and the beam intensity was 14 nA. The mineral chemistry was identified using EDS-spectra and quantitative analyses were performed using Co-calibration and the extended standard set provided by Oxford Instruments.

A spectrum that is produced from the emitted X-rays is the X-ray energy-dispersive spectroscopy (XEDS or EDS). The photons and their energy which are created by the X-rays, are gathered by a specific diode. The result compiles a spectrum of the wavelengths which is unique for every element. Quantitative data that may be acquired from these spectra, correspond to the chemical analysis of the mineral. (Egerton 2005).

The data obtained from the EDS analysis of each spot were used for calculation of wt-% elements and stoichiometry by software Aztec. Analyses resulting in wt% totals between 96 and 104% for dry silicate minerals were accepted for further quantitative composition calculations. Analyses that overpass the range of 96-104% have been discarded. Also, misplaced analyses, for which the beam hit on the surfaces of two minerals at the same time, have been excluded. A few mica and amphibole analyses with totals of 80-90 wt% have been also excluded from quantitative analyses.

Mineral compositions of rock-forming minerals were calculated based on the standard number of oxygens: 6 for pyroxenes, 12 for garnet, 11 for micas, 23 for amphiboles, 12.5 for epidotes, and 8 for feldspars. The amount of Fe^{3+} was calculated using the method of Droop (1987) in every case where the

calculated cation sum exceeded the maximum desired total that any given mineral can host in its' crystal structure. Amphiboles were classified following Leake et al. (1997), pyroxenes based on Morimoto (1988) and micas using Rieder et al. (1998). Site allocation in garnet is based on Grew et al. (2013).

3.3 Geothermobarometry

3.3.1 winTWQ

The winTWQ software has been used for geothermobarometry calculations for a sample of garnet-rich mafic knob (CM19R-11k). TWQ (Thermobarometry With Estimation of Equilibration State), is a program which calculates mineral (and mineral-fluid) equilibria. TWQ uses an internally consistent thermodynamic dataset for endmembers and solid solutions that has been derived from several thermodynamic experiments (Berman 1991). TWQ also allows the user to calculate reactions in P-T-X (composition) space, involving both pure and solid-solution phases and fluid phase compounds such as H_2O and CO_2. After input of the chemical compositions of the minerals in a sample and selection of endmembers for which the program will base the calculations, the outcome is a P-T diagram with a number of reaction lines. With petrographical criteria and observations on the petrographical microscope, the phases that equilibrated, and probably reacted with each other, are selected via a list of potential reaction curves. If the minerals are in equilibrium, the reaction curves will be intersecting in a point (ideally) or form a limited range of intersections in the P-T field. This way the user is able to define the metamorphic conditions during which the assemblage achieved equilibrium.

4 Results

4.1 Petrography

The studied rocks include four samples of each rock type, marble, calc-silicate and interlayered mafic pods and are described below. Marbles can be seemingly pure and white in colour, but all marble samples investigated here actually contain silicate minerals. Most minerals in the marbles are colourless or of faint colour, which is the reason why some minerals were identified or confirmed using EDS. Quartz, micas, pyroxene, and scapolite are occurring in them but in slight proportions. Pure marbles contain only carbonate minerals and quartz. Calc-silicate rocks are light in colour or melanocratic; the silicate minerals provide a greyish hue to the rocks. Mafic rocks are the heaviest of the samples and are found as rusty bodies in the calcareous succession. Their composition is close to that of a mafic granulite regarding parageneses and metamorphic textures. Some calc-silicate and mafic pods samples may look very similar under the petrographic microscope. However, calc-silicate rocks differ from the mafic rocks in terms of mineralogy, because only the former contain scapolite and phlogopite. This criterion has been used to classify these two rocks types in this study. Table 2 at the end of this chapter summarizes every sample by petrological type and their according mineral paragenesis observed.

4.2 Marbles

Marbles are one of the components of Einarsdalen Supracrustal Unit and the largest occurrence of marble is on the island of Allmenningen. The marbles on Allmenningen vary in colour from pure white to pink and yellow. Marbles also occur interfolded with calc-silicates right on the east of the Roan window, suggesting that ESU covered RIC as a tectonic nappe which now has been eroded. Four of the samples collected and characterized as marbles are described below.

4.2.1 Pink marble, sample CM16R-09c

Sample CM16R-09c is of a 1-meter wide layer of impure pink marble from the central part of the island. Quartz in this rock is forming coarse grained aggregates and is weathering-resistant in comparison to the carbonate matrix of the sample (Fig. 6a). Greenish-black clinopyroxene and vitreous quartz are visible macroscopically. Light green to yellow epidote and light pink to orange titanite are visible using the hand lens (Fig. 6b). The complete paragenesis of this rock is: Cal + Qtz + Ep + Cpx + Ttn + Scp ± Wmca ± Pl + Ap + Rt + Zrn + Op.

The matrix of this rock is medium to coarse-grained, predominantly composed of calcite, with 1–7 millimetres grains or aggregates of quartz, diopside, scapolite, and titanite. In some domains can also occur plagioclase and/or retrograde K-feldspar (Fig. 7 a-h). Clinopyroxene is colourless and occurring in two main

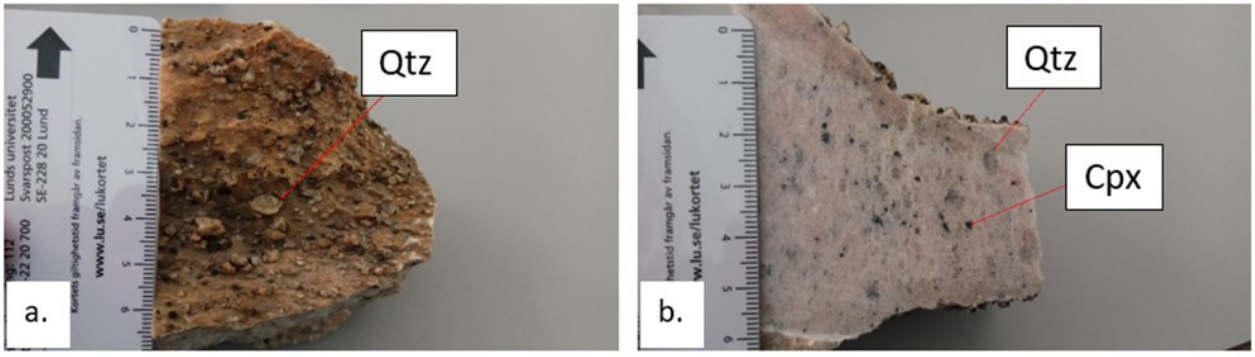

Figure 6. Hand sample of pink marble (sample CM16R-09c). a): The weathered surface showing a spiky appearance of Qtz crystals. b): Sawed surface in which Qtz and Cpx crystals are visible to the bare eye.

shapes: either prismatic with distinct cleavage subparallel to crystallographic c-axis, or in rounded grains of maximum 1-millimetre diameter. In every case though, Cpx is altering/pseudomorphing to a brown, cloudy, fine-grained aggregate which is composed of actinolite ± quartz ± calcite (Fig. 7 c-d). Clinopyroxene might also be at the form of detrital crystals (Fig. 7 a-b). The detrital crystals were probably deposited in the sedimentary protolith and 'survived' compaction and metamorphism. These crystals have dark-green colour and pleochroism. Retrograde amphibole has been formed in the cracks of these rock pieces. Epidote forms rounded subhedral grains maximum 0.5 millimetres in length. It is

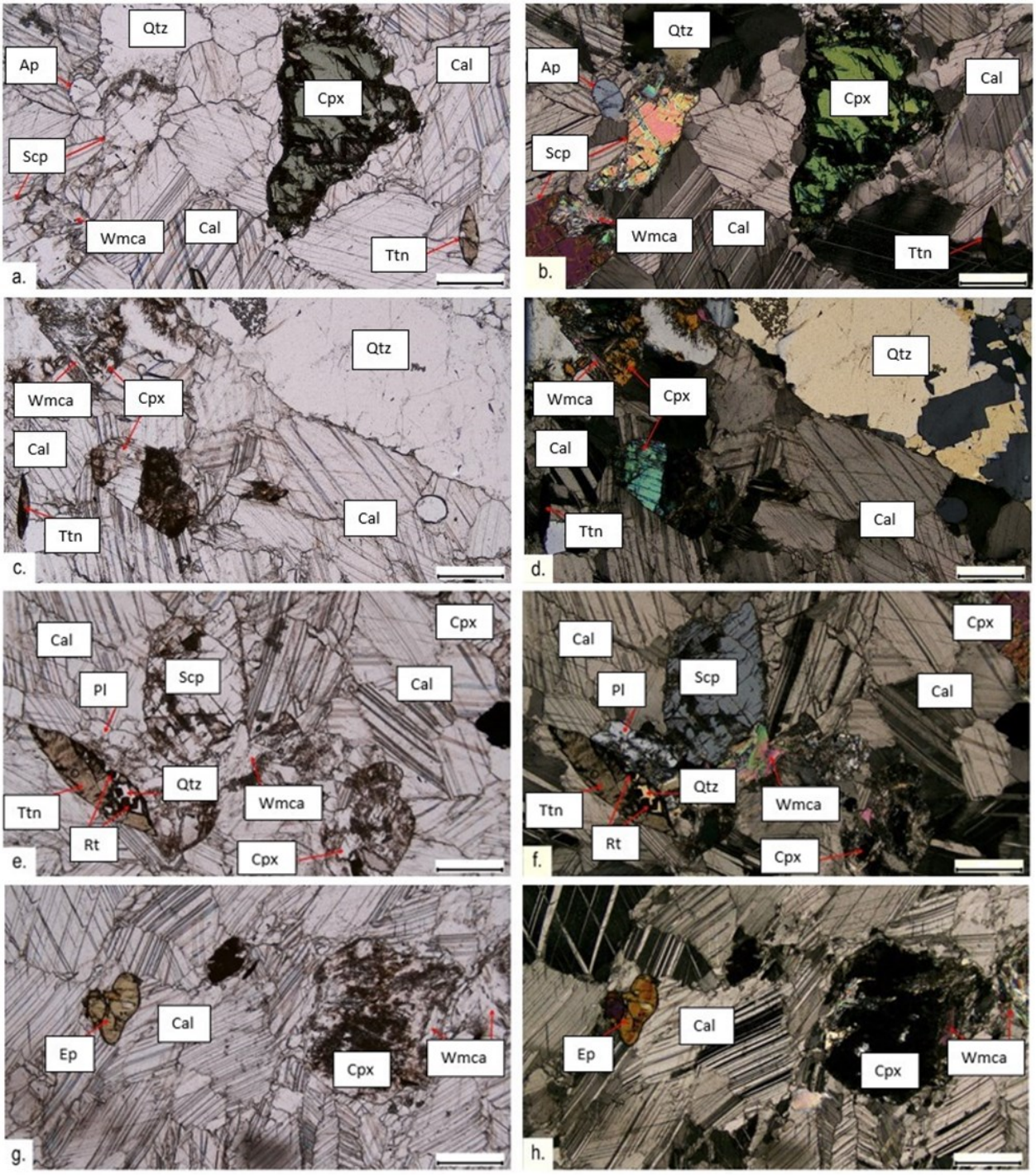

Figure 7. Photomicrographs of pink marble (sample CM16R-09c). PPL (parallel polars) on the left and corresponding XPL (crossed polars) on the right. Note the medium to coarse-grained matrix consisting of Cal + Qtz. a, b): Site with green detrital clinopyroxene crystal and scapolite. c, d): The light blue arrows without label show pseudomorph of diopside into a fine-grained aggregate of Act + Cal + Qtz. e, f): Rutile square-shaped crystals in quartz, pseudomorphs of diopside and unusual birefringence colours in Scp. g, h): Pseudomorphs of diopside into Act + Cal + Qtz and orange-yellow epidote crystals. Scale bar: 0.5 mm.

appearing as a yellow phase slightly pleochroic (Fig. 7 g-h). Scapolite is another abundant rock-forming mineral in this rock. It forms prismatic crystals like clinopyroxene. However, the two can be distinguished by clinopyroxene's higher relief and scapolite's higher birefringence colours. Scapolite is colourless and appears fractured (Fig. 7 a-b and e-f). Usually white mica occurs next to clinopyroxene and/or scapolite crystals and forms phyllo-morphed* aggregates (Fig. 7 a-h). Titanite is the dominant accessory mineral and is pleochroic as well, ranging from light pinkish to brownish. It locally occurs in euhedral sphenoidal crystals reaching 1 millimetre in length. One titanite grain contains a composite inclusion of square-shaped rutile in quartz (Fig. 7 a-f). Other accessory minerals include rutile, apatite, zircon, and opaque minerals.

*: Phyllo-morphed comes from the Greek 'phyllo' which stands for leaf. It is a textural term which is used in Greek petrology textbooks and describes the aggregate shape of phyllo-silicate minerals, like mica.

4.2.2 White marble, sample CM16R-09f1

Sample CM16R-09f1 is a white marble collected from an abandoned quarry in the middle part of Allmenningen. Its colour is pure white, and it contains thin faded-beige stripes of siliceous minerals. The rock is medium- to coarse-grained and its main component are carbonate minerals (Fig. 8). The mineral paragenesis of this marble is: Cal + Dol + Cpx + Phl + Ap + Ttn + Zrn ± Ep + Op.

The most plentiful minerals in this thin section are calcite and dolomite. The carbonaceous grains can be quite large and sometimes they approach 1 centimetre in length (Fig. 9 a-f). Clinopyroxene forms both prismatic and rounded crystals up to several millimetres long. Furthermore, perfect cleavage on 110 is visible even under PPL. The crystals are in most of the cases fractured and filled by talc and/or amphibole (Tr), a feature that probably reflects a late stage breakdown reaction of clinopyroxene (Fig. 9 a-f). Amphibole (Tr) is observed brownish, slightly pleochroic, forming fine grained masses as pseudomorphs after clinopyroxene (Fig. 9 c-f). White mica occupies the space between clinopyroxene grains, as phyllo-morphed aggregates (Phl). Talc forms very fine-grained masses in fractures within clinopyroxene (Fig. 9 a-f). Accessory minerals which could not been identified under the optical microscope but have been observed in SEM are apatite, titanite, zircon, epidote and Fe-sulphides.

4.2.3 White marble, sample CM19R-11d

In contrast to the two marbles above, this sample was collected from the southern shore of Allmenningen. It is a white, weathering-resistant, impure coarse-grained marble with yellow and brown-coloured crystals of silicic minerals. The major component of this rock is carbonate minerals. As noted by careful macroscopical examination, the carbonate minerals emit a pearly lustre on the crystals' cleavage surfaces (Fig. 10). The mineral paragenesis of this rock is Cal + Dol + Cpx + Am + Phl + Qtz ± Op.

Like in the previously described specimens, this rock is mainly composed of carbonate minerals. Most carbonate grains are coarse-grained, forming porphyroblasts up to some centimetres in diameter (Fig. 11 a-d). Clinopyroxene in this specimen is rather granular than prismatic. Its crystals are colourless and significantly smaller than the carbonate grains. Sometimes, perfect cleavage can be perceived. Usually the grains are fractured. Very fine-grained material is filling the cracks or, locally, pseudomorphing clinopyroxene. Following the pattern of these marbles it is breaking down producing tremolite and/or talc (Fig. 11 a-d). Amphibole occurs in the same way as clinopyroxene, in fine-grained aggregates, or forms sub-triangular shaped crystals. This mineral is colourless and occasionally single (parallel) or double cleavage (120°) is perceived (Fig. 11 a-d). Phlogopite crystals are generally euhedral in classic mica-shaped grains. Their colour changes from colourless to light brown in response to their pleochroism (Fig. 11 a-d).

4.2.4 Yellowish white marble, sample CM19R-11e

This specimen has been collected from the southern coast of Allmenningen, as well, just next to sample CM19R-11d, from a deeply weathered surface (Fig. 4e; 5). It is another impure marble of the same succession, but it differs both in colour and grain size from sample CM19R-11d and is prone to weathering. This variety of marble is yellowish but also contains greyish domains of minerals. The texture of this rock

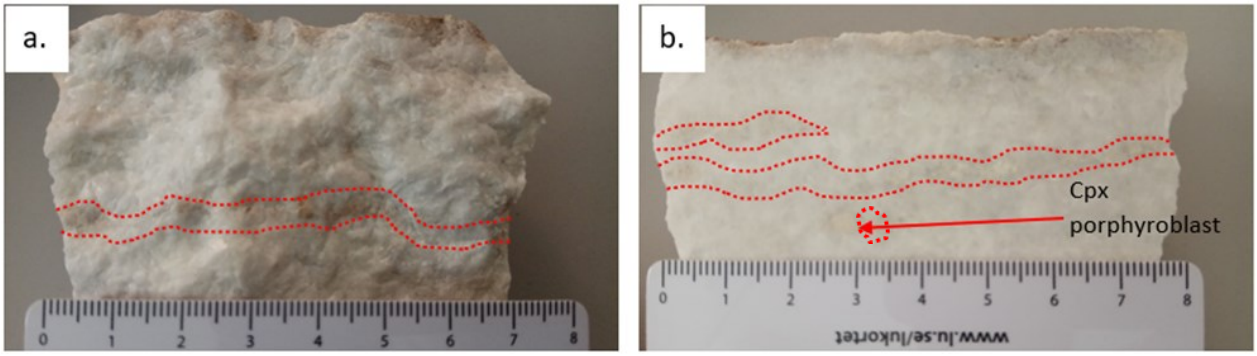

Figure 8. Hand sample of white marble (sample CM16R-09f1). The rock is pure white in colour and medium- to coarse-grained. a): Rough surface showing the coarse grain size of the carbonate crystals with a beige band marked with red dashed line. b): Sawed surface showing beige bands of siliceous minerals and a Cpx porphyroblast.

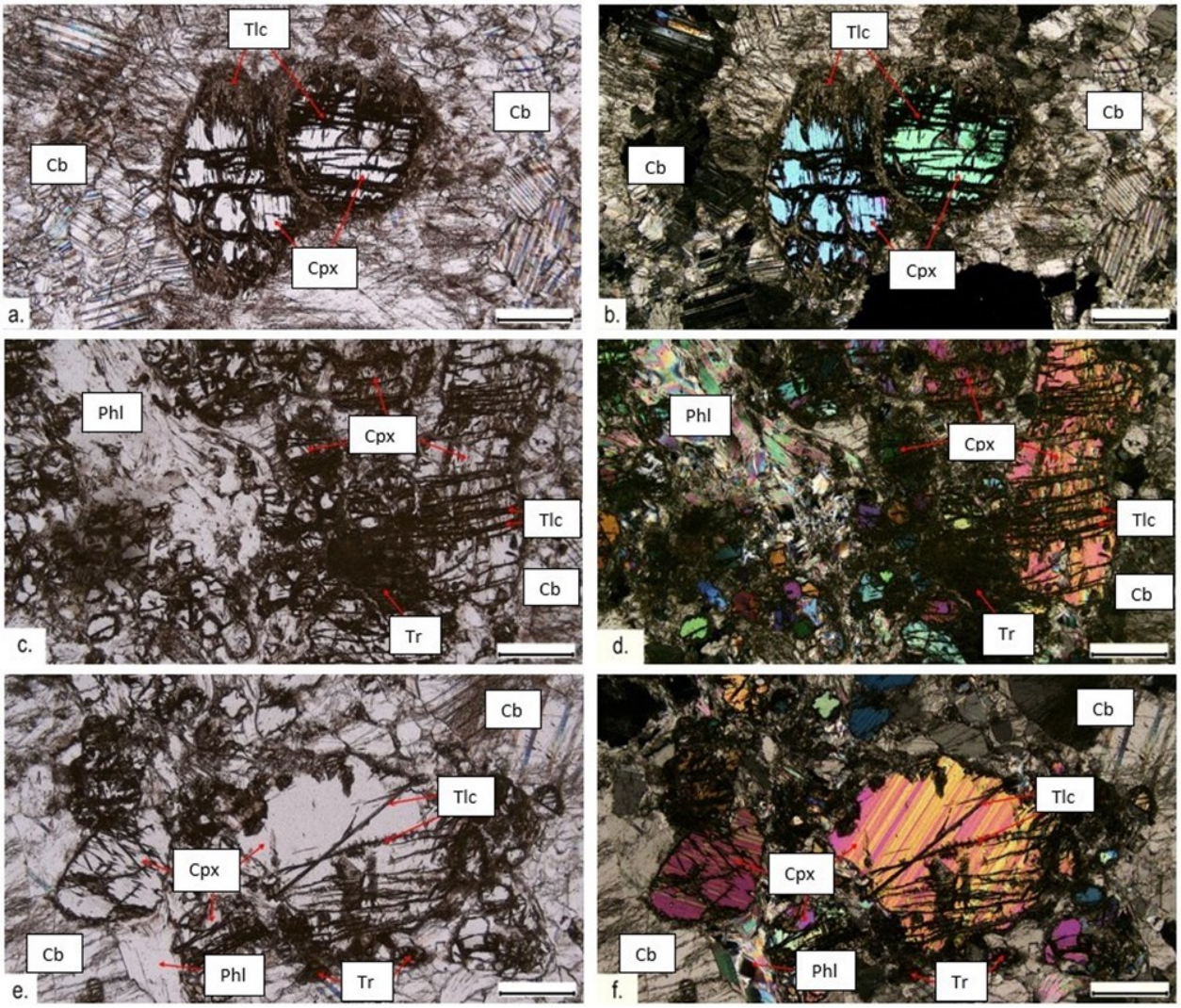

Figure 9. Photomicrographs of white marble (sample CM16R-09f1), PPL on the left and corresponding XPL on the right. a-f): The carbonate matrix (Cb; dolomite and calcite) is medium to coarse-grained, while clinopyroxene crystals present perfect cleavage. Clinopyroxene is partly replaced by very fine-grained masses of tremolite and/or talc, which also are present in thin fractures. Phlogopite is white due to Fe shortage. Scale bar: 0.5 mm.

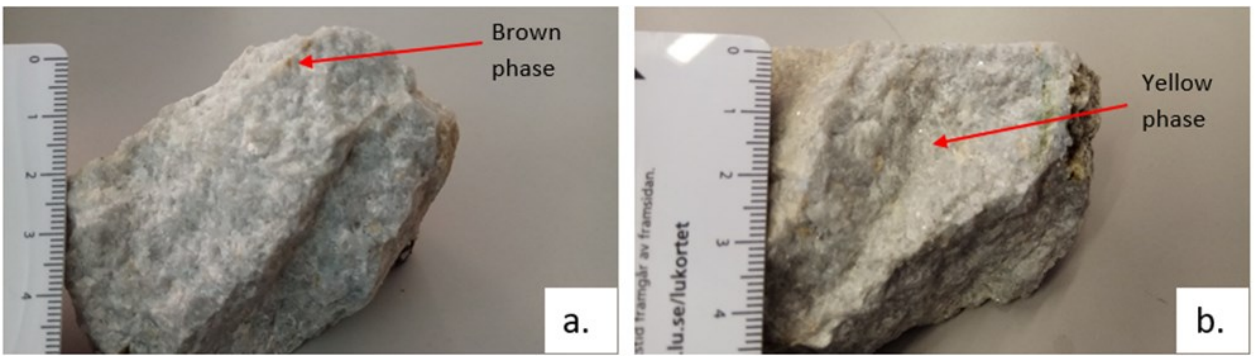

Figure 10. Hand sample of white marble (sample CM19R-11d). a): Raw surface with silicic brown phase. b): Raw surface with silicic yellow phase. It is worth looking on the carbonate crystal matrix, its grain size and lustrous cleavage.

is sugary, suggesting that this rock is rather finer-grained (Fig. 12). The mineral assemblage in this rock is Cal ± Dol + Cpx + Am + Scp + Bt + Ttn + Qtz ± Ap + Op.

The dominant phases in this marble are carbonate minerals. The carbonate crystals are generally anhedral and have the same grain size in average; however, rarely carbonate crystals are over 2 millimetres long. Occasionally triple points occur between these crystals (Fig. 13 a-b). Clinopyroxene is colourless and occurs as prismatic and rounded crystals of similar size as calcite. Nonetheless, clinopyroxene is less abundant

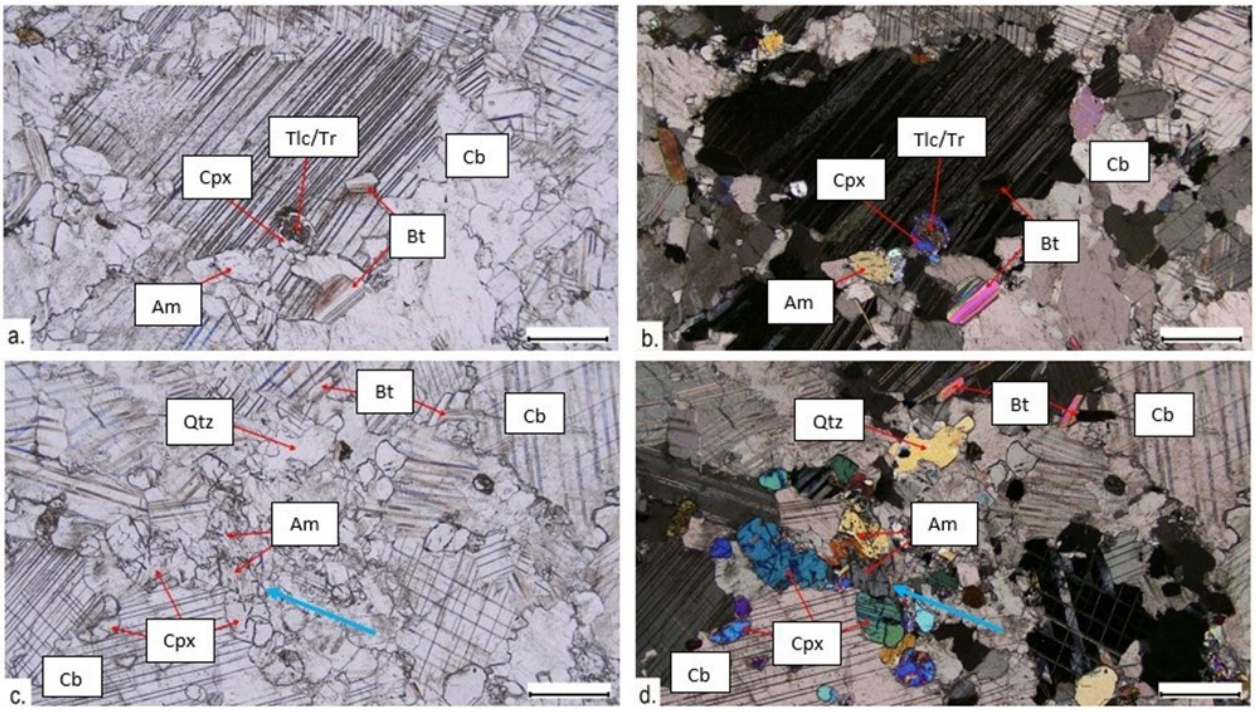

Figure 11. Photomicrographs of white marble (sample CM19R-11d), PPL on the left and same sites with XPL on the right. Note the difference in grain size between the large carbonate grains and the clinopyroxene, amphibole and almost colourless, faintly brownish, phlogopite mica. Phlogopite (Bt) is slightly coloured indicating Fe deficiency, similar to colourless clinopyroxene and amphibole. The light blue arrow points to the amphibole crystal with the single (parallel) cleavage. Scale bar: 0.5 mm.

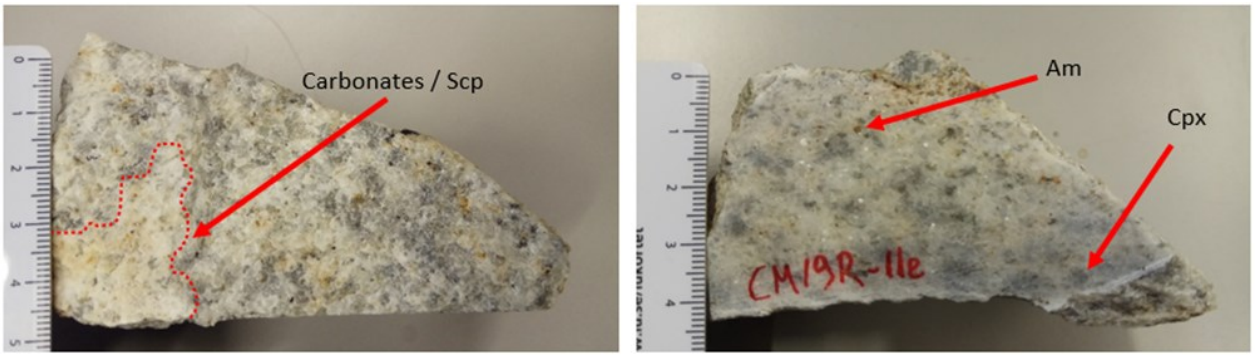

Figure 12. Hand sample of yellowish white marble with silicate minerals (sample CM19R-11e). a): Raw surface of the rock with a predominant carbonate-scapolite domain in the lower left (red dashed line). b): Sawed surface with a yellow phase which is probably amphibole and a greyish which is clinopyroxene. Brownish domains testify titanite grains.

than calcite and no triple points are observed. Cleavage lamellae parallel to 110 are common. Pseudomorphs of amphibole after clinopyroxene can be detected (Fig. 13 a-d). Amphibole is forming various types of crystals from euhedral prismatic and rhombohedral-shaped grains to subhedral and anhedral rounded grains (Fig. 13 c-d). This amphibole is white without pleochroism, and twinning has been observed. Their size is a few millimetres. Scapolite is colourless too and is identified in rounded grains less than a millimetre long. It has higher birefringence colours than clinopyroxene and amphibole and is often fractured. Mica content is low. However, when noticeable, it is white to brownish-pinkish and forms phyllo-morphed aggregates (Fig. 13 a-d). Titanite is an accessory mineral and develops thin, small, sphenoidal crystals less than a millimetre long. Its colour varies from colourless to light brown.

4.3 Calc-Silicate Rocks

Calc-silicate rocks are usually present in marble horizons. They occur in various types, either containing silicate layers alternating with marbles, or in welded siliceous knobs. Their colour varies, but in general terms is white for the carbonate minerals and light beige or greyish to greenish for the siliceous domains. Their colour is darker where closely associated with mafic rocks. The type of dark minerals and their proportions are responsible for the rock's colour. Mica rich bands are more greenish than their clinopyroxene-rich counterparts that appear black to grey. The white layers may include scapolite crystals, too.

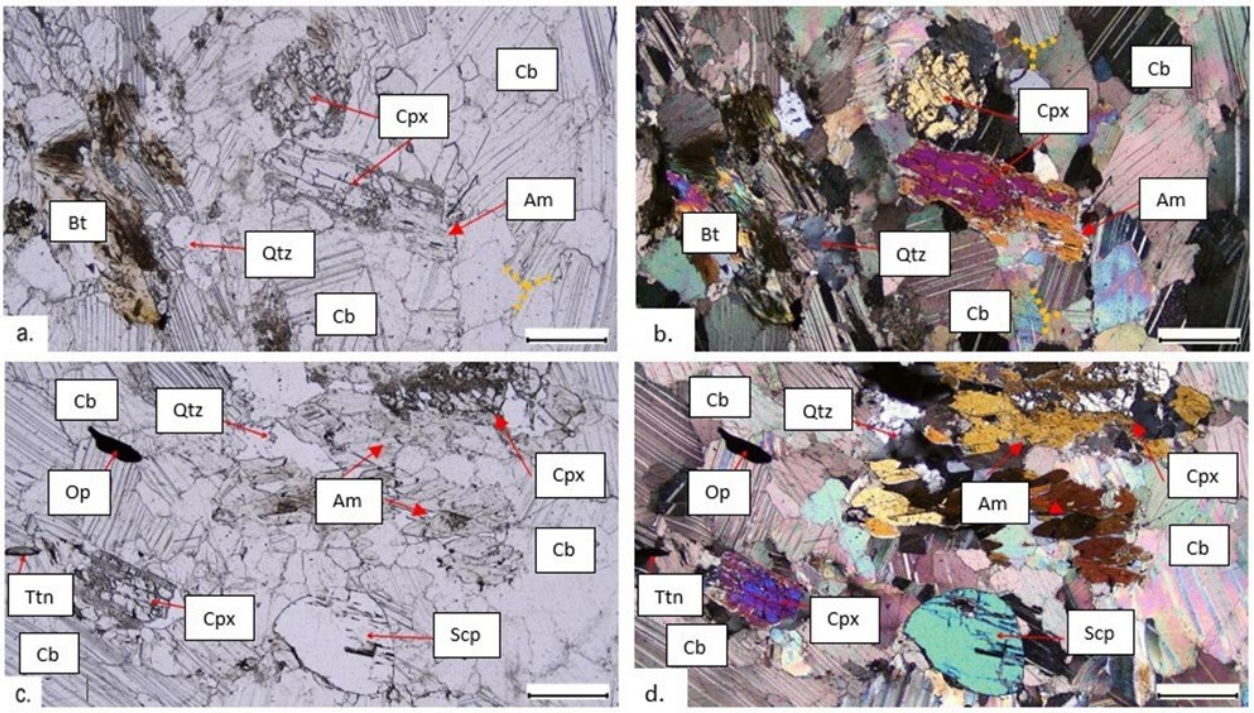

Figure 13. Photomicrographs of yellowish white marble (sample CM19R-11e), PPL on the left and XPL on the right. Note the pseudomorphs of amphibole after clinopyroxene and the suture-jagged triple points between carbonate mineral grains. Pseudomorphs of amphibole may form either euhedral rhombohedral grains or be partially covering the clinopyroxene. Scale bar: 0.5 mm.

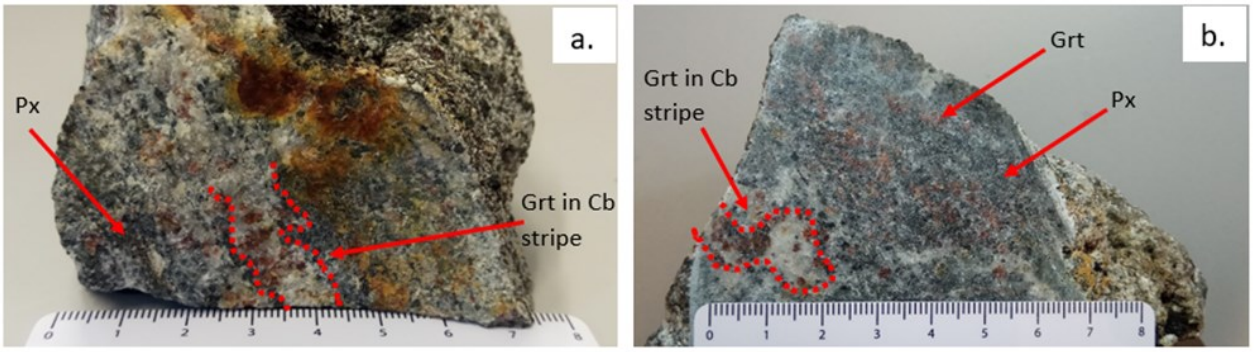

Figure 14. Hand sample of garnet- and clinopyroxene-rich calc-silicate rock (sample CM16R-03b1). a): Rough surface with garnet porphyroblasts inside carbonate and scapolite matrix (red dashed lines) and pyroxene masses which represent the siliceous layer. b): Sawed section of the rock where garnet, pyroxene and carbonate minerals can be identified.

4.3.1 Garnet- and clinopyroxene- rich calc-silicate rock, sample CM16R-03b1

This rock is a calc-silicate collected from the southern coast of the island. Specifically, it is a calc-silicate from a layered sequence within a white dolomitic marble (Fig. 4a, c). Macroscopically, the hand specimen of this rock is made up of thin white carbonate stripes in dark silicate horizons, the latter composed mainly of greyish pyroxene and reddish-brownish garnet. Garnet occurs inside the carbonate stripes (Fig. 14). Greenish areas visible with the hand lens indicate amphibole crystals. Euhedral calcite and/or scapolite crystals can be recognized inside narrow crevices. The mineral assemblage of this rock is Cpx + Grt + Ttn + Cal + Scp + Qtz + Op.

The major mineral in this sample is clinopyroxene. In thin section, the clinopyroxene is coloured light green with very slight pleochroism. Clinopyroxene crystals reach several millimetres long forming large porphyroblasts or make up small, less than millimetre-long, granular polygonal grains. Often, amphibole is pseudomorphing after clinopyroxene (Fig. 15 a-b). Its colour is dark green to brown pleochroic. Garnet crystals have a pinkish hue and also form porphyroblasts of some millimetres size. Garnet porphyroblasts have inclusions of zoisite, clinopyroxene, titanite, and scapolite (Fig. 15 c-d). The predominant mineral of the carbonate matrix is scapolite. Scapolite forms granoblastic aggregates with polygonal crystals (Fig. 15 a-d). Calcite is present but, surprisingly, not in large proportions. Triple points between scapolite and clinopyroxene grains are plentiful resulting in a polygonal granoblastic texture to the rock. Titanite is the accessory mineral which completes the paragenesis. It has a light pink to brown colour and is pleochroic. Small, euhedral and

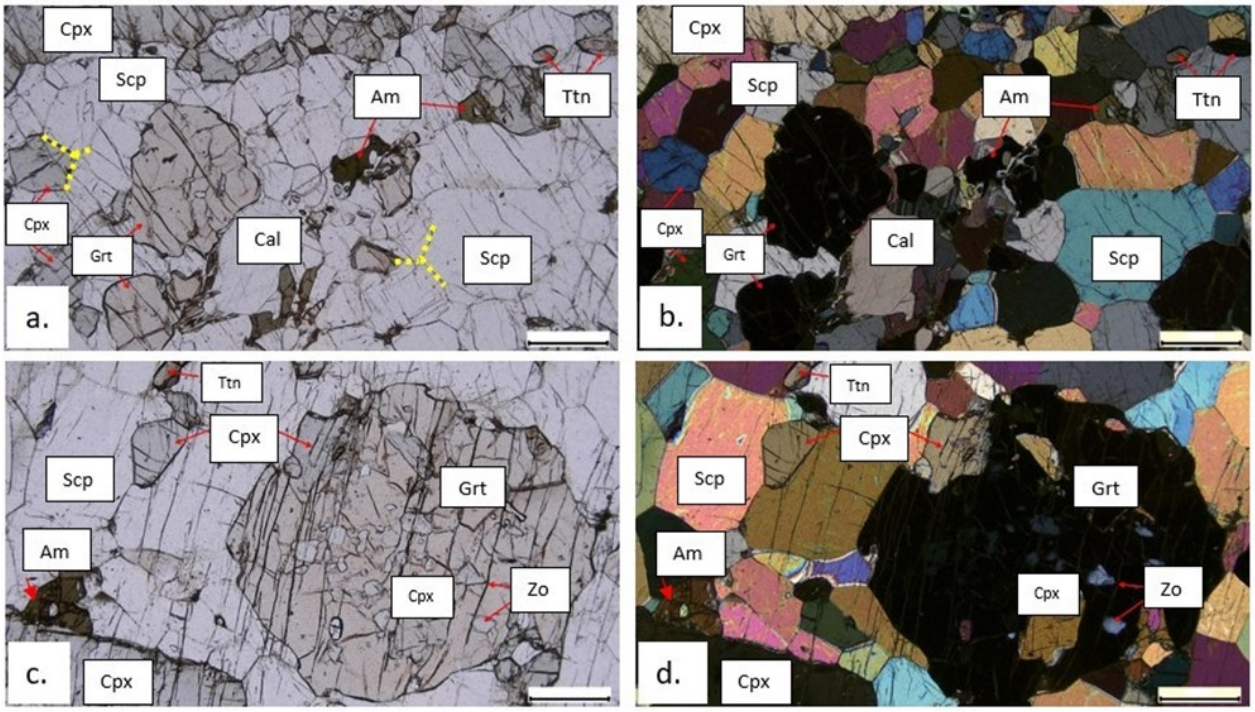

Figure 15. Photomicrographs of garnet- and clinopyroxene-rich calc-silicate rock (sample CM16R-03b1), PPL on the left and corresponding XPL on the right. Photographs of the full mineral assemblage. Observe the scapolite matrix with clinopyroxene and garnet. Pseudomorphs of amphibole after clinopyroxene and triple points between the mineral grains can be perceived. The garnet porphyroblasts contain various inclusions, mainly clinopyroxene and zoisite. Scale bar: 0.5 mm.

sphenoidal crystals occur throughout the sample (Fig. 15 a-d).

4.3.2 Carbonate-bearing mafic granulite, sample CM16R-03b2

The sample CM16R-03b2 (Fig. 4a,b) was collected from the same location as the sample CM16R-03b1. In this thesis, it has also been considered as a calc-silicate rock, with relatively high specific weight as the sample described above. However, this variety of the rock is more mafic and less rich in carbonates. In this rock, pyroxene porphyroblasts occur, but not even a single garnet grain has been observed (Fig. 16). Thus, the is blended with the mafic minerals (Fig. 16a). The mineral assemblage in this rock is Cpx + Scp + Ttn ± Cal ± Op.

The identical characteristics between CM16-03b1 and CM16R-03b2 are the formation of large clinopyroxene porphyroblasts and their granoblastic texture with triple points between polygonal crystals. Clinopyroxene is colourless to light green with high-relief grains. Their size can reach up to 1 centimetre long. Smaller, granoblastic/polygonal crystals occur as well (Fig. 17 a-d). Scapolite is found in the thin section filling voids between the clinopyroxene porphyroblasts (Fig. 17 c-d). Rarely, calcite is present. Titanite is an accessory, however abundant, phase. It

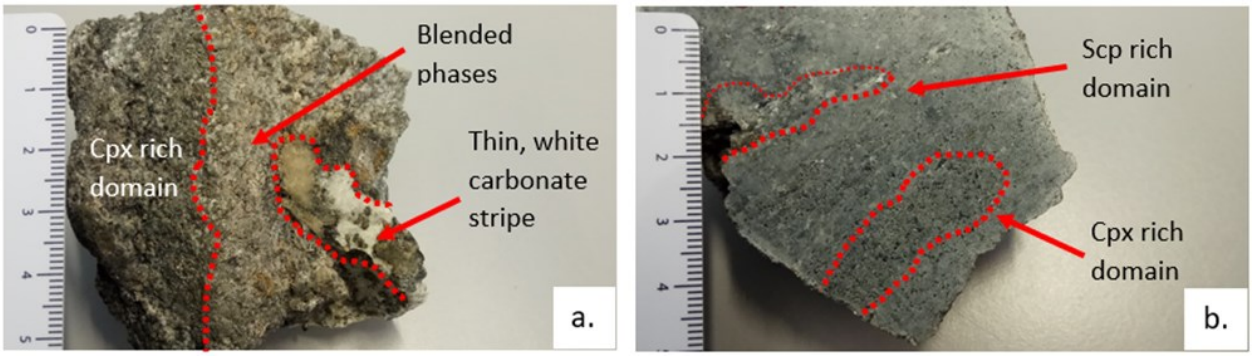

Figure 16. Hand sample of carbonate-bearing mafic granulite (sample CM16R-03b2). a): Rough surface with the three different compositional parts of the sample, b): Sawed section of the rock where the pyroxene rich areas are visible (clinopyroxene porphyroblasts).

colour of the rock is mainly dark greyish-greenish with thin white carbonate stripes. There are some domains in the hand specimen where the white carbonate phase forms euhedral crystals of maximum length ca. 0.5 millimetres. Its colour ranges from light pink to light brown due to pleochroism.

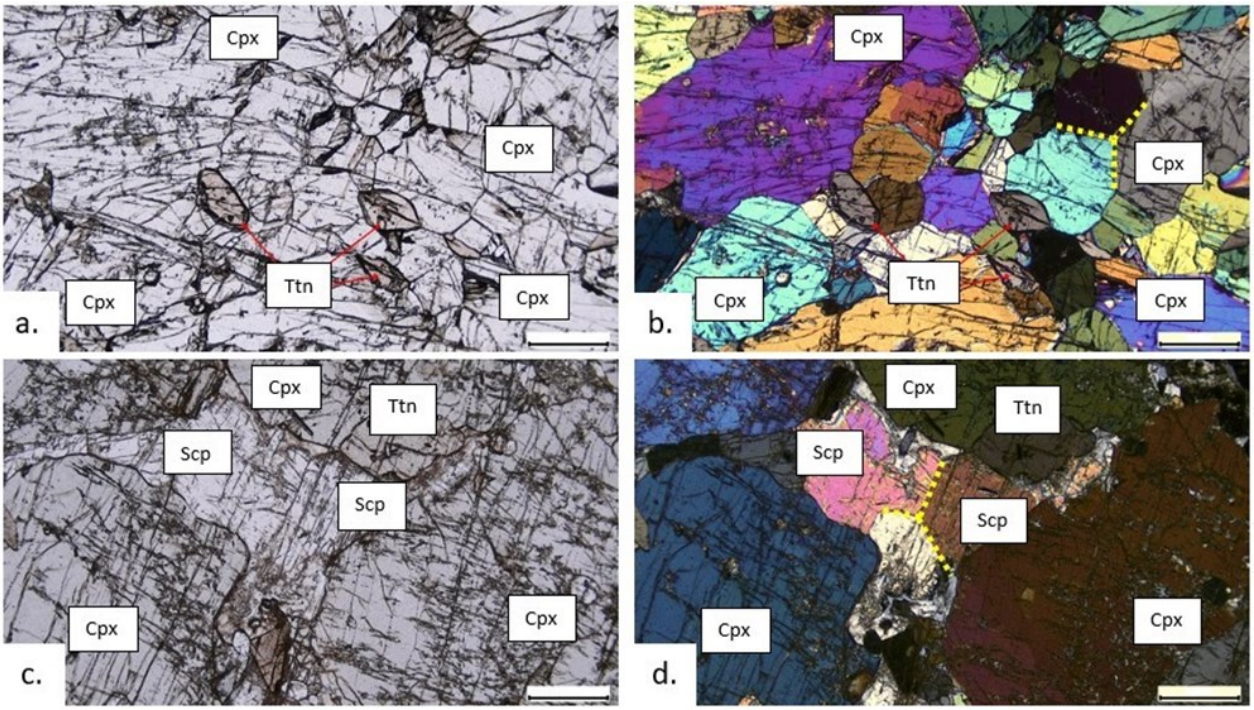

Figure 17. Photomicrographs of carbonate-bearing mafic granulite (sample CM16R-03b2), PPL on the left and XPL on the right. Note the clinopyroxene rich domain and associated small titanite crystals. The yellow dashed lines indicate triple points formation of the crystals. Scapolite crystals are occasionally filling the space between clinopyroxene porphyroblasts. Scale bar: 0.5 mm.

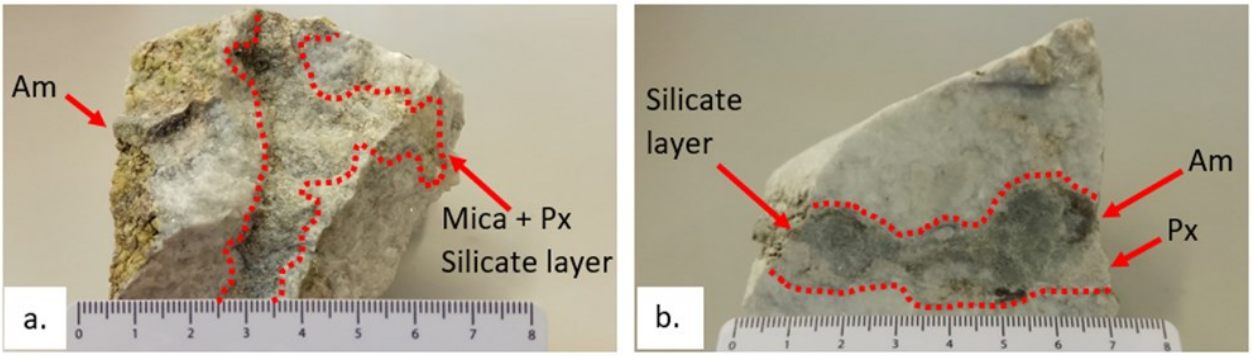

Figure 18. Hand specimen of calc-silicate layer in white marble (sample CM19R-11b). The rock is coarse-grained while some crystals can reach 0.5 cm in size. a): Rough surface with a greyish-green silicate layer. The grey phase are pyroxene grains, and the greenish aggregates contain micas. The latter own the characteristic glittery lustre of the mica mineral group. b): 1-2 cm thick, black-beige silicate layer. The dark grey minerals are amphiboles, and the beige phase is pyroxene.

4.3.3 Calc-silicate layer in white marble, sample CM19R-11b

The outcrop of this rock is located at the southern coast. This rock is a white calc-silicate with silicate layers of 1-3 centimetres long. The silicate layers are black-beige or greyish-green depending on whether they contain amphiboles and/or pyroxenes, or micas and/or pyroxenes, respectively (Fig. 18). The carbonate minerals in this specimen are mostly white. Scapolite is absent. The rock is coarse-grained and dominated by carbonate minerals and porphyroblasts of amphibole and pyroxene (Fig. 18). The mineral paragenesis in this sample is Cal + Dol + Cpx + Phl + Am +Ap + Op.

This sample is different from the calc-silicate rocks described above, both in mineralogy and texture. Granulitic texture is absent and triple points have not been formed. Clinopyroxene is colourless and forms large porphyroblasts (Fig. 19 a-b). Occasionally in some cracks, there is fine-grained alteration to talc and/or tremolite, similar to that in the marbles described above (Fig. 19 a-d). Rarely, perfect cleavage along 110 is observed in some diopside crystals. The very fine-grained, cloudy, aggregates are rich in tremolite pseudomorphing clinopyroxene (Fig. 19 c-d and g-h). Phlogopite is colourless and creates phyllo-morphed aggregates surrounding the large diopside and amphibole porphyroblasts. Pleochroism in phlogopite cannot be perceived (Fig. 19 c-f). Amphibole forms non-pleochroic, grand porphyroblasts of some millimetres long. Double cleavage of 120° angle, from perpendicular section to c-axis is distinguishable (Fig. 19 a-b and e-h). The

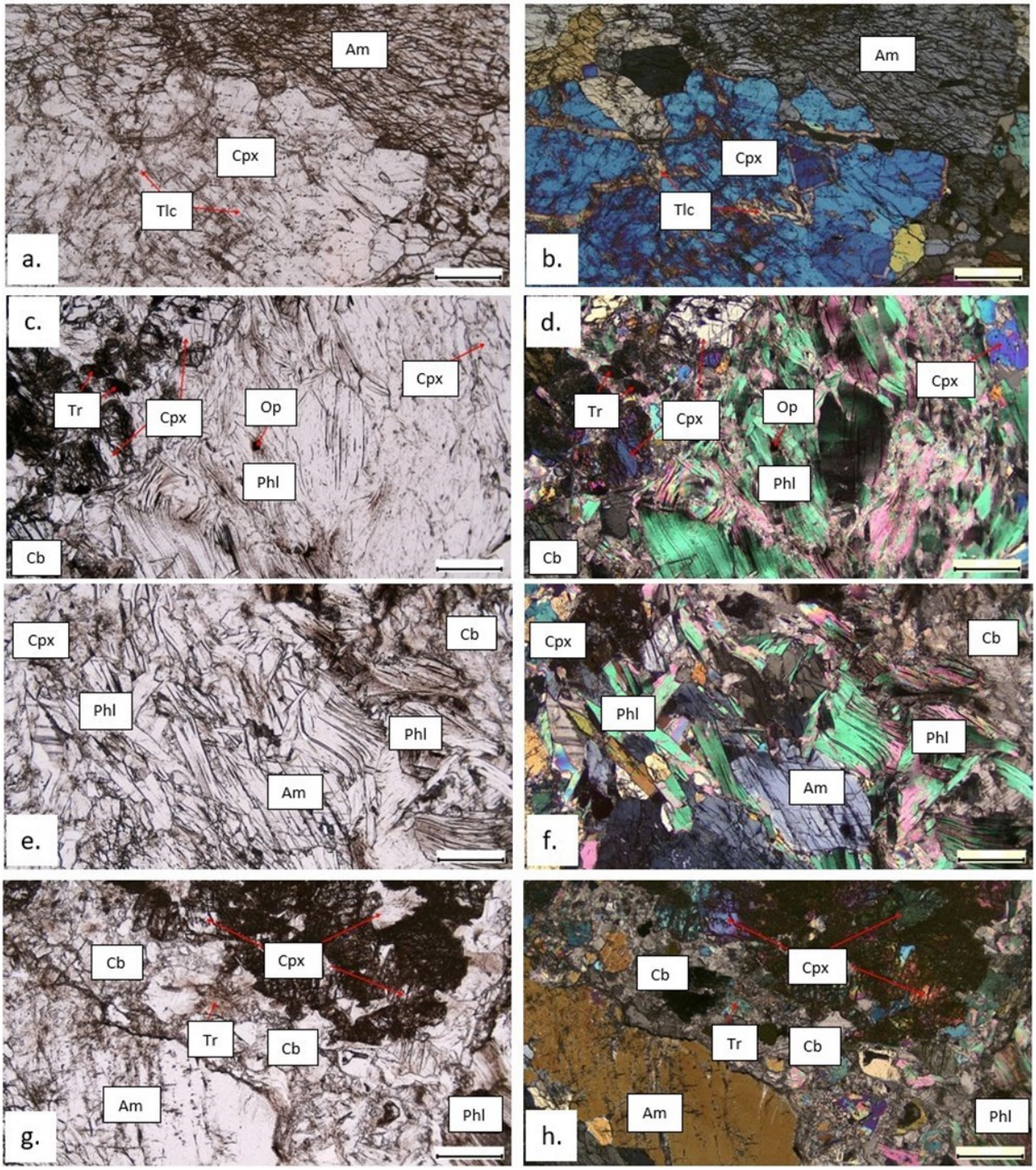

Figure 19. Photomicrographs of calc-silicate layer in white marble (sample CM19R-11b), PPL on the left and corresponding XPL on the right. a, b): Amphibole (edenite) and clinopyroxene porphyroblasts. Fractures in clinopyroxene is filled with talc. c-f): Surrounding the large porphyroblasts of diopside and amphibole are phyllo-morphed aggregates of phlogopite and fine-grained, second generation tremolite aggregates. Double cleavage (120°) is observed in one amphibole crystal (light blue arrow). g, h): Diopside and amphibole porphyroblasts and their surrounding carbonate matrix. The retrograde tremolite crystals are brown and cloudy, slightly pleochroic and substitute for diopside. Scale bar: 0.5 mm.

carbonate matrix of this sample is mainly composed of calcite (Fig. 19 c-h). However, dolomite crystals, even porphyroblasts, are also present. Accessory minerals are apatite and opaques.

4.3.4 Carbonate-rich calc-silicate rock, sample CM19R-11i1

This sample was collected from the southern coast of Allmenningen, and in the field was considered a variety of marble. However, it is a calc-silicate rock that is rich in scapolite and carbonate minerals. Macroscopically the rock is composed of white and

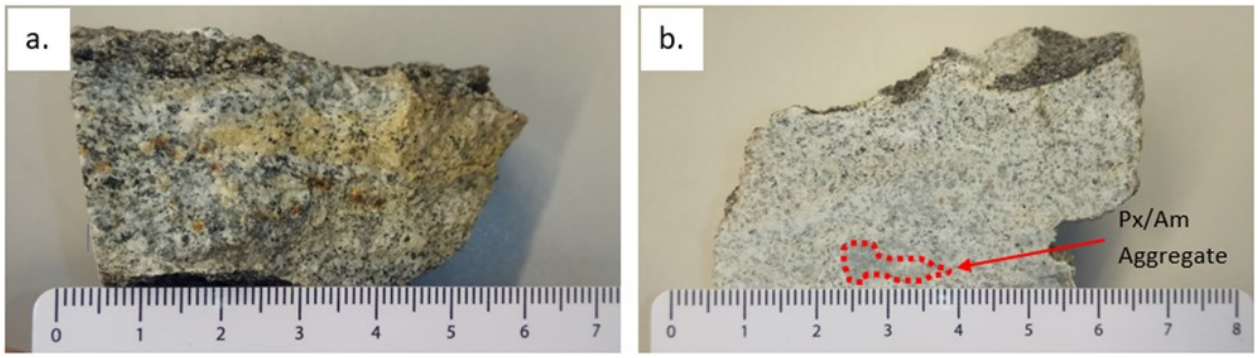

Figure 20. Hand specimen of carbonate-rich calc-silicate rock (sample CM19R-11i1). a): Sugary, granular, fine-grained crystals on the rough surface. The yellow and rusty areas are superficial discolouration. b): Sawed section with greyish-black aggregates of pyroxene/amphibole. The whitish areas are composed of carbonates and scapolite.

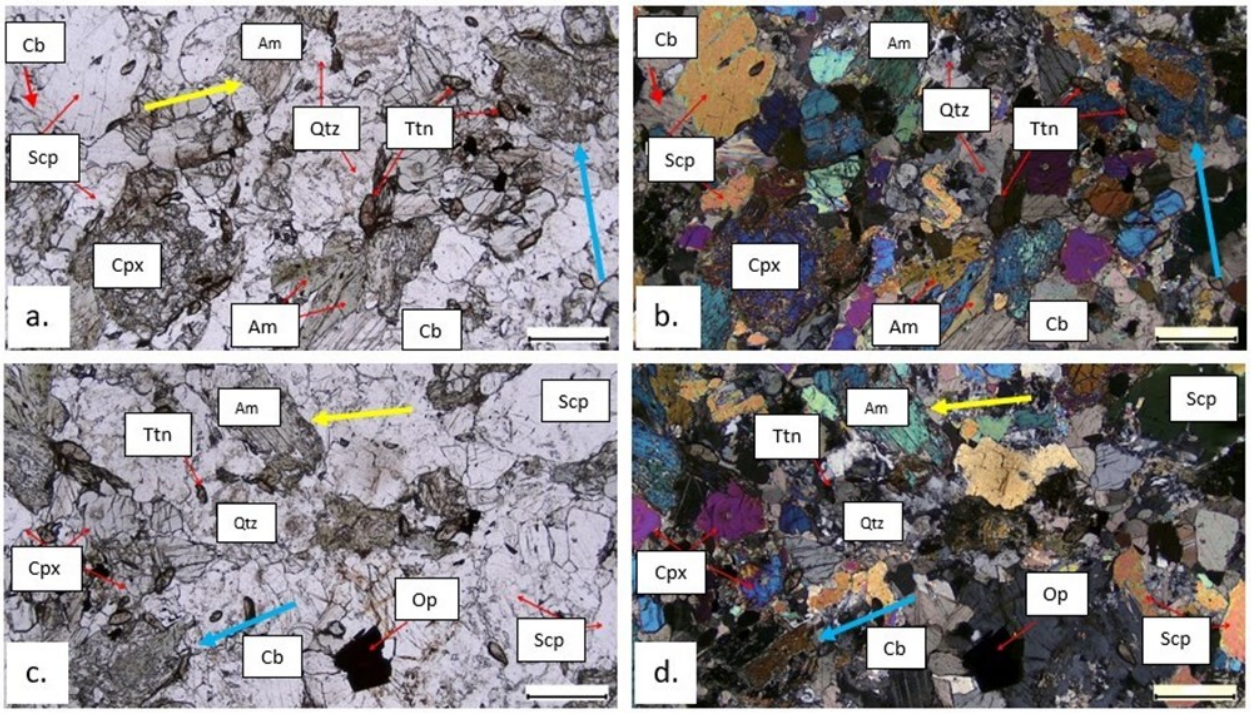

Figure 21. Photomicrographs of carbonate-rich calc-silicate rock (sample CM19R-11i1), PPL on the left and XPL on the right. The mineral paragenesis is made up of Cpx, Scp, Cb, Ttn and Qtz. The arrows without labels are pointing the pseudomorphs of Am after Cpx; light blue arrows and yellow arrows indicate partial and complete pseudomorphs, respectively. Scale bar: 0.5 mm.

black minerals. The white phases are carbonate minerals and scapolite, while the black and grey are pyroxenes and amphiboles. The hand specimen gives a fine-grained granular to sugary touch (Fig. 20). The mineral assemblage of this rock consists of: Cal ± Dol + Scp + Cpx + Ttn + Bt + Qtz + Op.

This sample is another scapolite-rich calc-silicate, in some ways comparable to sample CM16R-03b2 (Fig. 16-17). However, in this sample, garnet porphyroblasts and granulitic texture are absent. More common is that clinopyroxene occurs as rounded or prismatic, colourless grains. Complete or partial pseudomorphs of clinopyroxene by retrograde amphibole are also common (Fig. 21 a-b). Amphibole pseudomorphs are generally pale green, showing pleochroism. Clinopyroxene grains have well-developed cleavage that is maintained in the amphibole pseudomorphs, too (e.g., Fig. 21 a-d). The carbonate phase in this rock is made up of calcite and/or dolomite. Scapolite is abundant in every site of the thin section. A few quartz aggregates occur (Fig. 21 a-d). Titanite is the most common accessory mineral, forming very small subhedral to euhedral pleochroic grains, ranging from colourless to dark brown. The least common accessory minerals are biotite and chlorite. Many opaque minerals are also present (Fig. 21 a-d).

4.4 Mafic Rocks

Mafic rocks are another significant constituent of the ESU which are present in many outcrops throughout the marble-rich association on Allmenningen. The majority of the mafic samples are either from lenses inside the marble-rich succession, or from contact

zones between different kinds of rocks. These rocks tend to be relatively heavy and present very rusty surfaces, which are indicating Fe-enrichment. In these rocks carbonate phases are almost absent; however distinguishable white, non-carbonate phases exist in many samples. In these rocks garnet is very common and coexists with minerals which are representative of typical parageneses in mafic granulites.

4.4.1 Garnet-rich mafic granulite, sample CM16R -03e2

The sample was taken from a ca. 5 metre large rusty-weathering mafic lens on the south shore of Allmenningen. The hand sample is a rusty mafic rock with distinct garnet and pyroxene crystals. Under careful examination, dark green amphibole is visible with the hand lens as well. The layer of rust is the result of weathering of minerals rich in iron which causes discolouration (Fig. 22). The mineral paragenesis in this rock contains: Grt + Cpx + Am + Pl + Ttn + Ap ± Zrn ± Aln + Op.

Microscopically, this rock has the attributes of a porphyroblastic mafic granulite. There is no granoblastic texture, but the mineral assemblage is representative of a high-pressure granulite. Garnet has a light pink colour and forms porphyroblasts of several millimetres size (Fig. 23 a-d). The garnet crystals may have inclusions, but not enough to be considered as poikiloblasts. Clinopyroxene is the main phase in this rock and has a characteristic pale green colour and very slight pleochroism. Amphibole crystals have very strong pleochroism from olive green to very dark green (Fig. 23 a-d). Plagioclase grains are uncommon and occur scattered throughout the thin section. The most commonly observed accessory minerals are

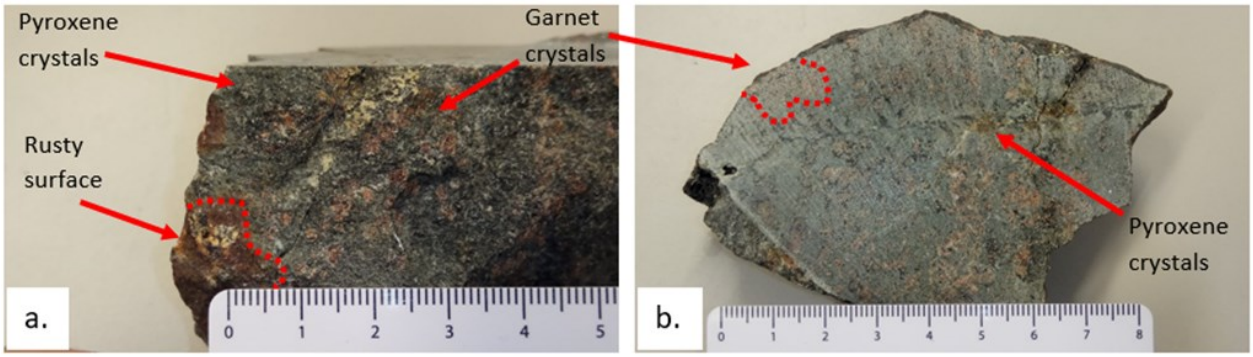

Figure 22. Hand sample of garnet-rich mafic granulite (sample CM16R-03e2). a): Raw surface with millimetre-sized garnet crystals in pyroxene-rich matrix of the rock and a rusty surface due to Fe discolouration. b): Sawed section with green clinopyroxene crystals and pinkish-brown garnet aggregates in the red-dashed lines.

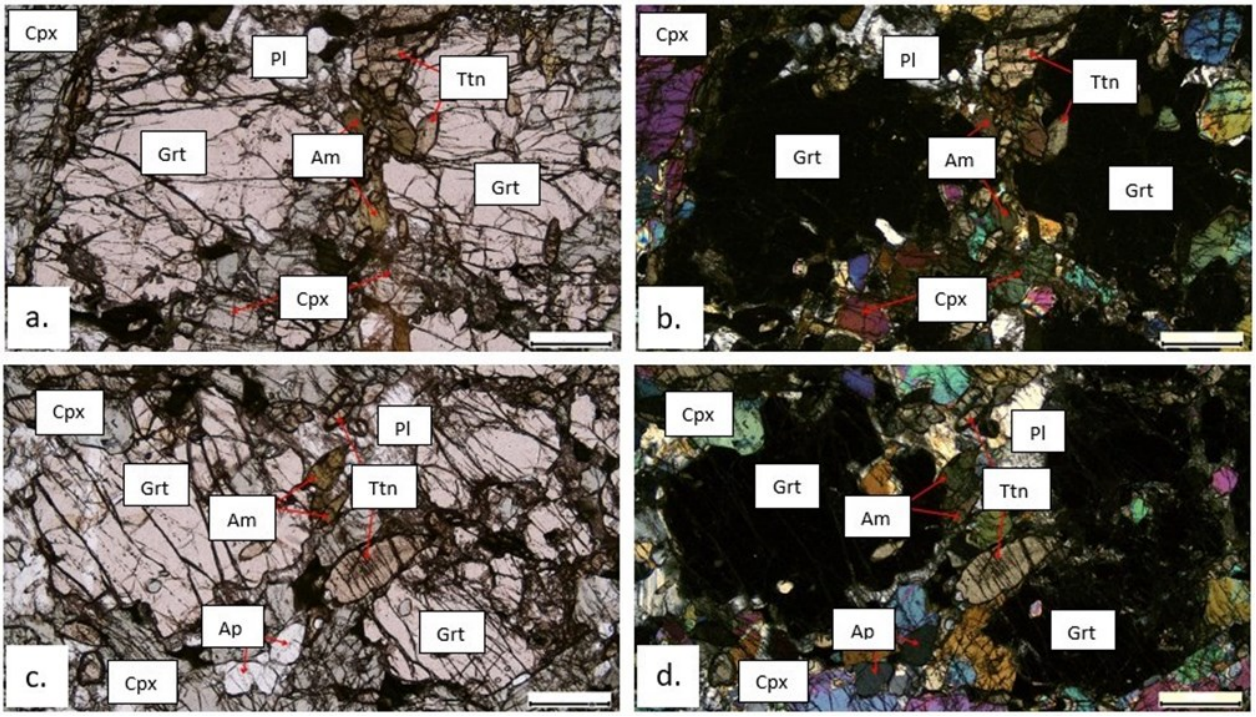

Figure 23. Photomicrographs of garnet-rich mafic granulite (sample CM16R-03e2), PPL on the left and corresponding XPL on the right. The mineral assemblage of this sample comprises garnet porphyroblasts in a matrix predominantly composed of clinopyroxene, with lesser amounts of amphibole, plagioclase and accessory minerals titanite and apatite. Scale bar: 0.5 mm.

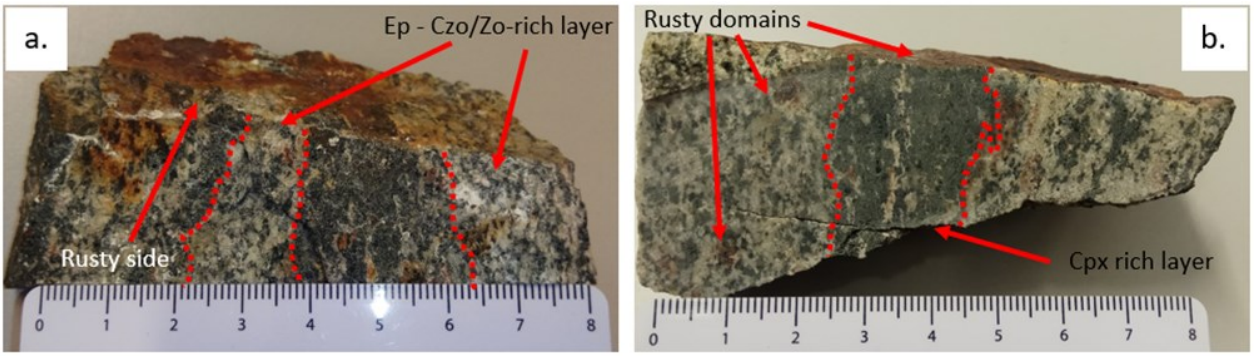

Figure 24. Hand specimen of zoisite-rich mafic granulite (sample CM16R-09d). a): Rough surface showing 2-3 cm wide zoisite-rich bands alternating with clinopyroxene-rich bands. The red arrow points to a rusty side suggesting Fe-oxidation. b): Sawed section showing the same alternating bands. In the zoisite bands there is also a brown rusty-looking substance.

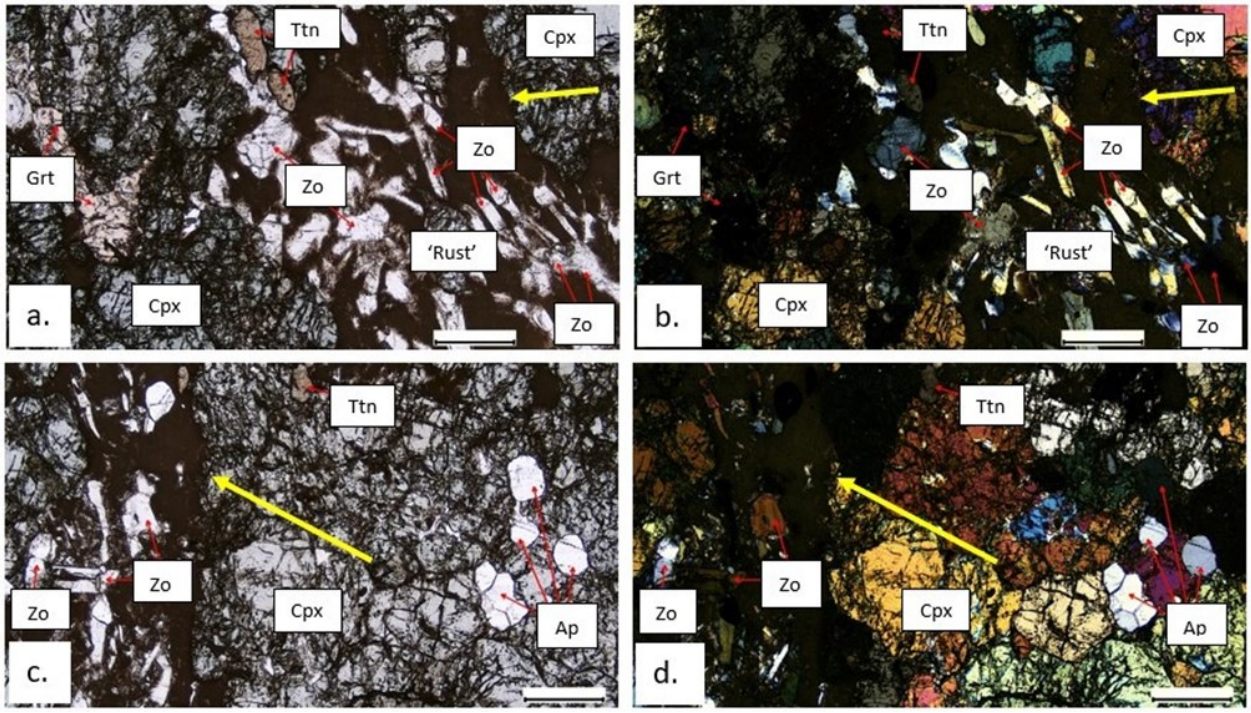

Figure 25. Photomicrographs of zoisite-rich mafic granulite (sample CM16R-09d), PPL on the left and XPL on the right. The mineral assemblage is made up of clinopyroxene, garnet, zoisite, apatite and titanite. The dark "rust" (yellow arrows) is covering only the zoisite bearing layers of the rock. Scale bar: 0.5 mm.

titanite and apatite; however, zircon and allanite are visible with higher magnification. Titanite is pleochroic with pinkish to brownish colours and apatite is colourless (Fig. 23 c-d). Opaque minerals are plentiful and probably are either Fe-sulphides or Fe-oxides.

4.4.2 Zoisite-rich mafic granulite, sample CM16R-09d

This sample was collected in the middle part of the island, in a wall near the abandoned quarry, at the contact between an amphibolite body and the white marble. Macroscopically it can be mistaken for a calc-silicate due to its white layers, but under the microscope it is a clinopyroxene-rich rock with plentiful zoisite, which forms the white layers. The greenish domains suggest pyroxene abundance and the rust on the hand specimen is due to the weathering of iron-rich minerals (Fig. 24). This rock is composed of Grt + Cpx + Zo + Ttn + Ap + rusty Op.

This sample is a mafic rock, with green clinopyroxene as primary constituent (Fig. 25). Occasionally clinopyroxene forms granoblastic aggregates, but alteration to fine-grained mineral aggregates in many places obscures the original metamorphic texture. Zoisite makes up for a remarkable proportion of this specimen. This mineral forms aggregates of colourless crystals, the individual grains being surrounded by a dark shroud of extremely fine-grained material with somewhat rusty appearance. This "rust" is mostly observed around zoisite crystals, while it is absent around clinopyroxene and garnet (Fig. 25 a-d). Garnet is light pink in colour with clinozoisite/zoisite micro drop-shaped inclusions and it is less abundant than clinopyroxene and zoisite (Fig. 25 a-b). Accessory phases in this thin section are titanite and apatite (Fig. 25 a-d).

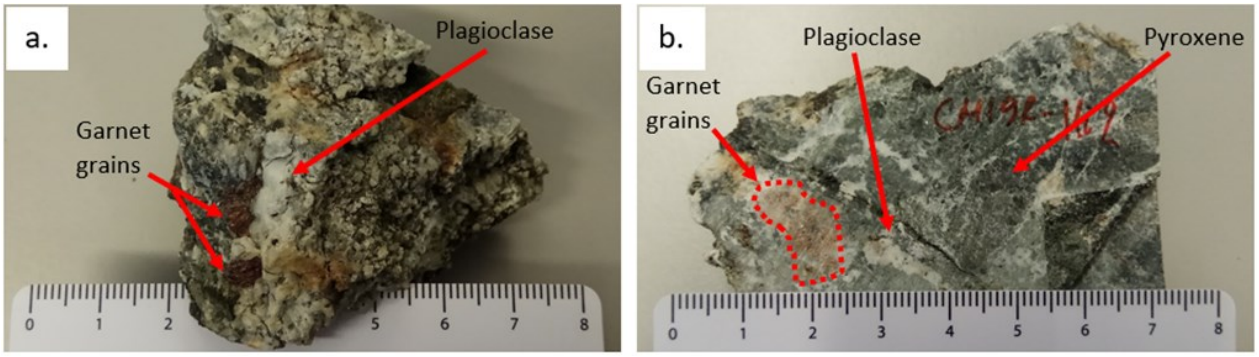

Figure 26. Hand sample of garnet-porphyroblastic knob in marble (sample CM19R-11i2). a): Rough surface with garnet porphyroblasts and plagioclase rich stripes. b): Sawed slab with garnet porphyroblasts and white plagioclase domains inside pyroxene-rich, green matrix.

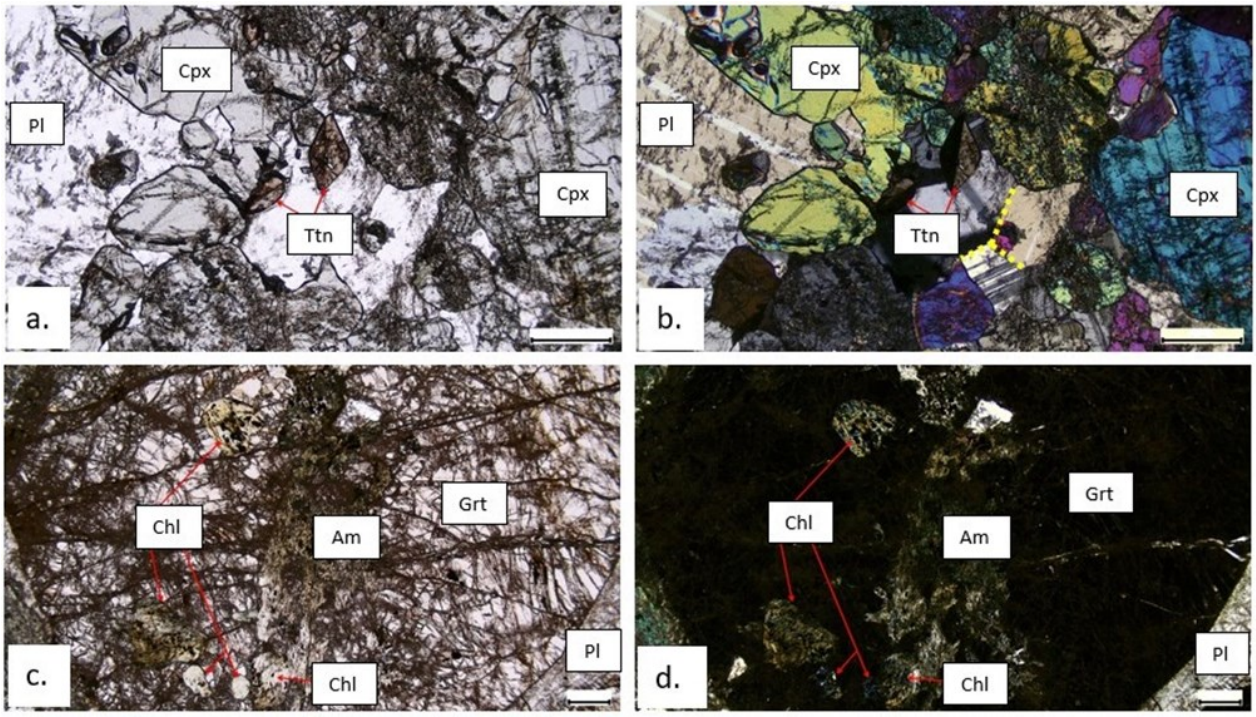

Figure 27. Photomicrographs of garnet-porphyroblastic knob in marble (sample CM19R-11i2), PPL on the left and corresponding XPL on the right. a, b): The unaltered rock contains green clinopyroxene with white plagioclase crystals in triple joints and twinned titanite crystals. c, d): Garnet porphyroblasts may include prismatic clinopyroxene inclusions which have been partly pseudomorphed by amphibole. Scale bar: 0.5 mm.

4.4.3 Garnet-porphyroblastic knob in marble, sample CM19R-11i2

This sample was found as a knob inside the calc-silicate rock, sample CM19R-11i1 described above (see Fig. 20). In comparison to the fine-grained scapolite rich host body, this rock is very coarse-grained and is composed predominantly of garnet, clinopyroxene and plagioclase porphyroblasts (Fig. 26). The minerals that comprise this rock are: Grt + Cpx + Pl + Ttn ± Qtz ± Ap + Op.

This pod can actually be categorized as a mafic granulite due to compositional minerals and granulitic texture that is observed among the mineral grains. Specifically, it can be classified as a partly retrogressed mafic granulite, due to pseudomorphs of amphibole after clinopyroxene and local chlorite growth at the expense of garnet (Fig. 27 c-d). Out of the three main phases, plagioclase is the most resistant to decomposition and alteration; however, in some sites it is sericitized. Garnet grains are pinkish and large, reaching 1 centimetre. The porphyroblasts are slightly starting breakdown to chlorite and also may contain clinopyroxene crystals which have been pseudomorphed into amphibole (Fig. 27 c-d). Clinopyroxene porphyroblasts are light green in colour and up to 1 centimetre long. Generally, triple points occur in unaltered plagioclase crystals in many sites, in response to polygonal granoblastic texture. Nonetheless, clinopyroxene grains next to garnets have been subjected to partial or complete pseudomorphing after dark green pleochroic amphibole. Plagioclase that appears to fill voids between garnet and clinopyroxene, is mostly unaltered and anhedral (Fig. 27 a-b). Titanite is the most abundant accessory mineral phase. It is pleochroic, ranging from light pink to brown, and often shows twinning (Fig. 27 a-b).

Figure 28. Hand sample of garnet-rich mafic knob in a marble-amphibolite contact zone (sample CM19R-11k). a), b): Rough surfaces of two separate pieces of the rock with distinguishable minerals of the main assemblage. The garnet rims are very thin thus, not visible even using the hand lens; however, the porphyroblasts are visible, and sometimes the clinopyroxene inclusions through very close observation.

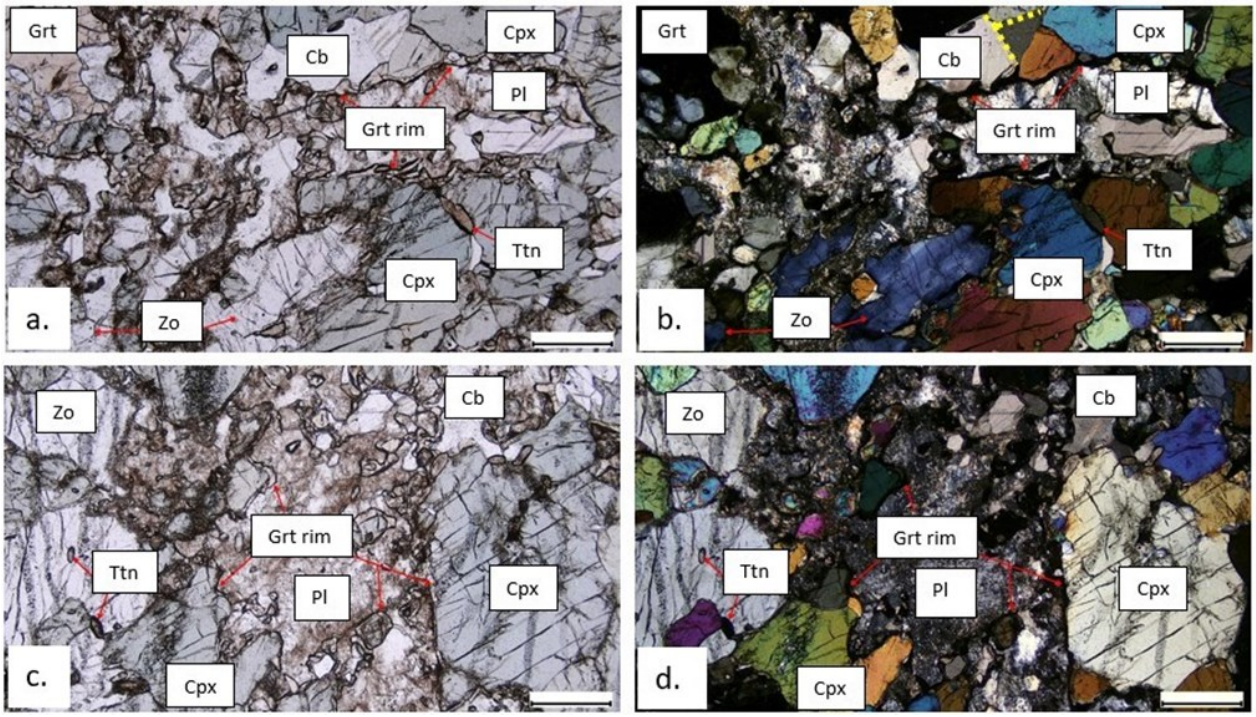

Figure 29. Photomicrographs of garnet-rich mafic knob in contact zone marble-amphibolite (sample CM19R-11k), PPL on the left and corresponding XPL on the right. Note the garnet grain (upper left) with zoisite inclusions, and garnet reaction rim around clinopyroxene, carbonates and zoisite crystals. The area in between garnet rim is the sericitized plagioclase. The yellow dashed marks indicate development of triple joints on carbonate-clinopyroxene boundary. The sericitization sites are accompanied by garnet reaction rim on its boundary, clinopyroxene and zoisite porphyroblasts, as well as calcite and titanite grains.

4.4.4 Garnet-rich mafic knob, sample CM19R-11k

The last sample included is a mafic knob in a marble-amphibolite contact zone in the southern coast of the study area. This rock is medium-grained, but garnet porphyroblasts can be seen with bare eye (Fig. 28). The main constituents of this sample are garnet, clinopyroxene, zoisite and carbonates. The complete mineral assemblage comprises: Grt + Cpx + Zo + Cal + Pl + Ttn + Op.

This mafic pod is very interesting due to its peculiar metamorphic texture. Under the microscope, thin garnet rims around the other minerals can be observed in many sites. Garnet also forms large poikiloblasts with clinopyroxene and zoisite inclusions. The rims have been formed around every type of main mineral i.e. clinopyroxene, calcite, zoisite, and plagioclase (Fig. 29 a-d). The colour of garnet is pink. Clinopyroxene is green and occurs in polygonal and prismatic aggregates forming triple joints that give a granoblastic texture in this sample (Fig. 29 a-d). Zoisite is the most plentiful colourless phase in the assemblage and it can be recognised by its anomalous birefringence colours (Fig. 29 a-d). Plagioclase is also present, however, has been partly altered into very fine-grained sericite and prehnite (Fig. 29 a-d). Carbonate minerals complete the assemblage and form polygonal crystals along with diopside that connect in triple points (Fig. 29 a-b). Titanite is the most bountiful accessory mineral. It forms small crystals, pleochroic, ranging from light

Sample	Rock Type	Minerals																	
		Grt	Cpx	Am	Scp	Ttn	Rt	Zo	Ep	Pl	Qtz	Chl	Bt*	Wmca	Cb	L*	R**	Ap	Op
CM16R-09c	Pink marble		ü		ü	ü	ü	/	ü	ü	ü			ü	ü		++	ü	ü
CM16R-09f1	White marble		ü			/			/				ü	/	ü	+	++	ü	/
CM19R-11d	White marble		ü	ü			ü				ü		ü		ü	+			/
CM19R-11e	Yellowish white marble		ü	ü	ü	ü					ü		ü		ü		++	/	ü
CM16R-03b1	Garnet- and clinopyroxene- rich calc-silicate rock	ü	ü		ü	ü		ü			/				ü		++		ü
CM16R-03b2	Carbonate- bearing mafic granulite		ü		ü	ü									ü				/
CM19R-11b	Calc-silicate layer in white marble		ü	ü							/		ü		ü	+		ü	ü
CM19R-11i1	Carbonate-rich calc-silicate rock		ü		ü	ü					ü	/	ü		ü		++		ü
CM16R-03e2	Garnet-rich mafic granulite	ü	ü	ü		ü				ü							++	ü	ü
CM16R-09d	Zoisite-rich mafic granulite	ü	ü			ü		ü	/									ü	/
CM19R-11i2	Garnet-porphyroblastic knob in marble	ü	ü			ü	/			ü	/	/					++	/	ü
CM19R-11k	Garnet-rich mafic knob	ü	ü			ü		ü	/	ü					ü	+			ü

Table 2: Overall table of samples included in the study with the associated mineral parageneses observed under the petrographic microscope. ü: present in the main assemblage of the sample, +: present in the sample as low-grade very fine-grained replacements, ++: present in the sample as retrograde amphibole replacing clinopyroxene, /: may have been observed in the sample, blank: not present in the sample.

L= low-grade very fine-grained replacements of sericite, tremolite and/or talc*

Bt= abbreviation for biotite stands also for phlogopite (Phl)*

*R**= retrograde amphibole replacing clinopyroxene*

pink to brown in colour (Fig. 29 a-d).

4.5 Mineral chemistry

Five out of the twelve samples described in the last chapter were examined in the scanning electron microscope to determine the exact type of each mineral, stoichiometry and respective chemical formulas. This chapter presents the SEM-EDS data of the dominant siliceous rock-forming minerals and the main accessory minerals of the assemblages. Mineral analytical data are given in tables in the appendix of this work (Tables 1-18). Plots for classification e.g. pyroxene and amphibole, are included in the main text body.

4.5.1 Garnet-rich mafic granulite, sample CM16R-03e2

Fifteen phases in total, including different textural amphibole types and retrograde phases, have been recognized during the SEM study of sample CM16R-03e2.

Garnet

Garnet is one of the major mineral components of this sample. Ten analyses have been performed to determine the composition of the main endmember species. Fig. 30 is a ternary diagram where the compositions of the endmembers have been plotted. The predominant constituents are almandine and grossular which add to, on average, 90%. The content of almandine is only slightly higher than that of grossular. The difference is approximately 4% and the average values are 47% and 43%, respectively. The pyrope component is far less than almandine and grossular, with an average value of 8% and a maximum of 9%. Minor constituents of less than 5%, are spessartine (2%) and andradite (0.5%). No zoning patterns have been observed; instead, the chemical composition of garnet grains appears homogeneous.

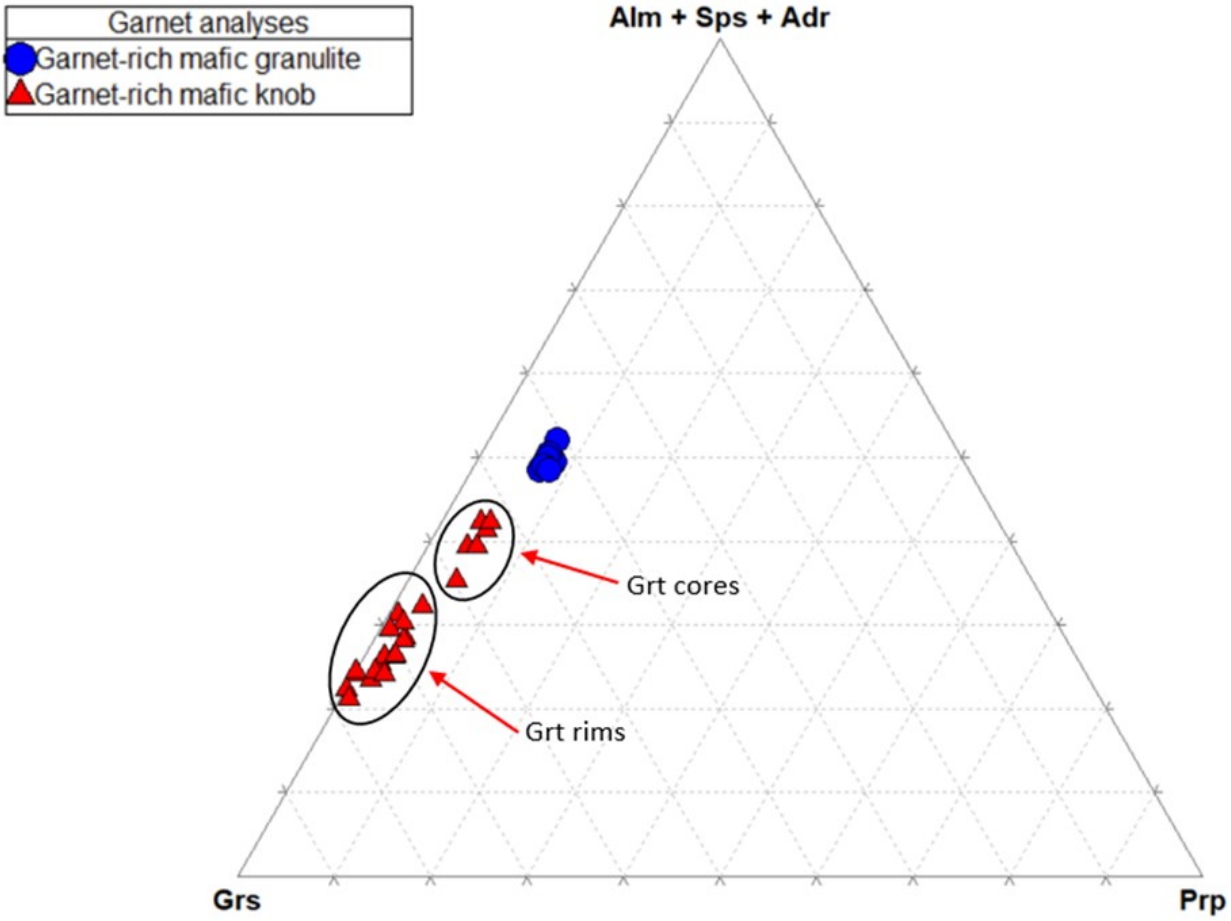

Figure 30. Garnet endmember ternary diagram with representative analyses of garnet in garnet-rich mafic granulite (sample CM16R-03e2) and garnet-rich mafic knob in contact zone marble amphibolite (sample CM19R-11k). In the sample CM19R-11k (red triangles), lower grossular composition is allocated in the garnet cores, while higher grossular composition is allocated to the rims. However, there are a few exceptions where in the garnet core the grossular composition is over 70%. In the other sample a chemical homogenization, is observed.

Pyroxene

Pyroxene is the most common mineral in this sample. Sixteen pyroxene analyses have been performed and plotted in a wollastonite-enstatite-ferrosilite (Wo-En-Fs) ternary diagram, following Morimoto (1988; Fig.

31a). The results plot entirely in the diopside field and thus, are classified as calcic clinopyroxenes (Mg / (Mg + Fe^{2+}) = 0.57-0.66). Any minor deficiency in Si in the tetrahedral position is filled by Al, which is present in lesser amounts, less than 2%. Slight contribution to the calcium (M2) site is provided by Fe^{2+}, Mn^{3+} and occasionally Na.

Amphibole

Amphibole is also a part of the main mineral assemblage. Sixteen amphibole spectra have been analysed from this thin section. As for the nomenclature and the plotting, the criteria that have been followed and diagrams used, are from Leake et al. (1997). Every amphibole spectrum has shown that these minerals belong to the calcic group (Figs 32). Amphibole follows the same compositional pattern as garnet, indicating abundant calcium and iron, while magnesium is relatively low (Mg / (Mg + Fe^{2+}) = 0.37-0.52). The values of the latter parameter (0.50-0.52) are referring to amphibole spectra which have been classified as actinolite (Fig. 32b). Actinolite is more siliceous than ferro-pargasite, more magnesium-rich and they do not contain any amounts of single valency cations, for instance sodium and potassium.

Feldspar

The feldspar that has been identified in this sample is plagioclase that varies significantly in composition. Eighteen spectra have been obtained from various sites throughout the thin section. Antiperthitic structures have not been identified in the crystals. The spectra can be distinguished into two groups: main assemblage plagioclase with medium-to-high anorthite component and low-grade albite plagioclase. The albitic plagioclase is classified as pure albite An_0, in contrast to its anorthitic counterpart which ranges from An_{57} to An_{95} (labradorite to anorthite). Minor Fe has been identified in some spectra (average of 0.5 wt% oxide). This iron component is assumed to be Fe^{3+}, which can substitute for Al.

Carbonates

Eight carbonate mineral spectra have been obtained from 5 different sites. The analyses show that these grains are calcite with an average content of 98% $CaCO_3$. The remaining proportion is Mg-, Mn-, and Fe - carbonate. Calcite has precipitated in a major crack in this sample during late fluid influx, accompanied with the retrograde actinolite from Fig. 32b.

Other phases

The most common accessory mineral is titanite. Other accessory phases include zircon and apatite. Rare allanite, and retrograde vesuvianite and muscovite have also been identified. Titanite contains some Al and Fe. Aluminium substitutes for Ti and the average oxide wt% value is 3%. Zircon is dominated by Si and Zr with detectable, yet uncertain amounts of Hf. Apatite does not contain any unusual elements, but some fluorine is present in the anion position, with an average value of 3 wt%. Allanite contains rare earth elements (REE), such as La, Ce and Nd. Peak overlap in the allanite spectra between the REEs, provide uncertain values for their wt%. In a site next to an ilmenite crystal, one grain of vesuvianite has been spotted. The 50-site method normalization suggested from Groat et al. (1992) has been used to calculate the chemical formula of vesuvianite and provide cation allocation. Lastly, the opaque minerals are mainly Fe-sulphide, Cu-Fe-sulphide, and ilmenite which can bear up to ~2 wt% Mn.

4.5.2 Pink marble, sample CM16R-09c

In total, nineteen phases have been identified in this sample, including various textural amphibole types, retrograde minerals and every accessory mineral observed.

Pyroxene

Pyroxene is one of the most common siliceous minerals in sample CM16R-09c. Eight pyroxene analyses have been obtained and plotted on a Wo-En-Fs ternary diagram (Fig. 31b). The results are plotting mostly inside the diopside, but also in the hedenbergite field Mg / (Mg + Fe2+) = 0.46 – 0.72.

In this sample, clinopyroxene formed during metamorphism, but also occurs in detrital crystals which were deposited in the limestone protolith. The tetrahedral position is filled by Si and slight amounts of Al or Fe3+ (<2 wt.% oxide). The presence of sodium suggests a minor jadeite component in pyroxenes. Other minor elements detected, are Cr and Ti.

Amphibole

Amphibole is common in this sample, like pyroxenes described above. Ten amphibole spectra have been acquired and categorized in their respective diagrams, based on their chemical composition and stoichiometry. This sample contains species of retrograde calcic amphibole (Fig. 32a-b), with various Mg#=0.30-0.66. Retrograde amphibole for instance, actinolite, is the most siliceous, while retrograde hornblende and ferro-pargasite amphibole are the least siliceous. The single valency cation position is filled by almost equal amounts of K and Na. Minor elements in the amphibole are Ti, Mn and Cl.

Epidote group minerals

Epidote group minerals are one of the most conspicuous phases in sample CM16R-09c. Eighteen spectra have been acquired for classification. For calculation of Fe^{3+} in these minerals, the method of Droop (1987) was used. The relative proportions of Fe^{3+} and Al, in the octahedral position, determines whether the mineral is classified as epidote or clinozoisite (boundary at 50%). The majority of the analyses are classified as epidote (11 spectra; Fig. 33). However, clinozoisite has been formed, where the iron component was not enough to form epidote. The classification between zoisite and clinozoisite was based on the proportion of Fe^{3+} in the octahedral position and crystal structure data acquired from polarized microscopy observations. The boundary is around 7% Fe^{3+} (zoisite contains less Fe^{3+} than clinozoisite; Brunsmann et al. 2000; Nesse 2011). In the case of a low FeO value (less than 2%),

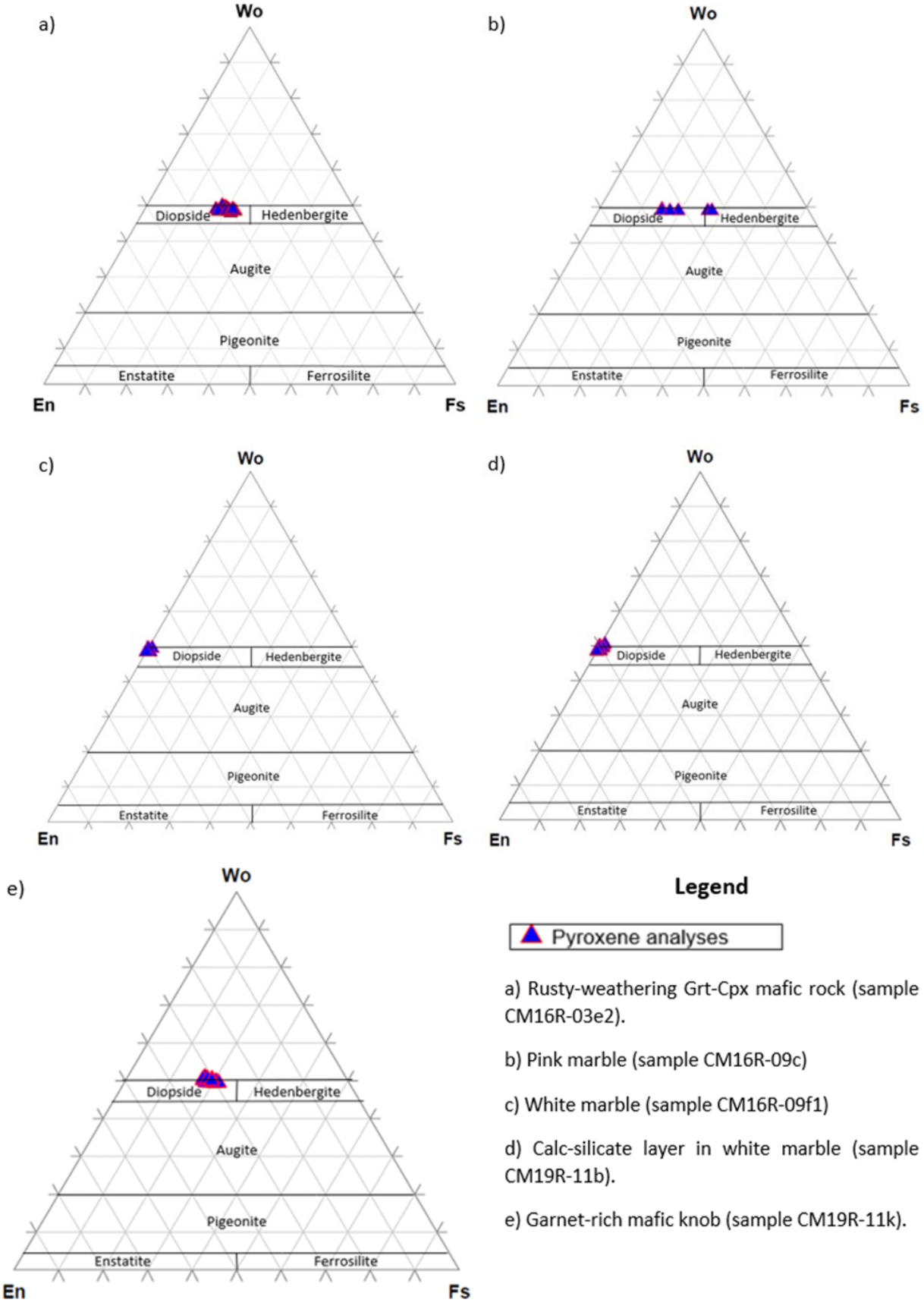

Figure 31. Wo-En-Fs ternary diagram with analyses of pyroxene from every rock studied in SEM-EDS. Almost all analyses plot in the diopside field. In the pink marble (sample CM16R-09c), diopside and hedenbergite come from the detrital crystals. The Fs component in a), b) and e) varies from ca. 15-23%.

magnesium is the main replacing cation. Other minor elements identified are: Cr, Mn, Ti, V, and Sr.

Scapolite

Scapolite is found in almost all sites of this sample and is a major constituent. Every spectrum analysed is categorized as meionite ($Ca_4Al_6Si_6O_{24}CO_3$), the calcic endmember of scapolite's solid solution. Pure meionite cannot be found in nature, but in this occasion, the calcic percentage in scapolite is much higher than the sodic (Mei% = 80-84%). The molecular fraction of CO_2 (XCO_2), has been calculated using the formula: $XCO_2 = CO_3 / (Cl + CO_3)$, where $CO_3 = 1 – Cl – SO_3$. The XCO_2 values are very high, ranging from 0.89 – 1.00. The percentage of "equivalent anorthite" (EqAn), is a parameter that can describe the composition of scapolite. This term was used by Orville (1975), in order to allocate the stability of lab-manufactured scapolite crystals to their plagioclase compositional counterparts. The mathematical formula to calculate EqAn is EqAn = 100 * (Al - 3) / 3, where Al, is the aluminium value of a.p.f.u. normalized to 16 cations (25 oxygens). Using the cation distribution to calculate the meionite component (Mei %), the mean value is 82%. Fig. 34 provides the relationship between the EqAn and XCO_2. As it is derived, scapolite is predominantly meionitic, slightly above the intermediate endmember, mizzonite (Mei_{50-80}; Evans et al. 1969). The sum of the main cations (Ca + Na + K) from 30 spectra is ca. 3.93 a.p.f.u., with a minor contribution of Fe_{2+} (0.04 a.p.f.u.). This slight deficiency (ideal total a.p.f.u. = 4.00), is probably due to Na evaporation during the analytical procedures (López Sánchez-Vizcaíno & Soto 1999). Minor elements in scapolite are K, Fe, Ti, Mg, Sc and Mn. In some of the spectra sulphur has been detected, which may indicate minor percentage of the calcic-sulphate scapolite endmember, sylvalite $(Ca,Na)_4Al_6Si_6O_{24}(SO_4,CO_3)$. No zonation patterns have been detected in single scapolite crystals.

Carbonates

Carbonate is the predominant phase of this sample. Forty-two analyses have been performed on carbonate grains, and all of them are categorized as calcites. The average percentage in CaCO3 is 98%, while the rest is mostly Mg, Fe and rarely Mn.

Mica

Twenty-four analyses on white micas have been executed. The data show that mica is muscovite (Fig. 35), but rarely margarite (i.e., calcic mica), is observed. Muscovite is characterized by high K content in the single valency cation position, which requires more than 0.7 a.p.f.u. (Rieder et al. 1998). Muscovite contains a mean of 0.86 K a.p.f.u., while the three margarite crystals analysed contain an average of 0.93 Ca a.p.f.u. Muscovite also contains various amounts of phengite mica. The sodic endmember, paragonite, has not been detected, but sodium is present (instead of potassium) in analysed muscovite grains (0 – 0.33 a.p.f.u.). Lesser minor elements < 1% are Mg, Fe^{2+}, Fe^{3+}, Mn, Ti and F.

Feldspar

Feldspar in sample CM16R-09c can be separated in two groups. The first group has high albite concentration, while the second is richer in potassium, forming K-feldspar. Pure albite crystals occur with An_{0-1}. Pure K-feldspar grains have not been detected,

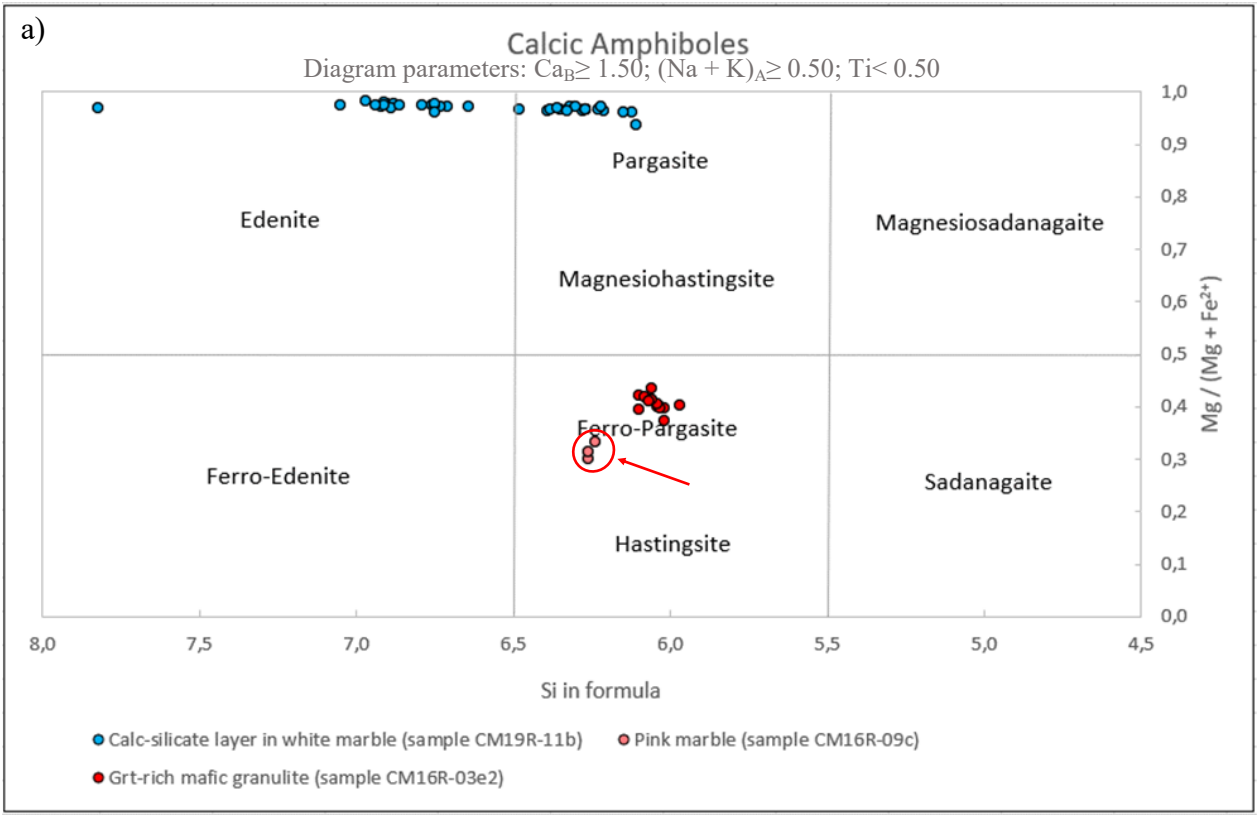

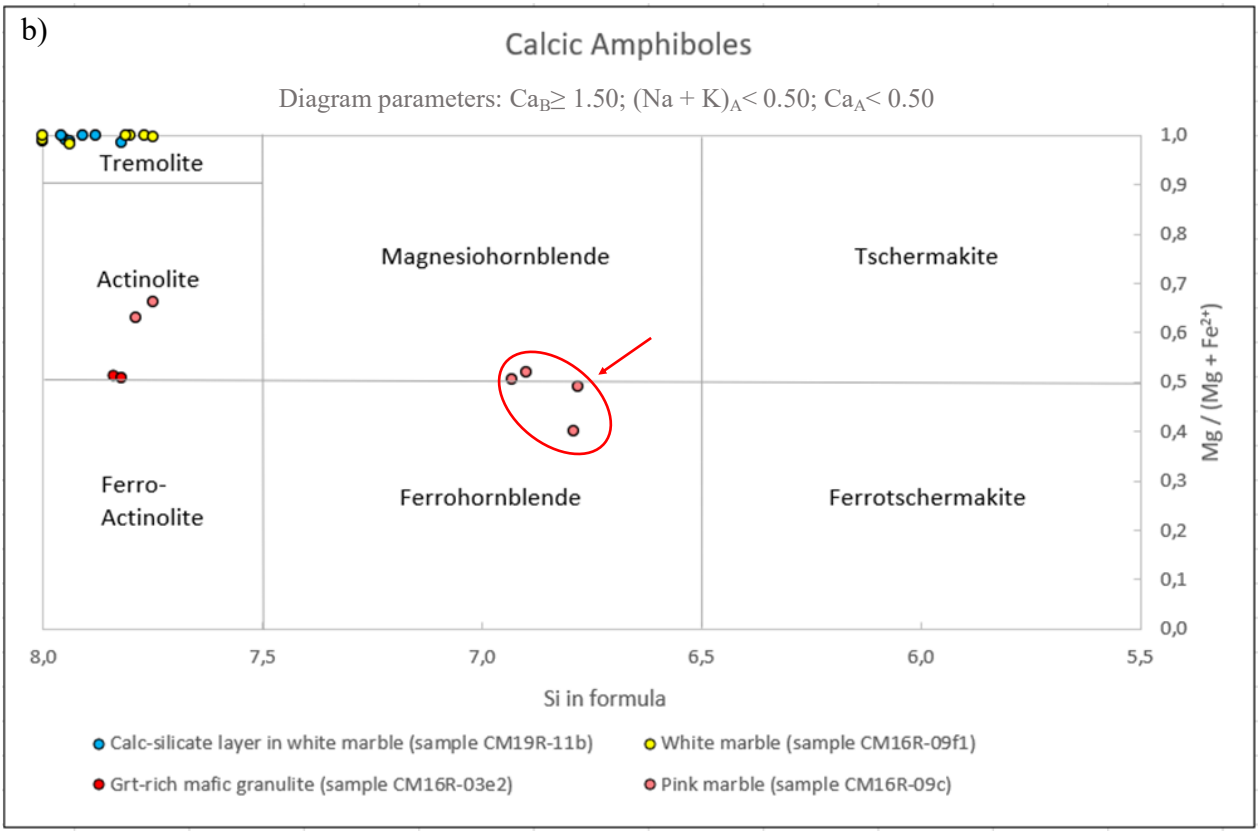

Figure 32. Summarized amphibole classification diagrams (criteria in Leake et al. 1997) from the studied rocks. a): Amphibole from the main mineral paragenesis. The group from Grt-rich mafic granulite (sample CM16R-03e2; red dots) plot in the ferro-pargasite field. The second group is the white dolomite marble with silicate layers (sample CM19R-11b; light blue dots) and plots in the edenite and pargasite fields. The pink dots from the pink marble (sample CM16R-09c; red encircled area with red arrow) represent retrograde amphibole. b): Retrograde amphibole from pseudomorphs or fine-grained replacements. Inside the actinolite field is contained retrograde amphibole from the Grt-rich mafic granulite (sample CM16R-03e2; red dots) and the pink marble (sample CM16R-09c; pink dots). Inside the tremolite field is contained retrograde amphibole from the calc-silicate layer in white marble (sample CM19R-11b; light blue dots) and the white marble (sample CM16R-09f1; yellow dots). In both hornblende fields is contained retrograde amphibole from the pink marble.

but their potassic component is generally over 90%. Perthitic and/or antiperthitic grains are absent. Textural positions could not be identified.

Other phases

The most important accessory minerals in this sample are apatite, titanite, rutile, zircon and opaques. Quartz is quite abundant in this sample. Apatite is generally rich in fluorine thus, categorized as fluorapatite. The average value of F is ~3 wt% calculated out of 5 analyses in 2 mineral grains. Minor Cl has been observed in the fluorapatite. Titanite is plentiful in this marble and also contains consistently minor amounts of Al and Fe (considered as Fe^{3+}). Other impurities observed are V and Mn. Rutile crystals have been observed in titanite. Rutile grains contain minor quantities of V and Fe^{3+}. Metallic minerals are Fe-rich oxides which are categorized as magnetite. Common minor elements are V, Ti, Cr and Co. Rarely can be perceived Fe-sulphides.

4.5.3 White marble, sample CM16R-09f1

Ten phases in total have been detected in sample CM16R-09f1, including main assemblage, retrograde and accessory mineral phases.

Pyroxene

Pyroxene is a common siliceous phase in sample CM16R-09f1. Fourteen spectra have been acquired and plotted on a Wo-En-Fs ternary diagram to determine the chemical composition of this mineral. As it is derived from Fig. 31c, the pyroxenes are very close to an ideal diopside composition. Fe is almost absent (Mg / (Mg + Fe^{2+}) = 0.98-1.00). In some spectra, occur low amounts of Al and Na (<1.00 wt%) suggesting a minor component of jadeite (~2 mole-%). No minor elements have been observed in the pyroxene of this sample.

Amphibole

Amphibole is highly calcic and magnesium-rich, similar to the pyroxene in the same sample. Amphibole totals are generally low (91-93%, table 3, appendix). However, an attempt for stoichiometry and classification has been conducted, which resulted in a classification as tremolite. Tremolite analyses show that the mineral is rich in Ca and Si, with Mg / (Mg + Fe^{2+}) = 0.98-1.00. Minor elements are Na, K, Al, Ti, Mn and Fe. Nine tremolite spectra have been acquired and plotted on a calcic amphibole classification diagram (Fig. 32b), according to Leake et al. (1997).

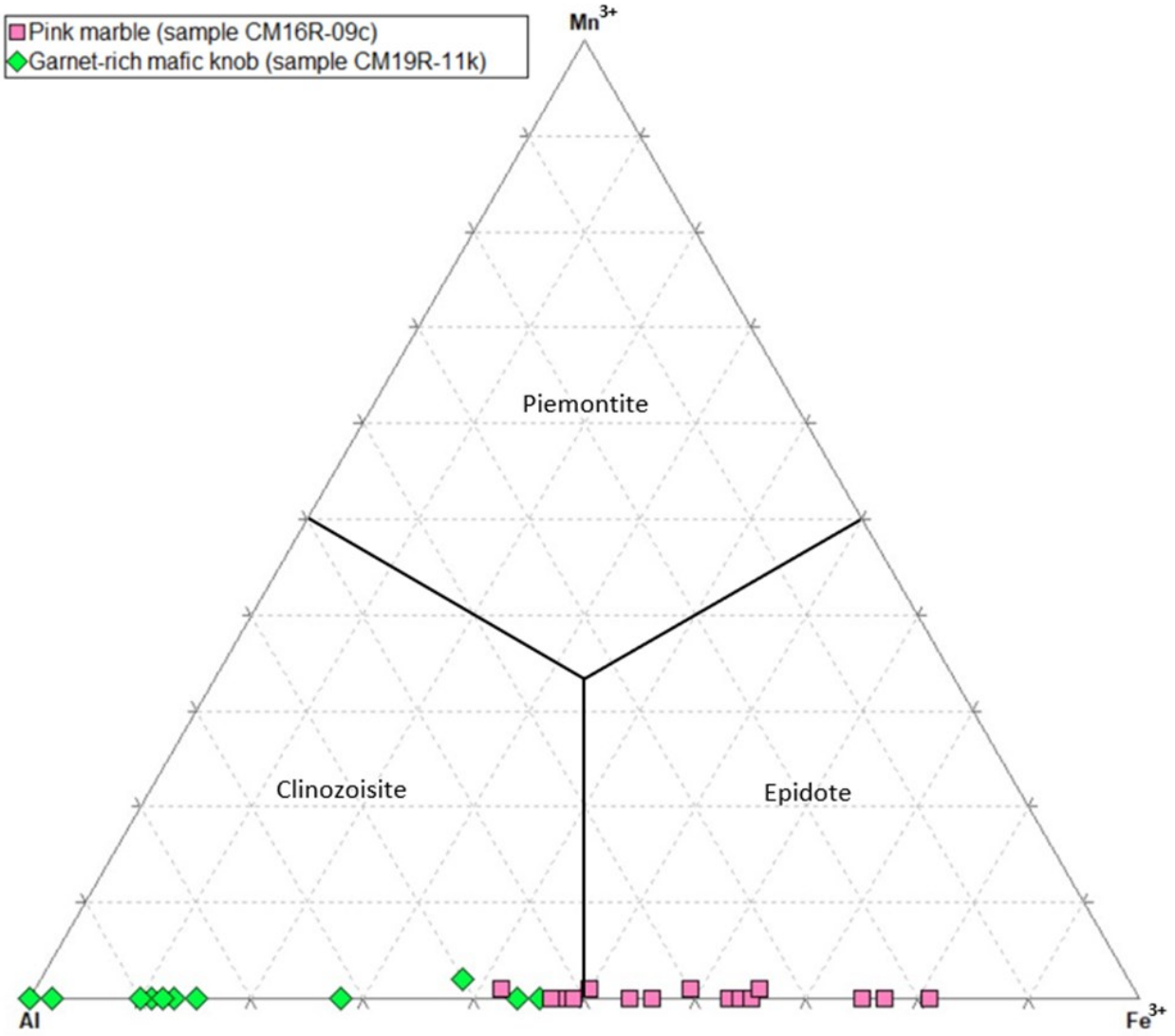

Figure 33. Mn^{3+}-Al-Fe^{3+} ternary plot with epidote group mineral analyses from the pink marble (sample CM16R-09c) and the garnet-rich mafic knob (sample CM19R-11k). In both samples there is significant spread in the proportion of Al and Fe^{3+}. Pure zoisite is located near the Al peak of the diagram, assuming that clinozoisite is generally a bit more ferric.

The single valency position in tremolites is either almost never filled (as it is suggested by its formula), or it sums up a maximum total of K + Na = 0.1 a.p.f.u. As has been described in the previous chapter, tremolite amphibole is very fine-grained retrograde mineral phase, replacing diopside.

Mica

Mica analyses from sample CM16R-09f1 show phlogopite composition (Fig. 35). Phlogopite is the Mg -rich endmember of the biotite solid solution. EDS analyses from this mineral indicate minor elements of Na and Fe^{2+}. The monovalent position receives K and Na and is never fully occupied (max sum: 0.98 a.p.f.u.). The ideal phlogopite composition [$KMg_3(AlSi_3O_{10})(F,OH)_2$], suggests 3.00 Si a.p.f.u. and 1.00 Al a.p.f.u. regarding the tetrahedral position. In this occasion a slight enrichment in Al, is observed (~1.1 a.p.f.u.).

Carbonates

Both calcite and dolomite have been recognized in this sample. Calcite and dolomite locally contain iron impurities, but pure crystals also occur. Dolomite analyses contain approximately 51.50% $CaCO_3$, and 49.50% $MgCO_3$. Calcite is mainly composed of $CaCO_3$ (94%), while the remaining cation positions are held mainly by Mg (6%).

Other phases

Other minerals that have been detected in this sample and are less abundant are talc, apatite, zircon, titanite and opaques. Talc occurs mainly inside the cracks of diopside. Apatite does not contain any minor elements in the cation positions, but contains approximately 1% of F + Cl, maximum 0.50 a.p.f.u. Two spectra of zircon crystals provide unreliable analytical data with low totals. However, Zr and Si peaks combined with very bright colour in the EDS images, confirm that these minerals are zircon. Titanite contains small amount of V, Fe and Al. These elements substitute for

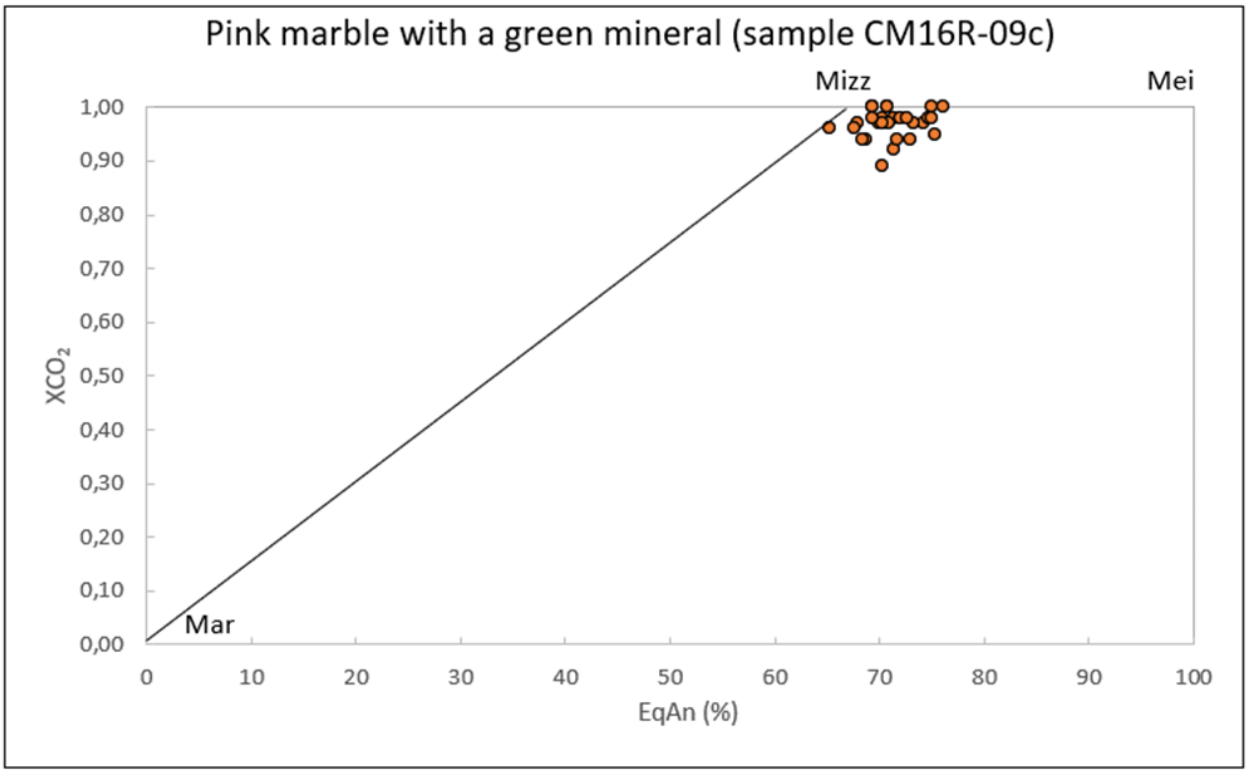

Figure 34. Diagram of chemical variation of scapolite expressed as the percentage of equal anorthite EqAn (%) vs. the molecular fraction of CO_2 (XCO_2). The analyses show highly meionitic (mizzonitic) scapolite and very high values of XCO_2.

Ti, which has a small deficiency (0.85 a.p.f.u.). Opaque minerals are Fe-sulphide.

4.5.4 Calc-silicate layer in white marble, sample CM19R-11b

This calc-silicate rock is composed of eleven phases. The main constituents are carbonate minerals, pyroxene, amphibole, and mica. F-bearing hydrous minerals are generally abundant in this sample.

Pyroxene

Thirty-two pyroxene spectra have been obtained, analysed and plotted on Wo-En-Fs ternary diagram (Fig. 31d). The clinopyroxene is Fe-poor and occasionally contain minor amounts of Na and Al (<1 wt%). Clinopyroxene of sample CM19R-11b has the closest composition to pure diopside together with the white marble (sample CM16R-09f1). The data show a concentration of approximately 50% Wo ($CaSiO_3$) and 50% En ($MgSiO_3$), which make up pure diopside ($CaMgSi_2O_6$; Fig. 31d). The Fs component ($FeSiO_3$), is very low (0-1,60%), Mg / (Mg + Fe^{2+}) = 0.97-1.00, and FeO concentrations is on average 0.61wt%. Occasionally, minor substitutions of Na (for Ca) and Al (for Mg), suggest a small jadeite constituent in these pyroxene crystals (3 mole-%).

Amphibole

Three different kinds of amphibole have been detected in sample CM19R-11b. The amphibole belongs to the calcic group and has high Mg / (Mg + Fe^{2+}) = 0.94-1.00. Forty-five amphibole spectra have been included in the classification diagrams (Fig. 32). The studied amphiboles are edenite to pargasite (hornblende) and tremolite (Fig. 32). Pargasite, in comparison to edenite and tremolite contains the highest amounts in aluminium. Pargasite and edenite show variation in Si a.p.f.u. A small number of spectra, mainly of pargasite and edenite (rarely of tremolite) contain trace amounts of fluorine (~0.30 wt% F). As their chemical formula suggest, both pargasite [$NaCa_2(Mg_4Al)(Si_6Al_2)O_{22}(OH)_2$] and edenite [$NaCa_2Mg_5(Si_7Al)O_{22}(OH)_2$] include Na in the single valency position. In fact, the latter in every spectrum obtained has a deficiency in cations. Na is the most abundant element in the monovalent cation position with ca. 0.70 a.p.f.u. Common minor elements in amphibole are K, Fe, Ti and Mn.

Mica

Twenty-five spectra of mica have been acquired and classified as phlogopite (Fig. 35). Phlogopite is high in magnesium and poor in iron while rich in Al, K and Na. The analysed phlogopite is also F-bearing with an average amount of 0.50 wt%. The single valency cation position is occupied mainly by K. Typical impurities in phlogopite include Ti and Fe.

Carbonates

Sample CM19R-11b contains calcite and dolomite. Both minerals contain low amounts of other elements, but also pure crystals have been spotted. Thirty-six of fifty-one spectra show that calcite crystals are composed of $CaCO_3$ (~ 95%), while the remaining component is $MgCO_3$. The rest fifteen spectra show that dolomite crystals in this rock are composed of $MgCO_3$ (~ 48%) and $CaCO_3$ (~ 51.5%) while the rest

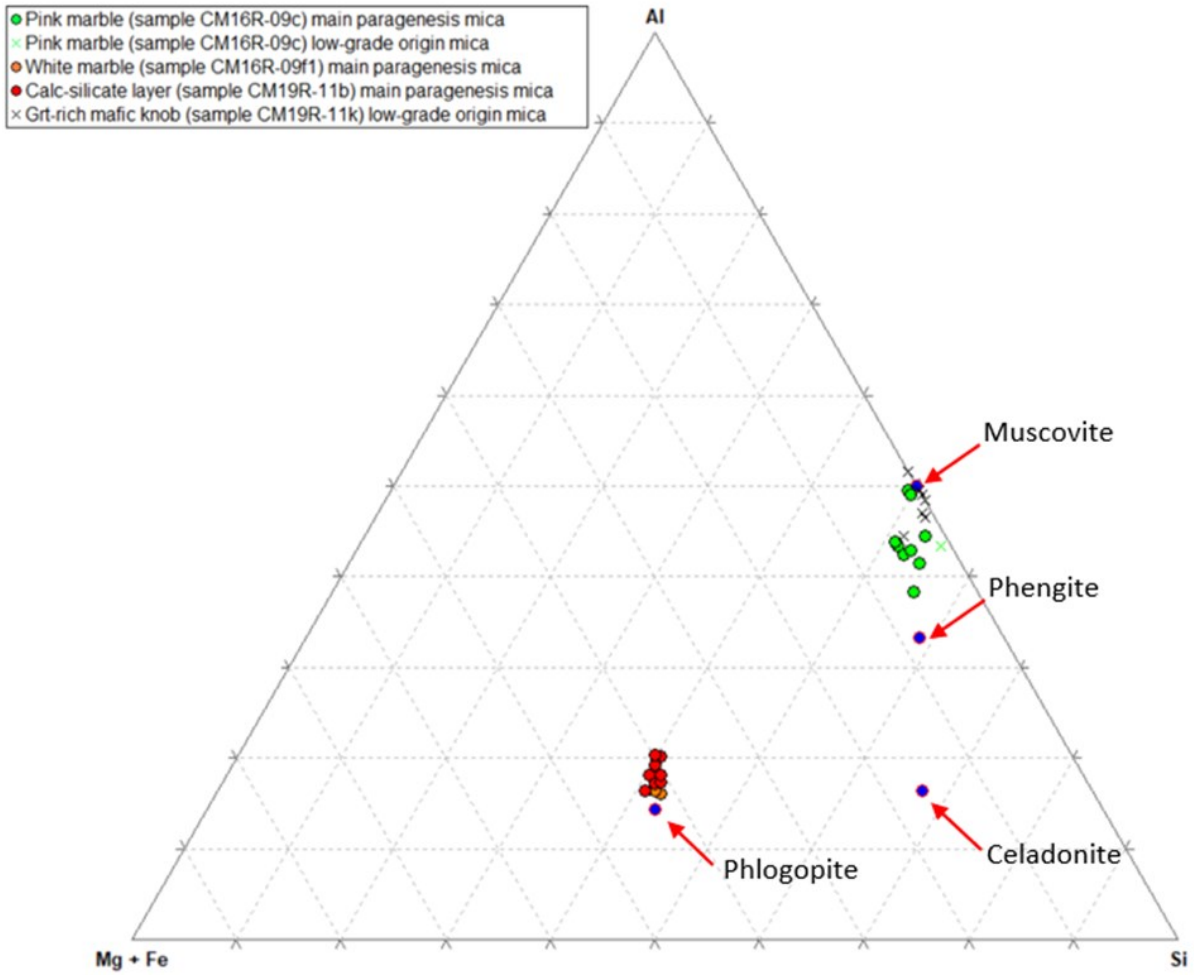

Figure 35. Al-Si-Mg + Fe ternary plot with mica composition from the pink marble (sample CM16R-09c), white marble (sample CM16R-09f1), calc-silicate layer in white marble (sample CM19R-11b) and garnet-rich mafic knob (sample CM19R-11k). The ideal composition of phlogopite, muscovite, phengite and celadonite are indicated with the blue dots. These values have been calculated based on the ideal chemical formulae of the minerals. The formulae have been acquired from mindat.org. The main paragenesis white mica in the dolomite marbles has composition very close to phlogopite, while in the dolomite-free pink marble has composition that varies from muscovite to phengite. Low-grade origin mica from the pink marble and the garnet-rich mafic knob has composition very close to muscovite (sericite).

0.50% is Fe impurities.

Other phases

Sample CM19R-11b is the only thin section without titanite. The most abundant accessory mineral is apatite. Apatite contains on average 2 wt% fluorine. Chlorine is also present but in lesser quantities (< 1 wt%). Opaque minerals are present in some sites and are mainly Fe-sulphides. One grain of a Platinum Group Mineral (PGM) has been detected, but its origin is uncertain (detrital crystal or dust crystal from coating material of fossils). The latter is composed of ca. 80 wt% Pt and 24 wt% Pd with traces of Fe and O. Rarely, talc and feldspar have been identified in some sites. The analyses show that it is plagioclase with a composition of An_{20}.

4.5.5 Garnet-rich mafic knob, sample CM19R-11k

This sample is one of the two amphibole-free rocks that are included in this study. The metamorphic texture with thin garnet rims around other minerals offers a possibility to infer the reaction history as well as to calculate P-T conditions.

Garnet

Garnet is present in every site explored in this sample. Forty spectra from both garnet porphyroblasts, poikiloblasts and reaction rim grains have been acquired. Chemical analyses and stoichiometric data from the garnet grains follow a pattern, showing a moderate deviation (Fig. 30). The predominant composition in garnet is a grossular-content of ca. 66%, with a maximum value observed of 77%. Almandine-content ranges from 28 to 41%. As it is observed, garnet rims are richer in grossular-content (65-77%) than the cores (53-59%). A small percentage of Fe^{3+} has been calculated with the Droop method, yielding an andradite content of ~ 2%. Garnet is low in Mg and Mn: pyrope is ca. 3%, and spessartine almost absent (0.3 %). In one spectrum, trace amounts of Cr have been observed (uvarovite ~1.5%).

Pyroxene

Twenty-five pyroxene spectra have been analysed and plotted in a Wo-En-Fs diagram. All analyses plot in the diopside field (Fig. 31e). This pyroxene is richer in Fe than those in samples CM19R11b and CM16R-09f1 and has Mg / (Mg + Fe^{2+}) = 0.58-0.66. Al is also present in these pyroxenes, with a mean value of ~1% Al_2O_3. Wo ($CaSiO_3$) component is ca. 50%, while enstatite ($MgSiO_3$) reaches 33%. Minor elements are Cr, Na, Fe^{3+}, V and Ti.

Epidote group minerals

Epidote group minerals in this thin section are mainly zoisite. The total calculated ions were slightly higher than 8 normalized to 12.5 oxygens, thus the Droop (1987) Fe^{3+} calculation was used for the determination of Fe_2O_3. The results show that 19 out of 23 spectra are zoisite, and the remaining 4 are clinozoisite (Fig 33). Zoisite contains low amounts in Fe_2O_3 (~2%), while clinozoisite is richer (~7%). Generally, none of the spectra is iron-rich enough to be categorized as epidote. Allanite crystals have not been detected in this sample. Zoisite crystals do not contain other minor elements.

Mica

Grains of sericite are present in this thin section, as alteration of plagioclase. Sericite and prehnite form very fine-grained aggregates and are interpreted as very low-grade alterations. Twenty-six spectra have been obtained from these fine-grained masses and all are classified as muscovite (K-rich mica; Fig. 35). The single valency position where K resides is never filled completely (max sum 0.99 a.p.f.u.) but K varies from 0.70 to 0.97. The minimum value of K a.p.f.u. in order to characterize a mica as muscovite is 0.70 (Rieder et al. 1998). K_2O presents an average value of 10%. The mica includes minor amounts of Ca, Na, Mg and Fe.

Prehnite

Prehnite has been observed in this thin section in the same sites as sericite. Prehnite's chemical formula is $Ca_2Al_2Si_3O_{10}(OH)_2$, thus is mostly occurring in Ca-Al-rich rocks, for instance plagioclase-rich marbles, or mafic rocks such as metabasalts and gabbros, with Ca-rich plagioclase. Ten prehnite spectra have been obtained from six different sites. Some spectra have Al excess, due to analytical errors. Prehnite forms very-fine-grained intergrowths with sericite and probably the Al excess occurs from spectra when the electron beam hits both prehnite and sericite. This situation is accompanied with a deficiency in Ca or in Si, where more Al than the regular amount is residing in the tetrahedral position. Prehnite contains variable minor amounts of Mg, Fe, K and Na. However, there are 'clean' analyses that fit well into prehnite stoichiometry without great excess in the cation allocation.

Carbonates

Eighteen spectra of carbonate minerals have been acquired. The results show that they are almost pure calcite with an average $CaCO_3$ proportion of 99%, the remaining being $MgCO_3$ and $FeCO_3$. Calcite forms both euhedral crystals and fine-grained aggregates that are mixed with sericite and prehnite.

Feldspar

The examination of feldspar showed that three types of plagioclase exist in sample CM19R-11k. Twenty-one of twenty-seven spectra have high anorthite component with an average of An_{97}. Calcic plagioclase with a lesser amount of anorthite (~An_{82}) has been detected. Another group of plagioclase analyses comprise three spectra obtained from a single albite crystal (~An_7). Plagioclase crystals are generally free of minor elements.

Other phases

The main accessory minerals in sample CM19R-11k are titanite, zircon, and apatite. Titanite crystals are peculiar, because their totals are not close to 100, but mostly closer to 98%. Titanite contains minor amounts of fluorine (~ 0.70 wt%). Aluminium also occurs (~ 3% Al_2O_3) substituting for Ti, in all titanite crystals. Common minor elements in titanite are Fe^{3+}, V and Cr. Eight zircon analyses have been acquired from this sample. Some are pure ($ZrSiO_4$), however Hf (uncertain element due to peak overlap) has been detected (substituting for Zr). In some cases, Fe^{3+} has been detected which can replace Si, as well. Four spectra from two apatite crystals were obtained, indicating that apatite is enriched in F (~ 3 wt% F), thus categorized as fluorapatite.

4.6 Geothermobarometry Calculations (winTWQ)

Five phase equilibrium diagrams have been created using the winTWQ program which indicate the mineral phase equilibrium in the garnet-rich mafic knob, sample CM19R-11k. The diagrams have been created based on the observed mineral assemblage under the petrographic microscope, i.e., garnet, clinopyroxene, zoisite, plagioclase, quartz, and carbonate, and their mineral chemical composition from EDS-analyses. The main aim of these diagrams was to investigate which reactions led to formation of the garnet rims. Therefore, respective EDS analyses have been selected from the garnet rim and adjacent main paragenesis mineral phases: diopside, plagioclase, calcite and zoisite. A second aim was to obtain, if possible, a P–T estimate for the equilibrium between garnet core, zoisite, clinopyroxene, calcite and quartz.

The unknown factor in P–T determination is the proportions between H_2O and CO_2 in the fluid phase. Therefore, four different calculations have been made assuming various proportions (20–80%) of these two fluid species. The calculations were based on a system containing the major chemical components, i.e., SiO_2, Al_2O_3, CaO, FeO, H_2O and CO_2. Also, only one type of Qtz has been selected (a-Qtz) and one type of zoisite (clinozoisite has been excluded). The TWQ calculation yielded 23 chemical reactions which are given in the appendix. Six out of the twenty-three reactions have been selected for the mineral phase equilibria determination. The selected reactions describe grossular-rich garnet formation by zoisite,

calcite, plagioclase and/or clinopyroxene consumption. These reactions were included in the calculation because they correspond to the observed garnet composition (Ca–Al rich garnet). The calculations that involved Mg endmembers of garnet and clinopyroxene were disregarded because of low contents in all constituent minerals other than Cpx. Also, any reaction(s) that could not provide an intersection point to explain grossular formation, was excluded. The results from geothermobarometry calculations are given below (Fig. 36 a-d).

Quartz is absent in sample CM19R-11k. If quartz is excluded from the mineral phases used in winTWQ, the available chemical reactions are dramatically

Fluid phase proportion (H_2O % - CO_2 %)	Pressure (kbar)	Temperature (°C)
75% - 25%	8.2	715
50% - 50%	10.8	800
25% - 75%	13.8	875
20% - 80%	16.5	910

Table 3. Pressure and temperature values for any given fluid phase composition from the intersection of the reactions 2, 14 and 15 in figure 36.

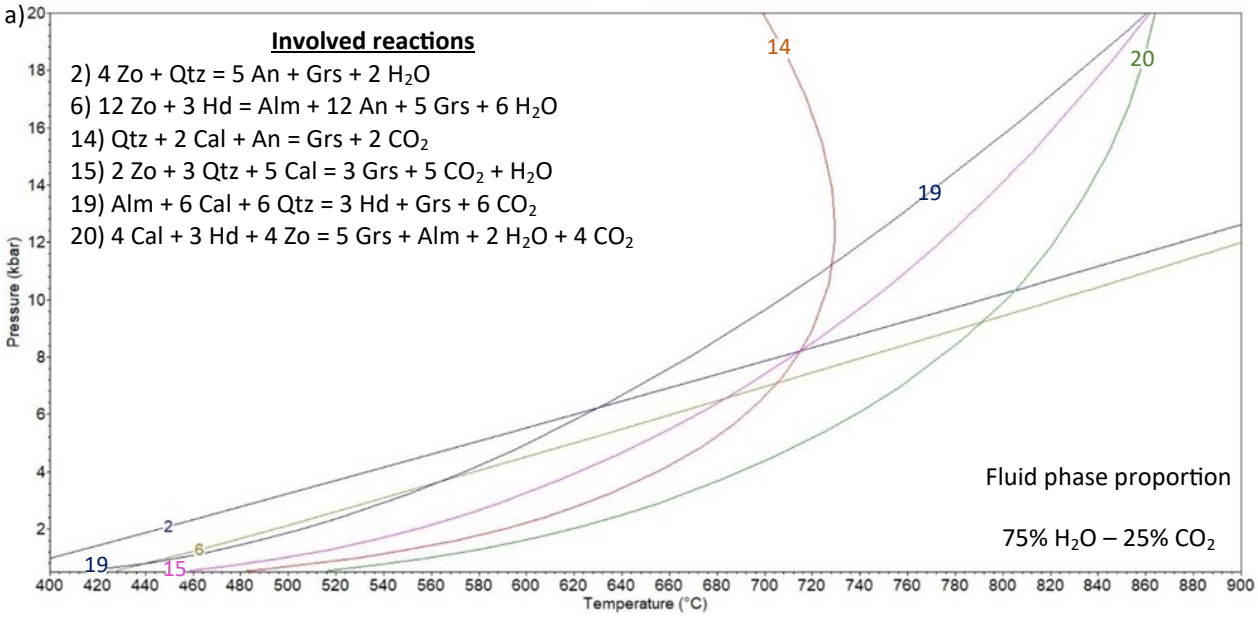

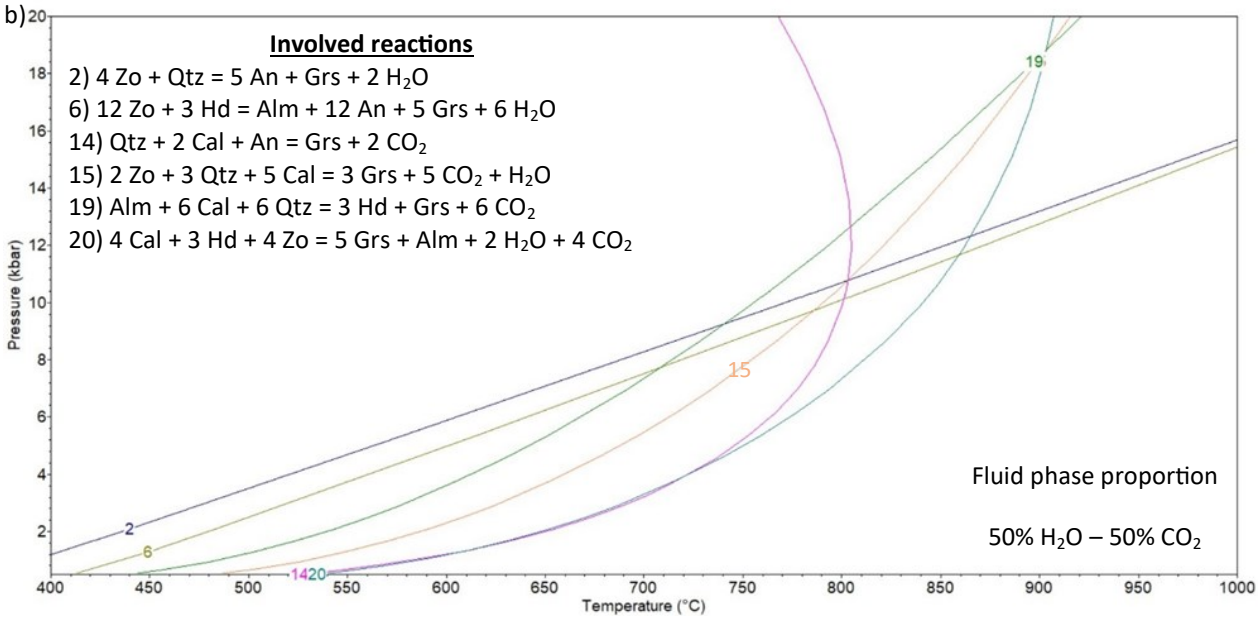

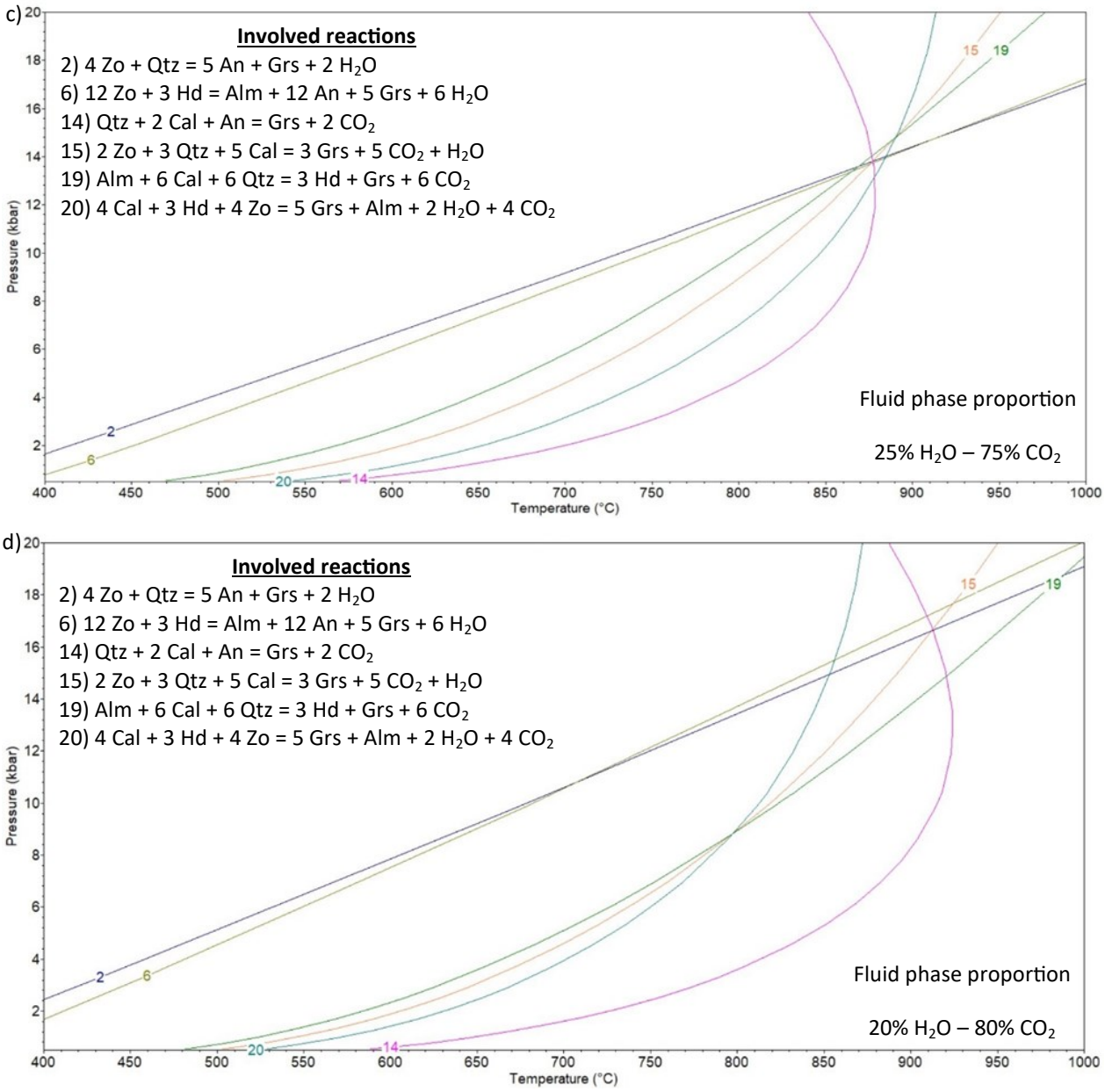

Figure 36. Temperature and pressure equilibrium diagram calculated using TWQ (Berman, 1991), with stable and metastable reactions of minerals in garnet-rich mafic knob in marble-amphibolite contact (sample CM19R-11k). The diagrams have been calculated assuming various CO_2 proportions of the fluid phase. The intersection of the chemical reactions implies that the metamorphic conditions during the formation of garnet rims reached amphibolite to high pressure granulite facies, at conditions indicated in diagram (c).

reduced to lower than 10, and an intersection point of the reactions does not occur. Therefore, it has been assumed that quartz was part of the main mineral assemblage until consumed by the reactions.

An intersection between the reactions 2, 14 and 15 has been observed in every diagram, suggesting a possible mineral phase equilibrium in sample CM19R-11k. Every reaction produces grossular-rich garnet and volatiles (H_2O and/or CO_2), while zoisite, quartz, calcite and/or anorthite are consumed. The intersection point between these three reactions changes in response to the fluid phase composition. The diagrams show that a fluid phase containing 75% CO_2 results in a well-defined intersection of reactions (Fig. 36c). Lower proportions of CO_2 (20 and 50%, respectively) result in poorly defined intersections (Fig. 36a, 36b), which are away from each other and very high CO_2 proportion (80%) in the fluid phase yield very high P–T values (Fig. 36d). The P–T values from every diagram are given in the table 3 below.

Reactions 4.1, 4.2 and 4.3 (below) have been calculated by the winTWQ software. Reaction 4.1 explains that grossular-rich garnet can be formed by consumption of zoisite, quartz and calcite. Assuming that the sample CM19R-11k had quartz in the main assemblage, then reaction 4.1 is one of the predominant grossular formation processes.

$$2\ Ca_2Al_3Si_3O_{12}(OH) + 3\ SiO_2 + 5\ CaCO_3 \rightarrow 3\ Ca_3Al_2Si_3O_{12} + 5\ CO_2 + H_2O \quad (4.1)$$

2 zoisite + 3 quartz + 5 calcite → 3 grossular + 5 carbon dioxide + water

Grossular-rich garnet is favoured by the consumption of calcic plagioclase, too. Reaction 4.2 describes another possible reaction, where grossular is formed at the expense of quartz, calcite and anorthite:

$SiO_2 + 2\ CaCO_3 + CaAl_2Si_2O_8 \rightarrow Ca_3Al_2Si_3O_{12} + 2\ CO_2$ (4.2)

quartz + 2 calcite + anorthite → grossular + 2 carbon dioxide

The third reaction (4.3) that intersects reactions 4.1 and 4.2 in figure 36 is a quartz and zoisite consuming reaction which produces anorthite, grossular and water.

$4\ Ca_2Al_3Si_3O_{12}(OH) + SiO_2 \rightarrow 5\ CaAl_2Si_2O_8 + Ca_3Al_2Si_3O_{12} + 2\ H_2O$ (4.3)

4 zoisite + quartz → 5 anorthite + grossular + 2 water

The P-T mineral equilibrium diagrams above (Fig. 36 a-d), involve rich-in-grossular garnet rims. The diagram in Figure 36c yields the best intersection of reactions using these grossular-rich compositions and is suggested to indicate the P–T conditions for this reaction.

To achieve a better understanding of the metamorphic conditions prior to this reaction, a calculation was made involving data from the garnet core which has lower grossular content. Figure 37 contains the same intersection point as in the diagrams in Figure 36. The intersection point using the garnet core composition is around 800°C and 12.5 kbar, slightly lower than the intersection point of the rims.

5 Petrological interpretation

5.1 Marbles

The marbles in the study area are dominated by carbonate minerals, but also contain siliceous minerals. The variation in parageneses observed is a function of the bulk compositions: dolomite-free protoliths form calcite marbles mainly associated with quartz and silicate minerals of detrital origin, while marbles originating from dolomite-rich protoliths interlayered with siliceous layers contain both dolomite and calcite but also siliceous minerals that are indicative of the metamorphic grade.

The white marbles from Allmenningen that have been examined in this study are typically dominated by diopside. Other important silicate minerals in the marbles are scapolite, amphibole, mica (mainly phengite and phlogopite), epidote/zoisite and titanite. Diopside in marble suggest that the rocks have been metamorphosed at high P–T conditions (Fig. 38; Bucher & Grapes 2011). Forsterite or wollastonite have not been found in these rocks, thus the metamorphic conditions did not reach ultrahigh temperature (UHT) conditions.

The textures suggest that the rocks equilibrated at the peak metamorphic conditions. However, during the retrograde path these rocks have followed, there were local replacements, e.g., of clinopyroxenes by tremolite, actinolite, ferro-pargasite or hornblende. Late fluid phase influx has formed talc inside the crevices of diopside crystals and the tremolite pseudomorphs. The fact that diopside, tremolite, and talc are present at the same time in the white marble (sample CM16R-09f1), can be explained by the rapid uplift that occurred in the general area of Roan during the retrogressive metamorphic path (Möller 1988), and also set the post-orogenic metamorphic conditions at low P and T. Another factor could be water influx during retrogression. More water in the metamorphic

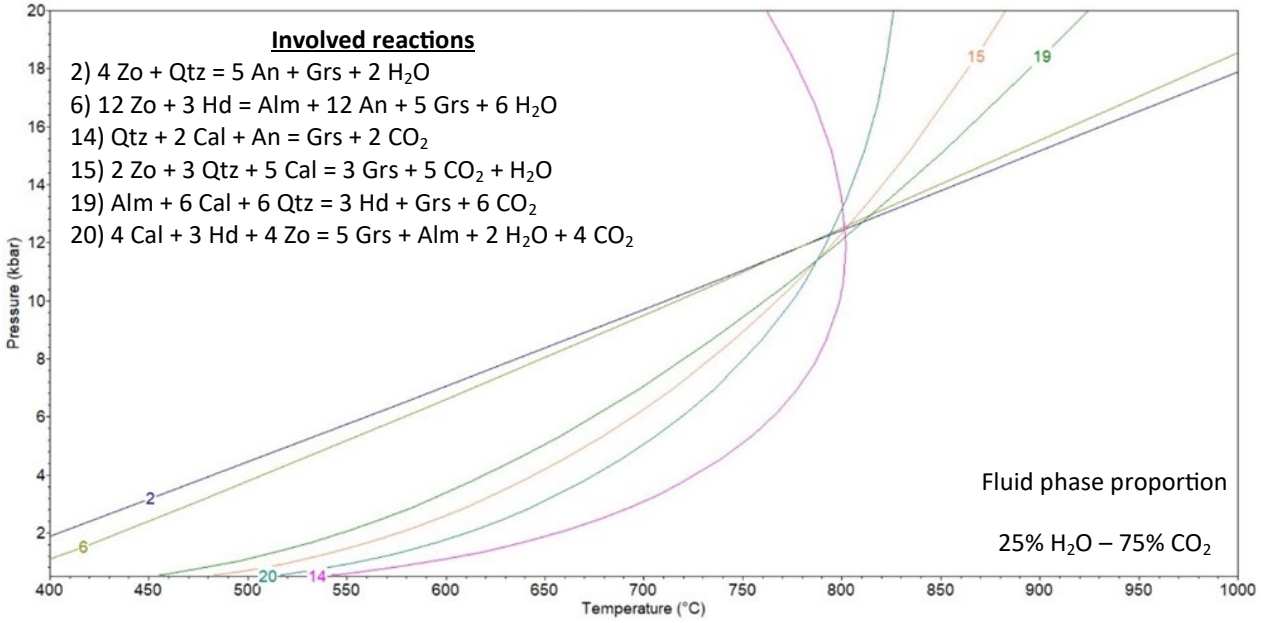

Figure 37. Temperature and pressure equilibrium diagram calculated using TWQ (Berman, 1991), with stable and metastable reactions of minerals in garnet-rich mafic knob in marble-amphibolite contact (sample CM19R-11k). Grossular analyses for this diagram have been selected from porphyroblast cores.

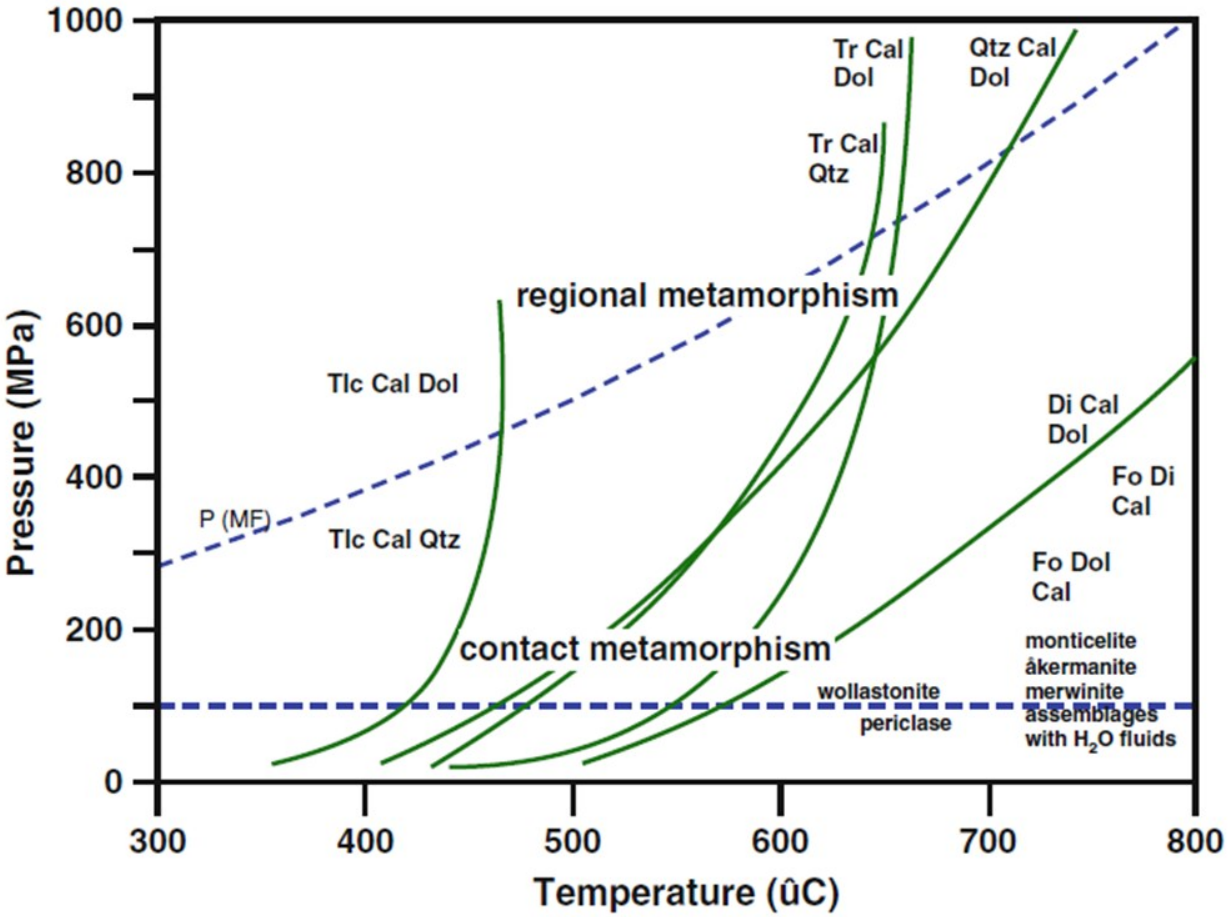

Figure 38. Mineral isograds from calc-silicate rocks projected on a P–T plot by Bucher & Grapes 2011. The stippled lines represent the metamorphic gradient for the respective type of metamorphism.

system could drive in the increase of the stability field of hydrous minerals like tremolite and talc resulting in the coexistence of these minerals in a wide P–T field. Of the three minerals only diopside is in equilibrium during peak metamorphism.

5.2 Calc-Silicates

The calc-silicate rocks from Allmenningen are the most peculiar in terms of mineralogy. Generally, the main paragenesis contain carbonates, diopside, garnet, phlogopite, amphibole, scapolite and titanite. As described above, the bulk composition plays a major role in the final assemblage. These rocks are interlayered with marbles, while mafic pods are found in their layers. Thus, Ca-rich minerals are formed, and Ca-rich endmembers of the siliceous minerals are observed. For instance, in most of the calc-silicates scapolite crystals occur, while in the most Mg-Fe-rich varieties garnet can also form.

Diopside is the mineral that occurs in all calc-silicate rocks examined. In most of the samples, diopside can coexist with amphibole. Amphibole can also form pseudomorphs after diopside, but single crystals have also been observed in the thin sections. Moreover, some calc-silicate rocks have granoblastic texture with polygonal crystals and distinctive mineral grain boundaries characteristic for granulite facies metamorphism.

The above observations with the equilibrium in the peak P-T metamorphic conditions suggest that this set of rocks have been metamorphosed in high-pressure granulite facies. The observed assemblages include garnet porphyroblasts (only in sample CM16R-03b1; Fig. 15), diopside (sometimes porphyroblastic, too), amphibole (only in sample CM19R-11b; Fig. 19) and scapolite. Mineral assemblages' observation from the photomicrographs suggest equilibrium of these mineral phases. Zoisite drop-shaped inclusions in garnet porphyroblasts suggest prograde garnet formation with zoisite consumption. The fact that dehydration reactions occur along with low amounts of amphibole and high amounts of diopside in the mineral paragenesis, suggest a transformation of amphibole to diopside. However, the signs of tremolite pseudomorphs strengthen the theory of retrogression of these rocks in a rapid tempo. That is because diopside and tremolite both occur in some samples in the form of partial and/or complete pseudomorphs. The pseudomorphs suggest disequilibrium; in the calc-silicate rocks, diopside equilibrated in peak metamorphism while tremolite formed later. The composition of scapolite and associated plagioclase crystals support equilibrium at high P-T conditions because of their calcic compositions (cp. Teertstra & Sherriff 1997). Post-metamorphic hydrothermal fluid influx partially altered the calcic plagioclase into

prehnite and sericite.

5.3 Mafic Rocks

The investigated samples of mafic rocks from Allmenningen are from mafic pods inside the marbles and calc-silicates. Both their microscopical and macroscopical characteristics (Fig. 22-29) are very close to those of mafic granulites. The mineral assemblages contain garnet, diopside, amphibole (only in sample CM16R-03e2), plagioclase and zoisite. In these mafic rocks, diopside appears almost in every site, while amphibole either is absent from some samples, or its proportion is very low compared to diopside appearance. Zoisite is stable in granulite facies temperatures in the mafic rocks due to bulk composition of the rocks. Usually, in mafic granulites, a small amount of water is incorporated in biotite. However, in the studied granulites, Mg and Fe form diopside and garnet, while Ca and Al are still in excess from grossular formation. The depletion in Mg and Fe means that phlogopite cannot be formed, while the excess in Ca and Al favour zoisite as the main water-bearing mineral phase. Scapolite is absent while carbonate minerals may occur in some rocks. The proportion of these minerals is low due to bulk composition.

The mineral pair that occur in every mafic rock sample is garnet and diopside. Plagioclase can be observed as well in three of four samples examined. These three minerals are characteristic of mafic high-pressure granulites regarding bulk composition and metamorphic P–T conditions. The texture of these rocks presents polygonal crystals and triple points, also typical of granulite facies metamorphism. Actinolite and/or tremolite occurs as pseudomorphs after diopside.

High anorthite component in plagioclase of the mafic rocks, suggest high temperature during peak metamorphism. During the retrograde path, actinolite pseudomorphs after diopside support partial disequilibrium in the mafic rocks. Specifically, in the Grt-rich mafic knob (sample CM19R-11k), fine-grained prehnite and muscovite (sericite) are indicative minerals of very low-grade, probably post-orogenic, alteration.

Four generations of minerals, in the three different rock types, have been distinguished and correspond to stages of the metamorphic P–T path. (1) During prograde metamorphism and equilibrium at peak metamorphic conditions, garnet, diopside, and scapolite formed. To this generation belong also calcic plagioclase, zoisite, phlogopite (in certain samples), titanite and recrystallized carbonate and/or quartz crystals. (2) Early amphibolitization, with partial replacement (pseudomorphs) of clinopyroxene by hornblende. (3) During late stages of the retrograde path, at greenschist-facies conditions, partial amphibolitization in the mafic rocks and the impure siliceous diopsidic marbles, caused the complete or partial replacement of high-pressure anhydrous minerals (diopside, garnet). The produced metamorphic minerals are amphibole (tremolite and/or actinolite) and chlorite, respectively. (4) Lastly, late influx of hydrothermal fluids led to low-grade mineral formation such as talc after Mg-rich minerals. Sericitization took place on plagioclase while prehnite also formed during that time.

6 Discussion

6.1 Petrography and chemical reactions

6.1.1 Marbles

Marble varieties in the study area are rich in diopside. Generally, during prograde metamorphism of carbonate rocks, diopside forms by tremolite consumption when the metamorphic conditions reach high enough temperature to enter the so-called “diopside zone” (Winter 2014). In a continental collision metamorphic gradient, the diopside zone starts at ca. 650°C, at pressure of 7 kbar (Bucher & Grapes 2011; Fig. 38).

Following a continental collision gradient, the diopside zone in marbles follows after the talc (first) and tremolite (second) zones, which correspond to low -grade (< 450°C, 4-5 kbar) and medium-grade metamorphism (< 600°C, ~7 kbar), respectively (Bucher & Grapes 2011; Fig. 38). It is suggested that the temperature during prograde-to-peak metamorphism of the calc-silicate rocks in Allmenningen reached at least 620°C and pressure more than 10 kbar. The “diopside-in” reaction in impure and siliceous dolostones has been described by Bowen (1940):

$$Ca_2Mg_5Si_8O_{22}(OH)_2 + 2\ SiO_2 + 3\ CaCO_3 \rightarrow 5\ CaMgSi_2O_6 + 3\ CO_2 + H_2O \quad (6.1)$$

tremolite + 2 quartz + 3 calcite → 5 diopside + 3 carbon dioxide + water

This is likely the case also for the studied rocks because the phases that have been recorded are diopside and calcite and/or dolomite, not quartz. Hence it is suggested that the protoliths of the respective rocks were originally rich in quartz dolostones and the order of the minerals formed may have been talc → tremolite → diopside.

Following the metamorphic gradient in Fig 38 the next diopside-forming reaction by quartz consumption is the reaction 6.2:

$$CaMg(CO_3)_2 + 2\ SiO_2 \rightarrow CaMgSi_2O_6 + 2\ CO_2 \quad (6.2)$$

dolomite + 2 quartz → diopside + 2 carbon dioxide

However, this scenario is very rare to happen because quartz was depleted by the reaction 6.1. Continued quartz consumption by reaction 6.1 during regional (orogenic) metamorphism leads to a new diopside formation reaction that has been described by Bucher and Grapes (2011):

$$3\ CaCO_3 + Ca_2Mg_5Si_8O_{22}(OH)_2 \rightarrow CaMg(CO_3)_2 + 4\ CaMgSi_2O_6 + H_2O + CO_2 \quad (6.3)$$

3 calcite + tremolite → dolomite + 4 diopside + water + carbon dioxide

Reaction 6.3 can explain diopside formation after

depletion of quartz right next to reaction 6.1 (Bucher & Grapes 2011; Fig. 38). Reactions 6.1 and 6.3 formed main-paragenesis diopside in prograde to peak metamorphic conditions. In the studied rocks, the diopside zone is probably between the isograds of reactions 6.1 and 6.3.

6.1.2 Calc-Silicates

Calc-silicate metamorphic rock systems are difficult to handle due to bulk compositional complexity (many chemical components) which strongly affects the equilibrated metamorphic mineral paragenesis. Calc-silicate rocks from Allmenningen are rich in diopside, amphibole, scapolite, titanite and calcite and/or dolomite. Some of the samples also contain amounts of phlogopite. Compared to the marbles, the calc-silicate rocks originally contained larger quantities of silicate minerals. The protoliths of these rocks represent calcite and/or dolomite marbles with various silicate-rich intercalations of clays, sands or mafic rocks. The studied calc-silicate rocks contain centimetre-long silicate layers. The dolomitic material reacted with the silica during metamorphism, hence the observed Ca-Mg minerals (diopside, amphibole) were created. In the calc-silicate rocks, diopside formed most likely from the reaction 6.1 or 6.3.

Since these rocks are not entirely characterized as marbles, the terms describing the index zone minerals (talc, tremolite, diopside, forsterite, periclase), are not completely applicable when it comes to metamorphic grade description. However, the calc-silicates were metamorphosed at P–T conditions similar to the marbles.

The calc-silicate rocks are also rich in scapolite. According to Goldsmith and Newton (1977) and Aitken (1983), the reaction which explains the equilibrium between plagioclase and meionitic (Ca-rich) scapolite is:

$$3\ CaAl_2Si_2O_8 + CaCO_3 \rightarrow Ca_4Al_6Si_6O_{24}CO_3 \qquad (6.4)$$

3 plagioclase (anorthite) + calcite → scapolite (meionite)

Reaction 6.4 describes scapolite formation in response to temperature increase, especially in upper granulite and upper amphibolite facies metamorphism (Aitken 1983). Aitken also stated that this reaction is pressure independent, whilst it is controlled exclusively by temperature and the P_{CO2} in the system. Reaction 6.4 is also called the *scapolitization reaction*, where the plagioclase minerals in a rock, are progressively turning into scapolite. The minimum temperature for reaction 6.4 to equilibrate is 525°C, and the concentration of CO_2 in the system must be higher than 13 moles %. Goldsmith and Newton (1977) proved that the mineral paragenesis of plagioclase and calcite is replaced by scapolite with increasing temperature. Pure meionite can be stable in a system with calcite only at temperatures > 875°C. Reaction 6.4 can explain plagioclase deficiency in the calc-silicate rocks of Allmenningen. Meionitic scapolite temperature stability field coincides with the peak metamorphic conditions (~ 860°C, 14.2 kbar) of the ESU, as calculated by Möller (1990).

During the retrograde metamorphic path, the calc-silicate rocks were also affected by local low-grade alterations. Amphibole formed as pseudomorphs after pyroxene and chlorite is locally replacing garnet. These two minerals and their associated appearance prove partial disequilibrium in these rocks and provide evidence of retrograde metamorphism.

Fine-grained amphibole intergrowths after diopside in calc-silicate rocks consist of tremolite. Hence, reaction (6.5) is suggested for this partial replacement:

$$CaMgSi_2O_6 + H_2O \rightarrow Ca_2Mg_5Si_8O_{22}(OH)_2 \qquad (6.5)$$

diopside + water → tremolite

6.1.3 Mafic Rocks

Mafic rocks on the island of Allmenningen contain mainly Ca-Fe-rich garnet, diopside, plagioclase, zoisite, amphibole and titanite, and can be characterized as mafic granulites. The grains are occasionally porphyroblasts, but the texture is mainly granoblastic. In this type of rocks, garnet is formed through a series of reactions during prograde metamorphism and temperature increase. As temperature rises, dehydration reactions take place (Winter 2014). For instance, when a rock is subject to changing conditions from the amphibolite-facies to the eclogite- or granulite-facies, a common reaction is the dehydration of amphibole and formation of clinopyroxene. It is suggested that diopside in mafic rocks has been created by reactions that consumed amphibole.

The major difference between the calc-silicate and the mafic rocks of the study area is the absence of scapolite in the latter. Scapolite is a common mineral in mafic granulites and can be formed only under specific circumstances, which are related to the protolith's bulk composition and/or the composition of the fluid phase.

The textural relations suggest that the occurrence of actinolite and/or tremolite amphibole in the mafic rocks is connected to retrogression. In the garnet-bearing knob in calc-silicate (sample CM19R-11i2), amphibole is not part of the main mineral paragenesis and also replaces diopside inclusions in garnet. In the garnet-rich mafic granulite (sample CM16R-03e2), actinolite occurs in pseudomorphs after clinopyroxene. On the other hand, in the same sample there is textural evidence that ferro-pargasite amphibole coexisted and equilibrated with clinopyroxene in the main mineral assemblage during peak metamorphism. Rhombohedral, euhedral amphibole crystals support this speculation (Fig. 23a, 23c). Ferro-pargasite is more abundant than actinolite in this sample.

Zoisite in these rocks is part of the main mineral assemblage. A rock can have mixed fluid components (e.g. H_2O and CO_2), hence both hydrous and carbonate minerals can equilibrate together and stabilize even at high-grade metamorphism. If we assume that the system was closed, the fluid composition was internally buffered by the mineral assemblage and the hydrous and carbonate mineral phases can coexist with anhydrous minerals. Before the peak metamorphism, dehydration and/or decarbonation reactions occur but, since the system is closed, thereafter the fluid

composition remains the same.

Tremolite and/or actinolite and chlorite locally replace diopside and garnet, respectively. This could suggest partial reequilibration of the rocks during retrograde greenschist-facies metamorphism and hydrous fluid influx. These minerals have retrograde origin, meaning that they are not in equilibrium with the peak-metamorphic assemblage of garnet, diopside etc.

6.2 The garnet rim of sample CM19R-11k

The sample CM19R-11k is unique with respect to that garnet forms rims around the other minerals (Cpx, Zoi, Cal, and Plag). The main mineral assemblage in this rock is grossular, clinopyroxene, anorthitic plagioclase, zoisite and calcite (+ titanite). In this study, garnet analyses have been obtained both from the garnet rims and the larger grains, showing that garnet cores are richer in almandine component and poorer in grossular component than the garnet rims. The garnet rims are everywhere grossular-dominated and not chemically affected by the adjacent mineral species that they surround. This observation suggests that the garnet cores were initially formed during prograde to peak metamorphism, consuming calcite, zoisite and plagioclase. As shown by the TWQ calculations (Fig. 36, 37), the garnet rims were probably formed later by zoisite, calcite and plagioclase consumption. Therefore, it is suggested that the garnet rim was created by heating and devolatilization.

In calc-silicate systems, calcite can provide Ca for garnet formation during temperature increase, thus leading to gradual decarbonation of the rock (Groppo et al. 2013). Grossular formation is favoured by temperature increase; thus, in these reactions grossular is located towards the high temperature part of the equilibrium (op cit.). In the case of Allmenningen, zoisite and calcite are the main mineral phases which contribute to grossular formation by devolatilization (reactions 4.1, 4.2, 4.3). Another calcic mineral which could contribute in grossular formation in calc-silicate metamorphic systems is diopside (Groppo et al. 2013). However, in the case of sample CM19R-11k, diopside is a reactant which provides iron (almandine) to the garnet rather than calcium (grossular).

Reaction 4.1, that consumes zoisite, quartz and calcite, is suggested as the most plausible reaction for the formation of grossular-rich rims in the Grt-rich mafic knob (sample CM19R-11k). In calc-silicate systems, quartz is necessary for the formation of many silicate minerals i.e., clinopyroxene, garnet, amphibole, scapolite and micas. Quartz is absent in sample CM19R-11k. Hence, it is suggested that quartz was once part of the main mineral assemblage but was consumed by a final grossular-producing reaction.

Anorthitic plagioclase is a main mineral phase in sample CM19R-11k, stable at high temperature during metamorphism. Prehnite and sericite alteration sites are abundant in the plagioclase crystals. Sericite and prehnite were formed at the expense of anorthite due to low-grade alteration in response to influx of hydrous fluid.

Figures 36 and 37 summarize the main chemical equilibria in sample CM19R-11k. These diagrams show intersections of univariant reactions at generally high temperature and pressure (> 700°C, > 8 kbar); some reactions are pressure-dependent (e.g., straight lines 2 and 6). It is assumed that the common intersection point represents the mineral equilibria in sample CM19R-11k including reactions 4.1, 4.2 and 4.3 (lines 2, 14, 15). In these reactions, grossular is a product on the high-temperature (HT) side of lines. Therefore, it is suggested that the grossular-rich garnet rim in sample CM19R-11k, has been formed during near-isobaric heating. Therefore, the system moved to the right sector of these curves passing by the common equilibrium point. The curve of reaction 4.2 (line 14) excludes the scenario of isothermal decompression, because in that case grossular decomposition takes place. This is derived from figure 36c, because in that occasion the system would move from the high-temperature domain of reaction 4.2 towards the low-pressure domain. In the Grt-rich mafic knob, garnet decomposition has not been observed, hence the garnet rims do not contain symplectites, which indicate retrogressive origin.

An estimation on the pressure and temperature conditions can be derived from the plot (Fig. 36). The accepted equilibrium is the intersection of reactions 4.1, 4.2 and 4.3 (lines 2, 14, 15). The initial estimation of peak metamorphism in Roan has been calculated at approximately 870°C and 14.5 kbar (Johansson & Möller 1986; Möller 1988, 1990). These values agree very well with the calculated values on the table 3 above (870°C – 13.8 kbar), assuming a fluid phase composition of 25% H_2O and 75% CO_2 (Fig. 36c). The other calculations are considered less valid because 1) they are not concordant with granulite facies pressure and temperature and 2) they present a larger spread between the intersection points, compared to Fig 36c and 37. Further confirmation on the fluid phase composition comes from the scapolite analytical data from adjacent rock formations that present high values of XCO_2. Based on new observations, pressure in Roan may have reached slightly higher values than 14.5 kbar. However, the general absence of coesite indicates that the peak pressure did not reach UHP conditions (Charlotte Möller, personal communication, June 2020).

6.3 The fluorine presence in ESU and fluid phase characterization

During SEM study of the samples, several spectra suggest the presence of fluorine in several minerals. Generally, the seeking of fluorine-bearing minerals in marbles is encouraged when these rocks are studied under SEM-EDS or electron microprobe (Bucher & Grapes 2011). Fluorine is a halogen element which can be dissolved in a CO_2 and H_2O mixed fluid phase. Elements like fluorine (Cl, Br, etc.) and alkali-metals (Na, K, etc.) are mobile when dissolved and can be transported easily in the metamorphic system by the fluid's phase activity (Winter 2014).

Apatite is the predominant phosphate accessory mineral and is very common in the studied rocks, as it

binds most of the P_2O_5 during metamorphism (Hughes & Rakovan 2015). Apatite usually contains some fluorine. The highest amounts of fluorine in apatite were found in the pink marble (sample CM16R-09c) and the Grt-rich mafic knob (sample CM19R-11k). The presence of fluorine in apatite and other minerals (e.g. phlogopite, amphibole) suggests an enrichment of this element in the fluid phase. Some of the apatite crystals contain lesser amount of chlorine, too.

The above observations suggest that the fluid phase in marbles and calc-silicates was a mixture of H_2O and CO_2 with changing proportions depending on the metamorphic reactions (e.g., Bucher & Grapes 2011), however their proportion in unknown. The reactions during the initial metamorphic stage produce hydrous minerals, consuming the intergranular water between the mineral grains and porous of the protolith (Bucher & Grapes 2011; Winter 2014). Thus, water is depleted from the free fluid phase and the latter is slightly enriched in CO_2. At the middle stages of metamorphism, the reactions in calc-silicate systems are getting more complicated. The majority of the reactions cause devolatilization and produce either CO_2, or H_2O, or both types of fluids. As a result, the contribution of these molecules to the fluid phase is difficult to calculate due to the complexity of the reactions and bulk composition of these rocks.

Figure 36c above proves that the proportion of the fluid phase in sample CM19R-11k at the time of peak metamorphism was 3:1 CO_2:H_2O. The predominant mechanism that adjusts the concentration of CO_2 in the fluid phase is calcite decomposition during heating. Furthermore, because ESU was a closed metamorphic system, the decomposition of calcite constantly buffers internally the XCO_2. The fluid phase in the studied rocks is CO_2 dominant, but not that high as has been calculated from scapolite analyses (cp. Fig. 34).

6.4 The effect of metamorphism of calcareous rocks on the CO_2 budget in the atmosphere

The metamorphic reactions in calc-silicate rocks release CO_2 gas that can contribute to the total amount of CO_2 in the atmosphere (Bucher & Grapes 2011; Groppo et al. 2013 and references therein). The geological environment that can produce the most CO_2 are large metamorphic provinces composed of calc-silicate rocks and impure marbles (Groppo et al. 2013). The metamorphic conditions for degassing include continental collisional zones with relatively high temperatures (op. cit.). The major minerals that produce CO_2 are calcite, dolomite and meionitic scapolite. Decarbonation occurs in granulite-facies terrains where marbles and calc-silicate rocks consist of wollastonite, grossular-rich garnet and scapolite (Groppo et al. 2013 and references therein).

In the calc-silicate rocks from Allmenningen there is no record of wollastonite-bearing rocks. Wollastonite is more common in contact metamorphism environments, including skarns and contact aureoles between igneous bodies and calc-silicate or impure marble layers (Bucher & Grapes 2011).

Taking into consideration the TWQ calculations (Fig. 36) and the work of Groppo et al (2013), it is assumed that the garnet corona-forming reactions were associated with CO_2 and/or H_2O production, during simultaneous breakdown of calcite and/or zoisite. The main diopside-forming reactions in marbles and calc-silicate rocks are 6.1 and 6.3, which also produce CO_2 and H_2O.

Finally, one can conclude that, in every calcareous rock at Allmenningen, reactions took place which produced a significant amount of CO_2. These rocks though, cannot hold all this fluid phase, so the release was probably happening continuously during prograde metamorphism. However, there is no evidence that the produced CO_2 from orogenic metamorphism of calcareous rocks can cause global warming, but definitely can be considered as a main factor that potentially could lead to climate change along with volcanic eruptions, ice cap melting etc.

7 Conclusions

- The main mineral assemblage in the marbles is Cal + Dol + Di + Scp + Phl + Am + Ttn ± Ep ± Qtz.

- The main mineral assemblage in the calc-silicate rocks is Cal + Dol + Di + Scp + Phl + Am + Grt + Ttn ± Qtz.

- The main mineral assemblage in the mafic rocks is Grt + Cpx + Pl + Zo + Am + Cal + Ttn.

- Retrograde minerals which are not in equilibrium with the main assemblage are tremolite, actinolite, chlorite, prehnite and sericite.

- P–T calculation using mineral equilibria from sample CM19R-11k yield ca. 875°C and 13.8 kbar.

- At these conditions, the fluid phase was composed of 75% CO_2 and 25% H_2O.

- The grossular-rich garnet rim in sample CM19R-11k was formed during heating and devolatilization. The main reactants are calcite, zoisite and plagioclase.

- The fluid phase contained dissolved elements, mainly halogens F and Cl.

- The main CO_2-producing processes are grossular and diopside formation reactions.

- The emitted CO_2 from the decarbonation during metamorphism can contribute to global warming along with other natural phenomena.

Acknowledgements

I would like to thank my supervisor, Charlotte Möller, who entrusted me this project and for her unflagging support and help throughout this thesis work. We went through a plethora of discussions both via email and in her office about this project and the challenges that arose during this work. The result was definitely above expectations and very edifying for me. I would also

want to thank my parents for their valuable support. If it weren't for them, I would not be able to write this work or even more just think of studying abroad and experience how life is outside of my country. Special thanks go to my colleague, Maria Eleni Taxopoulou for her constant encouragement during my work, countless discussions and advice about geological aspects in my project and important assistance regarding manuscript review. Lastly, I would like to thank the Associate Professor in the geology department of Aristotle University of Thessaloniki (A.U.Th.), Lambrini Papadopoulou, and my beloved colleague, Prodromos Nikolaidis, for their valuable advice about SEM-EDS observations. Special thanks go to my colleague Dino Leopardi, for his important help regarding apatite anion stoichiometry. I also send my gratitude to Mr. Tom Heldal from the Geological Survey of Norway (NGU) for using his photos of the Nidaros cathedral in Trondheim. This work is dedicated to my beloved father who sadly passed away by COVID-19.

References

Aitken, B. G., 1983: T-XCO2 stability relations and phase equilibria of a calcic carbonate scapolite. *Geochimica et Cosmochimica Acta*, *47*(3), 351-362.

Berman, R. G., 1991: Thermobarometry using multi-equilibrium calculations; a new technique, with petrological applications. *The Canadian Mineralogist, 29*(4), 833-855.

Birkeland, T., 1958: Geological and petrological investigations in northern Trøndelag, western Norway. *Nor. Geol. Tidsskr, 38*, 328-420.

Bowen, N. L., 1940: Progressive metamorphism of siliceous limestone and dolomite. *The Journal of Geology*, *48*(3), 225-274.

Brady, J. and Perkins, D., 2007: Mineral formulae recalculation. Excel spreadsheet acquired from: https://serc.carleton.edu/research_education/equilibria/mineralformulaerecalculation.html

Brueckner, H. K., 2018: The great eclogite debate of the Western Gneiss Region, Norwegian Caledonides: The in situ crustal v. exotic mantle origin controversy. *Journal of metamorphic geology. 36*(5), 517-527.

Brunsmann, A., Franz, G., Erzinger, J. & Landwehr, D., 2000: Zoisite-and clinozoisite-segregations in metabasites (Tauern Window, Austria) as evidence for high-pressure fluid-rock interaction. *Journal of Metamorphic Geology, 18(1),* 1-22.

Bucher, K. and Grapes, R., 2011: Petrogenesis of metamorphic rocks: Springer Science & Business Media.

Cuthbert, S. J., Harvey, M. A. & Carswell, D. A., 1983: A tectonic model for the metamorphic evolution of the Basal Gneiss Complex, Western South Norway. *Journal of Metamorphic Geology, 1(1),* 63-90.

Cuthbert, S. J., Carswell, D. A., Krogh-Ravna, E. J. & Wain, A., 2000: Eclogites and eclogites in the Western Gneiss region, Norwegian Caledonides. *Lithos, 52(1-4),* 165-195.

Dallmeyer, R. D., Johansson, L. & Möller, C., 1992: Chronology of Caledonian high-pressure granulite-facies metamorphism, uplift, and deformation within northern parts of the Western Gneiss Region, Norway. *Geological Society of America Bulletin, 104(4),* 444-455.

Droop, G. T. R., 1987: A general equation for estimating Fe 3+ concentrations in ferromagnesian silicates and oxides from microprobe analyses, using stoichiometric criteria. *Mineralogical magazine*, *51*(361), 431-435.

Egerton, R. F., 2005: Physical principles of electron microscopy (Vol. 56). New York: Springer.

Ellis, D. J. and Green, D. H., 1979: An experimental study of the effect of Ca upon garnet-clinopyroxene Fe-Mg exchange equilibria. *Contributions to Mineralogy and Petrology, 71 (1),* 13-22.

Engvik, A. K., Willemoes-Wissing, B., & Lutro, O., 2018: High-temperature, decompressional equilibration of the eclogite facies orogenic root (Western Gneiss Region, Norway). *Journal of Metamorphic Geology, 36(5),* 529-545.

Eskola, P., 1921: On the eclogites of Norway (No. 8). Рипол Классик.

Evans, B. W., Shaw, D. M. & Haughton, D. R., 1969: Scapolite stoichiometry. *Contributions to Mineralogy and Petrology, 24,* 293-305.

Gee, D.G., Kurnpulainen, R., Roberts, D., Stephens, M.B., Thon, A. & Zachrisson, E., 1985: Scandinavian Caledonides: Tectonostatigraphic Map. In: Gee, D.G. and Sturt, B.A., (ecs.) *The Caledonide Orogen: Scandinavia and Related Areas. John Wiley & Sons Chichester.* 843-857.

Gee, D. G., Fossen, H., Henriksen, N. & Higgins, A. K., 2008: From the early Paleozoic platforms of Baltica and Laurentia to the Caledonide Orogen of Scandinavia and Greenland. *Episodes, 31(1),* 44-51.

Grew, E. S., Locock, A. J., Mills, S. J., Galuskina, I. O., Galuskin, E. V. & Hålenius, U., 2013: Nomenclature of the garnet supergroup. *American Mineralogist, 98(4),* 785-811.

Goldsmith, J. R. and Newton, R. C., 1977: Scapolite-plagioclase stability relations at high pressures and temperatures in the system NaAlSi3O8-CaAl2Si2O8-CaCO3-CaSO4. *American Mineralogist, 62(11-12),* 1063-1081.

Gordon, S. M., Whitney, D. L., Teyssier, C., Fossen, H. & Kylander-Clark, A., 2016: Geochronology and geochemistry of zircon from the northern Western Gneiss Region: Insights into the Caledonian tectonic history of western Norway. *Lithos, 246,* 134-148.

Griffin, W. L., Austrheim, H., Brastad, K., Bryhni, I., Krill, A.G., Krogh, E.J., Mørk, M.B.E., Qvale, H. & Tørudbakken, B., 1985: High-pressure metamorphism in the Scandinavian Caledonides. In: Gee, D.G. and Sturt, B.A. (eds.). *The Caledonide Orogen – Scandinavia and Related Areas.* John Wiley & Sons Chichester, 783-801.

Griffin, W. L. and Brueckner, H. K., 1980: Caledonian Sm–Nd ages and a crustal origin for Norwegian eclogites. *Nature, 285(5763),* 319-321.

Groat, L. A., Hawthorne, F. C. & Ercit, T. S., 1992: The chemistry of vesuvianite. *Canadian Mineralogist, 30(1),* 19-48.

Groppo, C., Rolfo, F., Castelli, D. & Connolly, J. A., 2013: Metamorphic CO 2 production from calc -silicate rocks via garnet-forming reactions in the CFAS–H 2 O–CO 2 system. *Contributions to Mineralogy and Petrology, 166(6),* 1655-1675.

Hacker, B. R., 2006: Pressures and Temperatures of Ultrahigh-Pressure Metamorphism: Implications for UHP Tectonics and H2O in Subducting Slabs. *International Geology Review, 48 (12),* 1053-1066.

Hacker, B. R., Andersen, T. B., Johnston, S., Kylander -Clark, A. R., Peterman, E. M., Walsh, E. O. and Young, D., 2010: High-temperature deformation during continental-margin subduction & exhumation: The ultrahigh-pressure Western Gneiss Region of Norway. *Tectonophysics, 480 (1-4),* 149-171.

Heldal, T., 2012: Nidarosdomen ble bygd i 70 typer stein. Forskning.no, produsert og finansiert av NGU. https://forskning.no/bergfag-geofag/2012/11/nidarosdomen-ble-bygd-i-70-typer-stein

Hughes, J. M. and Rakovan, J. F., 2015: Structurally Robust, Chemically Diverse: Apatite and Apatite Supergroup Minerals. *Elements, 11(3),* 165-170.

Johansson, L., Andreasson, P.G. & Schaberg, H., 1987: An occurrence of the Gula Nappe in the Western Gneiss Region. Central Norwegian Caledonides. *Nor. Geol. Tidsskr. 67*. 85-92.

Johansson, L., 1986: Basement and cover relationships in the Vestranden - Grong-Olden region. Central Scandinavian Caledonides. Unpubl. Ph.D.-thesis. Univ. of Lund, 142 pp.

Johansson, L. and Möller, C., 1986: Formation of sapphirine during retrogression of a basic high-pressure granulite, Roan, Western Gneiss Region, Norway. *Contributions to Mineralogy and Petrology, 94(1),* 29-41.

Ketcham, R. A., 2015: Calculation of stoichiometry from EMP data for apatite and other phases with mixing on monovalent anion sites. *American Mineralogist, 100(7),* 1620-1623.

Kjerulf, T., 1871: Om Trondheims stifts geologi. Nyt. Mag. for Naturv. *Christiania 18,* 1-79.

Krogh, E. J., 1977: Evidence of Precambrian continent –continent collision in Western Norway. *Nature, 267(5606),* 17-19.

Krogh Ravna, E. J., and Terry, M. P., 2004: Geothermobarometry of UHP and HP eclogites and schists–an evaluation of equilibria among garnet–clinopyroxene–kyanite–phengite–coesite/ quartz. *Journal of metamorphic Geology, 22(6),* 579-592.

Krogh, T. E., Mysen, B. O. & Davis, G. L., 1974: A Paleozoic age for the primary minerals of a Norwegian eclogite. *Carnegie Institute Washington Yearbook, 73*, 575-576.

Kullerud, L., Torudbakken, B. O. & Ilebekk, S., 1986: A compilation of radiometric age determinations from the Western Gneiss Region, South Norway. *Bulletin-Norges geologiske undersokelse, (406),* 17-42.

Leake, B. E., Woolley, A. R., Arps, C. E., Birch, W. D., Gilbert, M. C., Grice, J. D., Hawthorne, F. C., Kato, A., Kisch, H. J., Krivovichev, V. G., Linthout, K., Laird, J., Mandarino, J. A., Maresch, W. V., Nickel, E. H., Rock, N. M. S., Schumacher, J. C., Smith, D. C., Stephenson, N. C. N., Ungaretti, L., Whittaker, E. J. W. & Youzhi, G., 1997: Nomenclature of amphiboles; report of the Subcommittee on Amphiboles of the International Mineralogical Association Commission on new minerals and mineral names. *Mineralogical magazine, 61(405),* 295-310.

Locock, A. J., 2014: An Excel spreadsheet to classify chemical analyses of amphiboles following the IMA 2012 recommendations. *Computers & Geosciences, 62,* 1-11.

López Sánchez-Vizcaino, V. and Soto, J. I., 1999: Metamorphism of calc-silicate rocks from the Alboran basement. In Proceedings of the Ocean Drilling Program. Scientific results (Vol. 161, pp. 251-261).

Mearns, E. W. and Lappin, M. A., 1982: A Sm–Nd isotopic study of 'internal'and 'external eclogites,'garnet lherzolite and grey gneiss from Almklovdalen, western Norway. *Terra cognita, 2(3),* 324-325.

Moecher, D. P., Essene, E. J. & Anovitz, L. M., 1988: Calculation and application of clinopyroxene-garnet-plagioclase-quartz geobarometers. *Contributions to Mineralogy and Petrology, 100(1),* 92-106.

Möller, C., Williams, D., Brueckner, H., Szilas, K., Johansson, L., Naeraa, T. & Whitehouse, M., 2020: Eclogite, garnet peridotite, and amphibolite complexes in the Precambrian basement of Vestranden (northernmost Western Gneiss Re-

gion), western Norway. Presented abstract at the IEC (International Eclogite Conference).

Möller, C., Andersson, J., Dyck, B. & Antal Lundin, I., 2015: Exhumation of an eclogite terrane as a hot migmatitic nappe, Sveconorwegian orogen. *Lithos 226,* 147-168.

Möller, C., 1990: Metamorphic and tectonic history of high-pressure granulite facies crust, Roan, Western Gneiss Region, Norwegian Caledonides. University of Lund. Institute of Geology. Department of Mineralogy and Petrology.

Möller, C., 1988: Geology and metamorphic evolution of the Roan area, Vestranden, Western Gneiss Region, Central Norwegian, Caledonides. *Bulletin-Norges geologiske undersokelse, (413),* 1-31.

Morimoto, N., 1988: Nomenclature of pyroxenes. *Mineralogy and Petrology, 39(1),* 55-76.

Mørk, M. B. E. and Mearns, E. W., 1986: Sm Nd isotopic systematics of a gabbro-eclogite transition. *Lithos, 19(3-4),* 255-267.

Mørk, M. B. E., 1985: A gabbro to eclogite transition on Flemsøy, Sunnmøre, western Norway. *Chemical Geology, Volume 50, Issues 1–3,* 283 -310

Nesse, W. D., 2011: Introduction to Mineralogy, 2nd edition. *Oxford University Press, 2nd edition.*

Orville, P.M., 1975: Stability of scapolite in the system Ab-An-NaCl-CaCO3 at 4kb and 750°C. *Geochimica et Cosmochimica Acta 39,* 1091-1095.

Ramberg, H., 1966: The Scandinavian Caledonides as studied by centrifuged dynamic models. *Bull. Geol. Inst. Univ. Uppsala*, 43(1).

Ramberg, H., 1943: En undersøkelse av Vestrandens Regionalmetamorfe bergarter (Doctoral dissertation, Oslo).

Ramberg, I. B., Bryhni, I., Nøttvedt, A. & Rangnes, K., (Eds) 2008: The Making of a Land – Geology of Norway. *Geological Society of London.*

Rieder, M., Cavazzini, G., D'yakonov, Y. S., Frank-Kamenetskii, V. A., Gottardi, G., Guggenheim, S., Koval, P. V., Müller, G., Neiva, A. M. R., Radoslovich, E. W., Robert, J-L., Sassi, F. P., Takeda, H., Weiss, Z., & Wones, D. R., 1998: Nomenclature of the micas. *Clays and clay minerals, 46(5),* 586-595.

Root, D. B., Hacker, B. R., Gans, P. B., Ducea, M. N., Eide, E. A. & Mosenfelder, J. L., 2005: Discrete ultrahigh-pressure domains in the Western Gneiss Region, Norway: implications for formation and exhumation. *Journal of Metamorphic Geology, 23(1),* 45-61.

Røhr, T. S., Bingen, B., Robinson, P. & Reddy, S. M., 2013: Geochronology of Paleoproterozoic augen gneisses in the Western Gneiss Region, Norway: evidence for Sveconorwegian zircon neocrystallization and Caledonian zircon deformation. *The Journal of Geology, 121(2),* 105-128.

Schouenborg, B. E., Johansson, L. & Gorbatschev, R., 1991: U/Pb zircon ages of basement gneisses and discordant felsic dykes from Vestranden, westernmost Baltic Shield and central Norwegian Caledonides. *Geologische Rundschau, 80 (1),* 121-134.

Schouenborg, B. E., 1989: Primary and tectonic basement-cover relationships in northernmost Vestranden, central Norwegian Caledonides. Norsk geologisk tidsskrift, 69(4), 209-223.

Siivola, J. and Schmid, R., 2007: List of mineral abbreviations. Metamorphic Rocks: A Classification and Glossary of Terms. *Recommendations of the International Union of Geological Sciences Subcommission on the Systematics of Metamorphic Rocks, 93-110.*

Solli, A., Bugge, T. & Thorsnes, T., 1997: Geologisk kart over Norge, berggrunnskart Namsos, M 1:250 000. *Norges geologiske undersøkelse.*

Teertstra, D. K. and Sherriff, B. L., 1997: Substitutional mechanisms, compositional trends and the end-member formulae of scapolite. *Chemical Geology, 136(3-4),* 233-260.

Tveten, E., Lutro, O., & Thorsnes, T., 1998: Berggrunnskart Alesund. 1: 250,000 (Alesund, western Norway). *NGU Trondheim (bedrock map).*

Vrijmoed, J. C., Van Roermund, H. L. M. & Davies, G. R., 2006: Evidence for diamond-grade ultrahigh pressure metamorphism and fluid interaction in the Svartberget Fe–Ti garnet peridotite–websterite body, Western Gneiss Region, Norway. *Mineralogy and Petrology, 88(1-2),* 381-405.

Wain, A., 1997: New evidence for coesite in eclogite and gneisses: Defining an ultrahigh-pressure province in the Western Gneiss region of Norway. *Geology, 25(10),* 927-930.

Winter, J. D., 2014: Principles of igneous and metamorphic petrology (p. 738). *Harlow, UK: Pearson education*.

Young, D. J., Hacker, B. R., Andersen, T. B. & Corfu, F., 2007: Prograde amphibolite facies to ultrahigh-pressure transition along Nordfjord, western Norway: Implications for exhumation tectonics. *Tectonics, 26(1).*

Appendix 1 – Common abbreviations of petrogenetic minerals

List of the minerals' abbreviations used in the text, figures and appendices of this work.

Abbreviations	Mineral Name	Abbreviations	Mineral Name	Abbreviations	Mineral Name
Actinolite	Act	K-feldspar	Kfs	Wollastonite	Wo
Albite	Ab	Margarite	Mrg	Zoisite	Zo
Allanite	Aln	Marialite	Mar	Zircon	Zrn
Almandine	Alm	Meionite	Mei		
Amphibole	Am	Mizzonite	Mizz		
Andradite	Adr	Muscovite	Ms		
Anorthite	An	Opaque minerals	Op		
Apatite	Ap	Phlogopite	Phl		
Biotite	Bt	Plagioclase	Pl		
Calcite	Cal	Prehnite	Prh		
Carbonate mineral	Cb	Pyrope	Prp		
Chlorite	Chl	Pyroxene	Px		
Clinopyroxene	Cpx	Quartz	Qtz		
Clinozoisite	Czo	Rutile	Rt		
Diopside	Di	Scapolite	Scp		
Dolomite	Dol	Sericite	Ser		
Enstatite	En	Spessartine	Sps		
Epidote	Ep	Talc	Tlc		
Ferrosilite	Fs	Titanite	Ttn		
Garnet	Grt	Tremolite	Tr		
Grossular	Grs	White Mica	Wmca		
Hedenbergite	Hd				

Appendix 2 – Chemical reactions of phase equilibria

List of chemical reactions calculated in winTWQ.

The number in front of the reactions coincide with the respective numbered reaction curve on the diagram.

The reactions in bold font have been selected for the P-T diagram formation.

Alm + 5 Qtz + 8 Zo = 3 Hd + 13 An + 4 H_2O

2) 4 Zo + Qtz = 5 An + Grs + 2 H_2O

Prp + 5 Qtz + 8 Zo = 3 Di + 13 An + 4 H_2O

2 Zo + CO_2 = Cal + 3 An + H_2O

3 Qtz + 2 Grs + Alm = 3 An + 3 Hd

12 Zo + 3 Hd = Alm + 12 An + 5 Grs + 6 H_2O

12 Qtz + 13 Grs + 5 Alm + 6 H_2O = 15 Hd + 12 Zo

Alm + 3 Di = Prp + 3 Hd

5 Qtz + 4 Cal + Alm = An + 3 Hd + 4 CO_2

15 Qtz + 13 Cal + 3 Alm + H_2O = 9 Hd + 2 Zo + 13 CO_2

3 Qtz + Prp + 2 Grs = 3 An + 3 Di

3 Di + 12 Zo = Prp + 5 Grs + 12 An + 6 H_2O

13) 12 Qtz + 5 Prp + 13 Grs + 6 H_2O = 15 Di + 12 Zo

14) Qtz + 2 Cal + An = Grs + 2 CO_2

15) 2 Zo + 3 Qtz + 5 Cal = 3 Grs + 5 CO_2 + H_2O

16) 4 Cal + Prp + 5 Qtz = 3 Di + An + 4 CO_2

17) 15 Qtz + 3 Prp + 13 Cal + H_2O = 9 Di + 2 Zo + 13 CO_2

18) Alm + 5 Grs + 6 CO_2 = 3 Hd + 6 Cal + 6 An

19) Alm + 6 Cal + 6 Qtz = 3 Hd + Grs + 6 CO_2

20) 4 Cal + 3 Hd + 4 Zo = 5 Grs + Alm + 2 H_2O + 4 CO_2

21) Prp + 5 Grs + 6 CO_2 = 6 An + 6 Cal + 3 Di

22) 6 Cal + Prp + 6 Qtz = Grs + 3 Di + 6 CO_2

23) 4 Cal + 3 Di + 4 Zo = Prp + 5 Grs + 2 H_2O + 4 CO_2

Appendix 3 – Representative EDS analyses of petrogenetic minerals

The tables 1-18 below list wt% oxides and atoms per formula unit of minerals analysed from the five samples which were used for SEM-EDS analyses.

Table 1. Garnet. Fe^{3+} has been calculated with the method of Droop (1987). Textural positions: PR: porphyroblast rim, PC: porphyroblast core, RD: thin rim on diopside, RP: thin rim on plagioclase, RC: thin rim on calcite, RL: thin rim on low-grade alterations (sericite, prehnite).

Sample	CM16R-03e2							
Lithology	Mafic Granulite (meta-mafic rock)							
Analysis	GRT-1	GRT-2	GRT-3	GRT-4	GRT-5	GRT-6	GRT-7	GRT-8
Textural position	PR	PR	PC	PR	PC	PR	PC	PC
SiO_2	38.47	38.89	38.61	38.21	38.19	38.30	38.46	38.67
Al_2O_3	21.86	21.96	21.54	21.48	21.58	21.68	21.98	22.50
Fe_2O_3	1.03	-	0.51	1.02	1.02	0.51	1.03	-
FeO	21.33	21.93	21.12	21.60	21.07	21.34	21.35	21.41
MgO	1.96	2.07	1.90	1.99	1.93	1.93	2.01	2.30
MnO	1.09	1.14	1.10	1.29	1.20	1.11	0.94	0.90
CaO	15.73	15.83	16.07	14.96	15.52	15.52	15.66	15.64
Total	101.46	101.82	100.85	100.55	100.51	100.39	101.43	101.43
Formula based on:	12.00 Oxygens							
Si	2.97	2.99	3.00	2.98	2.98	2.99	2.99	2.98
Al	2.00	1.99	1.97	1.98	1.99	2.00	2.01	2.04
Fe^{3+}	0.06	-	0.03	0.06	0.06	0.03	0.03	-
Fe^{2+}	1.38	1.41	1.37	1.41	1.38	1.39	1.39	1.38
Mn^{2+}	0.07	0.07	0.07	0.09	0.08	0.07	0.06	0.06
Mg	0.23	0.24	0.22	0.23	0.22	0.23	0.23	0.26
Ca	1.31	1.30	1.34	1.25	1.30	1.30	1.30	1.29
Total	8.01	8.01	8.01	7.99	8.00	8.00	8.00	8.00
Grossular %	42.80	43.33	44.00	40.84	42.54	42.97	42.98	43.14
Almandine %	46.86	46.33	45.67	47.67	46.84	46.84	46.64	46.15
Pyrope %	7.59	8.00	7.33	7.67	7.31	7.64	7.72	8.70
Spessartine %	2.31	2.33	2.33	3.00	2.66	2.33	2.01	2.01
Andradite %	0.43	-	0.67	0.83	0.65	0.22	0.64	-
Name	Almandine-Grossular	Almandine-Grossular	Almandine-Grossular	Almandine-Grossular	Almandine-Grossular	Almandine-Grossular	Almandine-Grossular	Almandine-Grossular

Table 1 (cont). Garnet. Fe^{3+} has been calculated with the method of Droop (1987). Textural positions: R: rim, PC: porphyroblast core, RD: thin rim on diopside, RP: thin rim on plagioclase, RC: thin rim on calcite, RL: thin rim on low-grade alterations (sericite, prehnite).

Sample	CM19R-11k							
Lithology	Mafic Granulite (meta-mafic rock)							
Analysis	GRT-9	GRT-10	GRT-11	GRT-12	GRT-13	GRT-14	GRT-15	GRT-16
Textural position	RP	RC	RL	PC	RL	RD	PC	PC
SiO_2	39.14	38.74	38.59	38.39	38.76	38.90	38.55	38.46
Al_2O_3	21.26	21.16	20.96	21.47	21.27	21.30	21.32	21.64
Fe_2O_3	0.52	2.04	-	2.02	-	1.02	1.03	1.03
FeO	11.83	11.39	11.03	14.50	14.04	11.92	17.92	18.19
MgO	1.00	1.02	0.94	1.30	0.93	1.02	1.38	1.37
MnO	-	-	-	-	0.42	-	0.56	0.47
CaO	25.94	25.60	27.14	21.67	24.13	25.63	19.70	19.53
Total	99.69	99.95	98.66	99.35	99.55	99.79	100.46	100.69
Formula based on:	12.00 Oxygens							
Si	3.02	2.99	3.00	2.99	3.02	2.99	2.99	2.97
Al	1.93	1.93	1.92	1.97	1.94	1.94	1.96	1.98
Fe^{3+}	0.03	0.12	-	0.12	-	0.06	0.06	0.06
Fe^{2+}	0.76	0.74	0.72	0.95	0.92	0.78	1.16	1.18
Mn^{2+}	-	-	-	-	0.02	-	0.04	0.04
Mg	0.12	0.12	0.10	0.16	0.10	0.12	0.16	0.16
Ca	2.15	2.11	2.26	1.81	2.00	2.11	1.64	1.62
Total	8.00	8.00	8.00	8.00	8.00	8.00	8.00	8.00
Grossular %	70.81	67.30	75.33	59.13	67.11	68.22	53.12	52.38
Almandine %	25.42	25.91	24.00	34.33	30.87	26.00	38.87	39.33
Pyrope %	2.68	3.99	0.67	5.33	1.34	3.67	5.32	5.33
Spessartine %	-	-	-	-	0.67	-	1.33	1.33
Andradite %	1.10	2.80	-	1.21	-	2.11	1.36	1.62
Name	Grossular	Grossular	Grossular	Grossular	Grossular	Grossular	Grossular	Grossular

Sample	CM19R-11k							
Lithology	Mafic Granulite (meta-mafic rock)							
Analysis	GRT-17	GRT-18	GRT-19	GRT-20	GRT-21	GRT-22	GRT-23	GRT-24
Textural position	PC	RP	RD	RD	RD	RL	RL	PC
SiO_2	39.04	39.17	39.26	38.76	39.13	38.78	39.38	38.73
Al_2O_3	21.58	21.50	21.77	21.24	21.05	21.18	21.09	21.19
Fe_2O_3	-	1.04	2.08	2.06	1.04	1.03	1.02	2.09
FeO	15.03	11.51	10.60	10.20	12.42	11.44	8.58	9.69
MgO	1.26	0.92	0.80	0.75	0.92	0.81	0.6	0.72
MnO	-	-	-	-	0.39	-	-	-
CaO	23.27	26.44	26.57	27.08	25.91	25.94	28.69	27.57
Total	100.19	100.57	101.08	100.09	100.85	99.18	99.36	99.99
Formula based on:	12.00 Oxygens							
Si	3.02	2.99	2.99	2.99	2.99	3.01	3.03	2.99
Al	1.96	1.94	1.95	1.93	1.90	1.94	1.92	1.93
Fe^{3+}	-	0.06	0.12	0.12	0.06	0.06	0.06	0.12
Fe^{2+}	0.96	0.74	0.68	0.66	0.80	0.74	0.56	0.62
Mn^{2+}	-	-	-	-	0.02	-	-	-
Mg	0.14	0.10	0.10	0.08	0.10	0.10	0.06	0.08
Ca	1.92	2.17	2.17	2.23	2.13	2.15	2.37	2.27
Total	8.00	8.00	8.00	8.00	8.00	8.00	8.00	8.00
Grossular %	64.43	70.16	69.93	71.12	68.87	69.75	77.40	72.40
Almandine %	32.21	24.67	24.58	23.26	26.67	24.75	18.86	21.93
Pyrope %	3.36	3.00	3.32	2.66	1.67	3.34	1.35	2.66
Spessartine %	-	-	-	-	0.67	-	-	-
Andradite %	-	2.17	2.16	2.96	2.13	2.16	2.39	3.02
Name	Grossular	Grossular	Grossular	Grossular	Grossular	Grossular	Grossular	Grossular

Table 2. Clinopyroxene. Fe^{3+} has been calculated with the method of Droop (1987). Textural positions: m: Main assemblage, r: amphibolite-facies retrograde mineral, l: low-grade origin mineral, u: cannot be texturally classified.

Sample	CM16R-03e2							
Lithology	Mafic Granulite (meta-mafic rock)							
Analysis	CPX-1	CPX-2	CPX-3	CPX-4	CPX-5	CPX-6	CPX-7	CPX-8
Textural position	m	m	m	m	m	m	m	m
SiO_2	53.54	53.17	51.50	51.25	52.56	51.26	51.08	51.02
TiO_2	-	-	-	-	-	-	-	-
Al_2O_3	-	0.52	2.05	2.28	-	2.29	2.13	2.23
FeO	12.32	11.40	13.46	12.54	11.40	12.32	12.87	13.47
Fe_2O_3	-	-	-	-	-	-	-	-
MgO	11.24	11.77	10.15	10.20	11.76	10.62	10.40	10.04
MnO	-	0.32	-	-	0.27	-	-	0.22
CaO	24.47	24.19	23.15	22.93	23.72	22.88	22.87	23.03
Total	101.57	101.37	100.31	99.18	99.72	99.37	99.35	100.00
Formula based on:	6.00 Oxygens							
Si	2.00	1.99	1.96	1.96	2.00	1.96	1.96	1.95
Ti	-	-	-	-	-	-	-	-
Al	-	0.02	0.09	0.10	-	0.10	0.10	0.10
Fe^{2+}	0.39	0.36	0.43	0.40	0.36	0.39	0.41	0.43
Fe^{3+}	-	-	-	-	-	-	-	-
Mg	0.63	0.66	0.58	0.58	0.67	0.60	0.59	0.57
Mn	-	0.01	-	-	0.01	-	-	0.01
Ca	0.98	0.97	0.94	0.94	0.97	0.94	0.94	0.94
Total	4.00	4.00	4.00	3.99	4.00	3.99	4.00	4.00
#Mg	0.62	0.65	0.57	0.59	0.65	0.61	0.59	0.57
Name	Diopside	Diopside	Diopside	Diopside	Diopside	Diopside	Diopside	Diopside

Sample	CM16R-09c							
Lithology	Marble							
Analysis	CPX-9	CPX-10	CPX-11	CPX-12	CPX-13	CPX-14	CPX-15	CPX-16
Textural position	m	m	m	m	u	u	u	m
SiO_2	51.32	51.34	52.44	52.62	50.05	49.89	49.50	52.51
TiO_2	-	-	-	-	-	-	-	-
Al_2O_3	1.30	1.21	0.76	-	2.58	2.58	2.63	0.79
FeO	11.27	12.09	9.88	8.72	16.12	14.06	14.39	10.88
Fe_2O_3	1.04	-	-	1.04	-	2.04	2.04	-
Cr_2O_3	-	-	0.17	-	-	-	-	-
MgO	10.99	10.90	12.40	12.79	8.20	8.01	7.91	11.68
MnO	-	-	-	-	-	-	-	0.18
CaO	23.45	23.45	24.14	24.21	22.67	22.69	22.65	23.50
Na_2O	-	-	-	-	-	0.55	0.40	0.18
Total	99.37	98.99	99.79	99.37	99.63	99.81	99.52	99.72
Formula based on:	6.00 Oxygens							
Si	1.97	1.97	1.98	1.99	1.94	1.93	1.92	1.99
Ti	-	-	-	-	-	-	-	-
Al	0.06	0.05	0.03	-	0.12	0.12	0.12	0.04
Fe^{2+}	0.36	0.39	0.31	0.28	0.52	0.46	0.47	0.34
Fe^{3+}	0.03	-	-	0.03	-	0.06	0.06	-
Cr	-	-	0.01	-	-	-	-	-
Mg	0.63	0.62	0.70	0.72	0.47	0.46	0.46	0.66
Mn	-	-	-	-	-	-	-	0.01
Ca	0.96	0.96	0.98	0.98	0.94	0.94	0.95	0.95
Na	-	-	-	-	-	0.06	0.05	0.01
Total	4.00	4.00	4.00	3.99	4.00	4.00	4.00	4.00
#Mg	0.64	0.61	0.69	0.72	0.47	0.47	0.46	0.66
Name	Diopside	Diopside	Diopside	Diopside	Hedenbergite	Hedenbergite	Hedenbergite	Diopside

Table 2 (cont). Clinopyroxene. Fe^{3+} has been calculated with the method of Droop (1987). Textural positions: m: Main assemblage, r: amphibolite-facies retrograde mineral, l: low-grade origin mineral, u: cannot be texturally classified.

Sample	CM16R-09f1						
Lithology	Marble						
Analysis	CPX-17	CPX-18	CPX-19	CPX-20	CPX-21	CPX-22	CPX-23
Textural position	m	m	m	m	m	m	m
SiO_2	56.09	56.41	55.92	56.20	55.98	55.65	56.05
TiO_2	-	-	-	-	-	-	-
Al_2O_3	-	-	-	0.94	1.06	0.94	0.94
FeO	-	-	-	-	-	-	-
Fe_2O_3	-	-	-	0.68	0.58	0.76	0.71
MgO	19.59	19.59	19.32	18.71	18.62	18.75	18.98
MnO	-	-	-	-	-	-	-
CaO	25.74	25.54	25.68	25.83	25.60	25.30	25.29
Na_2O	-	-	-	0.22	0.23	0.25	0.23
Total	101.43	101.54	100.91	102.59	102.07	101.65	102.20
Formula based on:	6.00 Oxygens						
Si	1.99	2.00	2.00	1.98	1.98	1.98	1.98
Ti	-	-	-	-	-	-	-
Al	-	-	-	0.04	0.04	0.04	0.04
Fe^{2+}	-	-	-	-	-	-	-
Fe^{3+}	-	-	-	0.02	0.02	0.02	0.02
Mg	1.04	1.03	1.03	0.98	0.98	0.99	1.00
Mn	-	-	-	-	-	-	-
Ca	0.98	0.97	0.98	0.97	0.97	0.96	0.96
Na	-	-	-	0.02	0.02	0.02	0.02
Total	4.01	4.00	4.00	4.01	4.01	4.01	4.01
#Mg	1.00	1.00	1.00	0.98	0.98	0.98	0.98
Name	Diopside	Diopside	Diopside	Diopside	Diopside	Diopside	Diopside

Sample	CM16R-09f1						
Lithology	Marble						
Analysis	CPX-24	CPX-25	CPX-26	CPX-27	CPX-28	CPX-29	CPX-30
Textural position	m	m	m	m	m	m	m
SiO_2	55.61	55.77	56.27	55.39	56.09	55.48	55.98
TiO_2	-	-	-	-	-	-	-
Al_2O_3	0.97	0.88	0.56	0.57	0.56	0.55	0.41
FeO	0.63	0.73	-	-	-	-	-
Fe_2O_3	-	-	-	-	-	-	-
Cr_2O_3	-	-	-	-	-	-	-
MgO	18.55	18.59	18.99	18.65	18.97	18.80	18.89
MnO	-	-	-	-	-	-	-
CaO	25.58	25.00	25.42	25.56	25.44	25.26	25.65
Na_2O	-	0.24	-	-	-	-	-
Total	101.34	101.21	101.23	100.16	101.07	100.10	100.93
Formula based on:	6.00 Oxygens						
Si	1.98	1.99	2.00	1.99	1.99	1.99	2.00
Ti	-	-	-	-	-	-	-
Al	0.04	0.04	0.02	0.02	0.02	0.02	0.02
Fe^{2+}	0.02	0.02	-	-	-	-	-
Fe^{3+}	-	-	-	-	-	-	-
Cr	-	-	-	-	-	-	-
Mg	0.98	0.99	1.00	1.00	1.01	1.01	1.00
Mn	-	-	-	-	-	-	-
Ca	0.98	0.95	0.97	0.98	0.97	0.97	0.98
Na	-	0.02	-	-	-	-	-
Total	4.00	4.00	3.99	4.00	3.99	4.00	4.00
#Mg	0.98	0.98	1.00	1.00	1.00	1.00	1.00
Name	Diopside	Diopside	Diopside	Diopside	Diopside	Diopside	Diopside

Table 2 (cont). Clinopyroxene. Fe^{3+} has been calculated with the method of Droop (1987). Textural positions: m: Main assemblage, r: amphibolite-facies retrograde mineral, l: low-grade origin mineral, u: cannot be texturally classified.

Sample	CM19R-11b							
Lithology	Calc-silicate							
Analysis	CPX-31	CPX-32	CPX-33	CPX-34	CPX-35	CPX-36	CPX-37	CPX-38
Textural position	m	m	m	m	m	m	m	m
SiO_2	55.62	55.64	57.26	56.56	55.97	57.32	56.90	56.71
Al_2O_3	-	-	-	0.93	2.26	-	-	2.53
FeO	-	0.43	0.47	0.59	0.96	-	-	0.86
Fe_2O_3	0.41	-	-	-	-	0.36	-	-
MgO	19.07	19.28	19.41	18.56	17.79	19.38	19.44	17.77
CaO	25.65	25.04	25.86	25.53	25.13	26.15	25.98	24.72
Na_2O	-	-	-	0.34	0.51	-	-	0.69
Total	100.75	100.39	103.00	102.51	102.63	103.22	102.32	103.28
Formula based on:	6.00 Oxygens							
Si	1.99	2.00	2.00	1.99	1.97	2.00	2.00	1.98
Al	-	-	-	0.04	0.09	-	-	0.10
Fe^{2+}	-	0.01	0.01	0.02	0.03	-	-	0.03
Fe^{3+}	0.01	-	-	-	-	0.01	-	-
Mg	1.02	1.03	1.01	0.97	0.93	1.01	1.02	0.92
Ca	0.98	0.96	0.97	0.96	0.95	0.98	0.98	0.92
Na	-	-	-	0.02	0.03	-	-	0.05
Total	4.01	4.00	4.00	4.00	4.00	4.00	4.00	4.00
#Mg	0.99	0.99	0.99	0.98	0.97	0.99	1.00	0.97
Name	Diopside	Diopside	Diopside	Diopside	Diopside	Diopside	Diopside	Diopside

Sample	CM19R-11b							
Lithology	Calc-silicate							
Analysis	CPX-39	CPX-40	CPX-41	CPX-42	CPX-43	CPX-44	CPX-45	CPX-46
Textural position	m	m	m	m	m	m	m	m
SiO_2	56.58	55.69	55.91	56.45	56.39	56.69	56.38	56.52
TiO_2	-	-	-	-	-	-	-	-
Al_2O_3	0.99	-	0.91	-	-	-	-	-
FeO	0.58	-	-	-	-	-	-	-
Cr_2O_3	-	-	-	-	0.35	-	-	-
MgO	18.77	18.72	18.46	19.34	19.42	19.55	19.17	19.65
MnO	-	-	-	-	-	-	-	-
CaO	25.73	25.28	25.58	25.29	25.68	25.82	25.55	25.65
Na_2O	-	-	-	-	-	-	-	-
Total	102.64	99.69	100.86	101.08	101.83	102.06	101.10	101.81
Formula based on:	6.00 Oxygens							
Si	1.99	2.01	1.99	2.01	2.00	2.00	2.00	2.00
Ti	-	-	-	-	-	-	-	-
Al	0.04	-	0.04	-	-	-	-	-
Fe^{2+}	0.02	-	-	-	-	-	-	-
Cr	-	-	-	-	0.01	-	-	-
Mg	0.98	1.01	0.98	1.03	1.02	1.03	1.01	1.04
Mn	-	-	-	-	-	-	-	-
Ca	0.97	0.98	0.98	0.96	0.98	0.98	0.98	0.97
Na	-	-	-	-	-	-	-	-
Total	3.99	3.99	3.99	4.00	4.00	4.00	3.99	4.00
#Mg	0.98	1.00	1.00	1.00	1.00	1.00	1.00	1.00
Name	Diopside	Diopside	Diopside	Diopside	Diopside	Diopside	Diopside	Diopside

Table 2 (cont). Clinopyroxene. Fe^{3+} has been calculated with the method of Droop (1987). Textural positions: m: Main assemblage, r: amphibolite-facies retrograde mineral, l: low-grade origin mineral, u: cannot be texturally classified.

Sample	CM19R-11k							
Lithology	Mafic Granulite (meta-mafic rock)							
Analysis	CPX-47	CPX-48	CPX-49	CPX-50	CPX-51	CPX-52	CPX-53	CPX-54
Textural position	m	m	m	m	m	m	m	m
SiO_2	50.47	50.91	51.16	51.27	51.10	50.55	50.87	51.14
TiO_2	-	-	-	-	-	-	0.36	-
Al_2O_3	3.10	2.33	2.31	2.51	2.31	2.20	2.95	2.27
FeO	10.99	11.31	11.70	10.24	12.81	11.84	10.56	11.31
Fe_2O_3	-	-	1.05	2.13	-	1.04	-	-
Cr_2O_3	0.39	-	-	-	0.38	-	-	-
MgO	10.58	10.68	10.39	10.45	9.96	9.85	11.14	10.77
MnO	-	-	-	-	-	-	-	-
CaO	23.85	23.87	23.81	23.88	23.41	22.98	24.09	23.86
Na_2O	-	-	-	0.36	-	0.37	-	-
Total	99.38	99.10	100.43	100.84	99.97	98.83	99.97	99.35
Formula based on:	6.00 Oxygens							
Si	1.92	1.95	1.94	1.93	1.95	1.95	1.92	1.95
Ti	-	-	-	-	-	-	0.01	-
Al	0.14	0.10	0.10	0.11	0.10	0.10	0.13	0.10
Fe^{2+}	0.35	0.36	0.37	0.32	0.41	0.38	0.33	0.36
Fe^{3+}	-	-	0.03	0.06	-	0.03	-	-
Cr	0.01	-	-	-	0.01	-	-	-
Mg	0.60	0.61	0.59	0.59	0.57	0.57	0.63	0.61
Mn	-	-	-	-	-	-	-	-
Ca	0.97	0.98	0.97	0.97	0.96	0.95	0.98	0.97
Na	-	-	-	0.03	-	0.03	-	-
Total	4.00	4.00	3.99	4.00	3.99	4.00	4.00	4.00
#Mg	0.63	0.63	0.61	0.65	0.58	0.60	0.66	0.63
Name	Diopside	Diopside	Diopside	Diopside	Diopside	Diopside	Diopside	Diopside

Table 3. Amphibole. Fe^{3+} has been calculated with the method of Droop (1987). Textural positions: m: Main assemblage, r: amphibolite-facies retrograde mineral, l: low-grade origin mineral, u: cannot be texturally classified.

Sample	CM16R-03e2							
Lithology	Mafic Granulite (meta-mafic rock)							
Analysis	AM-1	AM-2	AM-3	AM-4	AM-5	AM-6	AM-7	AM-8
Textural position	m	m	m	r	m	m	m	m
SiO_2	40.20	40.37	40.35	54.08	39.93	39.58	39.53	39.75
TiO_2	1.99	1.63	1.57	-	1.65	1.76	1.83	1.53
Al_2O_3	14.90	14.43	14.86	1.59	14.88	14.26	13.96	15.74
FeO	19.44	19.22	20.09	18.94	19.27	19.20	19.32	20.38
Fe_2O_3	-	-	-	0.55	-	-	-	-
Cr_2O_3	-	-	-	-	-	-	0.20	-
MgO	7.42	7.83	7.36	11.62	7.61	7.58	7.51	6.79
MnO	-	-	-	0.35	-	-	0.22	-
CaO	11.99	12.00	11.93	12.82	11.91	11.65	11.71	11.76
Na_2O	1.78	1.74	1.76	-	1.79	1.75	1.77	2.20
K_2O	1.68	1.84	1.64	-	1.62	1.81	1.68	0.40
F*	-	-	-	-	-	-	-	-
Cl*	-	-	-	-	-	0.14	0.13	-
Total	99.40	99.07	99.55	99.94	98.66	97.73	97.86	98.55
Formula based on:	23.00 Oxygens							
Si	6.06	6.10	6.10	7.83	6.06	6.06	6.06	6.02
Ti	0.23	0.19	0.19	-	0.19	0.20	0.21	0.17
Al	2.64	2.57	2.65	0.27	2.66	2.58	2.53	2.81
Fe^{2+}	2.45	2.43	2.53	2.30	2.44	2.46	2.48	2.58
Fe^{3+}	-	-	-	0.06	-	-	-	-
Cr	-	-	-	-	-	-	0.02	-
Mg	1.67	1.76	1.65	2.51	1.72	1.73	1.72	1.53
Mn	-	-	-	0.04	-	-	0.03	-
Ca	1.93	1.94	1.92	1.99	1.93	1.91	1.93	1.91
Na	0.52	0.51	0.50	-	0.53	0.52	0.53	0.65
K	0.32	0.35	0.31	-	0.31	0.35	0.33	0.08
F**	-	-	-	-	-	-	-	-
Cl**	-	-	-	-	-	0.04	0.03	-
OH**	2.00	2.00	2.00	2.00	2.00	1.96	1.97	2.00
Total	17.82	17.86	17.83	16.99	17.84	17.81	17.85	17.76
#Mg	0.43	0.42	0.39	0.52	0.41	0.41	0.41	0.37
Name	Ferro-Pargasite	Ferro-Pargasite	Ferro-Pargasite	Actinolite	Ferro-Pargasite	Ferro-Pargasite	Ferro-Pargasite	Ferro-Pargasite

* Value is input as Wt%

**Calculated based on Locock, A. J., 2014.

Table 3 (cont). Amphibole. Fe^{3+} has been calculated with the method of Droop (1987). Textural positions: m: Main assemblage, r: amphibolite-facies retrograde mineral, l: low-grade origin mineral, u: cannot be texturally classified.

Sample	CM16R-09c						
Lithology	Marble						
Analysis	AM-9	AM-10	AM-11	AM-12	AM-13	AM-14	AM-15
Textural position	r	r	r	r	r	r	r
SiO_2	39.74	45.21	45.93	52.90	45.41	54.05	46.71
TiO_2	0.69	0.50	0.46	-	0.60	-	0.32
Al_2O_3	12.59	9.21	9.37	1.36	8.26	2.28	8.57
FeO	22.91	19.34	19.20	12.05	17.60	11.48	18.58
Fe_2O_3	-	-	0.27	3.35	0.26	2.77	0.27
Cr_2O_3	-	-	-	-	-	-	-
MgO	6.38	10.23	10.40	14.45	10.74	15.50	10.65
MnO	-	-	0.30	0.28	-	-	-
CaO	11.95	12.07	12.38	12.48	11.96	12.37	12.36
Na_2O	0.87	0.88	0.92	0.15	0.65	0.19	0.70
K_2O	1.57	0.84	0.68	0.07	0.69	0.13	0.70
F*	-	-	-	-	-	-	-
Cl*	0.26	-	-	-	-	-	-
Total	96.96	98.28	99.91	97.09	96.29	98.78	98.90
Formula based on:	23.00 Oxygens						
Si	6.24	6.79	6.78	7.73	6.90	7.70	6.93
Ti	0.08	0.06	0.05	-	0.07	-	0.04
Al	2.33	1.63	1.63	0.24	1.48	0.38	1.50
Fe^{2+}	3.01	2.43	2.37	1.48	2.24	1.38	2.30
Fe^{3+}	-	-	0.03	0.37	0.03	0.30	0.03
Cr	-	-	-	-	-	-	-
Mg	1.49	2.29	2.29	3.14	2.43	3.29	2.35
Mn	-	-	0.04	0.04	-	-	-
Ca	2.01	1.94	1.96	1.95	1.95	1.89	1.96
Na	0.27	0.25	0.26	0.04	0.19	0.05	0.20
K	0.31	0.16	0.13	0.01	0.13	0.02	0.13
F**	-	-	-	-	-	-	-
Cl**	0.07	-	-	-	-	-	-
OH**	1.93	2.00	2.00	2.00	2.00	2.00	2.00
Total	17.74	17.55	17.53	17.00	17.44	17.00	17.43
#Mg	0.33	0.40	0.49	0.63	0.52	0.66	0.51
Name	Ferro-Pargasite	Ferro-Hornblende	Ferro-Hornblende	Actinolite	Magnesio-Hornblende	Actinolite	Magnesio-Hornblende

* Value is input as Wt%

**Calculated based on Locock, A. J., 2014.

Table 3 (cont). Amphibole. Fe^{3+} has been calculated with the method of Droop (1987). Textural positions: m: Main assemblage, r: amphibolite-facies retrograde mineral, l: low-grade origin mineral, u: cannot be texturally classified.

Sample	CM16R-09fl							
Lithology	Marble							
Analysis	AM-16	AM-17	AM-18	AM-19	AM-20	AM-21	AM-22	AM-23
Textural position	r	r	r	r	r	r	r	r
SiO_2	56.50	54.23	53.50	54.00	55.80	55.49	51.81	53.45
TiO_2	-	-	-	0.10	-	-	-	-
Al_2O_3	0.38	1.29	1.56	1.68	0.31	0.27	2.93	1.68
FeO	0.26	-	-	-	0.26	-	-	-
Fe_2O_3	0.28	0.57	0.63	0.10	-	-	0.31	0.22
Cr_2O_3	-	-	-	-	-	-	-	-
MgO	22.11	21.70	21.17	21.39	21.76	21.53	20.70	20.88
MnO	-	-	-	0.09	-	-	-	-
CaO	13.75	13.28	13.28	14.00	13.87	13.76	13.87	13.69
Na_2O	0.27	0.67	0.76	0.61	0.10	-	1.05	0.68
K_2O	0.13	0.16	0.14	0.13	-	-	0.22	-
F*	-	-	-	-	-	-	-	-
Cl*	-	-	-	-	-	-	-	-
Total	93.68	91.89	91.04	92.11	92.09	91.05	90.90	90.62
Formula based on:	23.00 Oxygens							
Si	8.00	7.80	7.77	7.75	8.05	8.05	7.50	7.81
Ti	-	-	-	0.01	-	-	-	-
Al	0.06	0.22	0.27	0.29	0.04	0.04	0.49	0.30
Fe^{2+}	0.03	-	-	-	0.04	-	-	-
Fe^{3+}	0.03	0.07	0.08	0.01	-	-	0.04	0.04
Cr	-	-	-	-	-	-	-	-
Mg	4.67	4.65	4.59	4.58	4.68	4.68	4.48	4.53
Mn	-	-	-	0.01	-	-	-	-
Ca	2.09	2.04	2.07	2.15	2.15	2.15	2.15	2.13
Na	0.07	0.19	0.22	0.17	0.04	-	0.30	0.19
K	0.02	0.03	0.03	0.02	-	-	0.04	-
F**	-	-	-	-	-	-	-	-
Cl**	-	-	-	-	-	-	-	-
OH**	2.00	2.00	2.00	2.00	2.00	2.00	2.00	2.00
Total	16.98	17.00	17.02	16.99	16.99	16.91	17.00	17.00
#Mg	0.99	1.00	1.00	1.00	0.99	1.00	1.00	1.00
Name	Tremolite	Tremolite	Tremolite	Tremolite	Tremolite	Tremolite	Tremolite	Tremolite

* Value is input as Wt%

**Calculated based on Locock, A. J., 2014.

Table 3 (cont). Amphibole. Fe^{3+} has been calculated with the method of Droop (1987). Textural positions: m: Main assemblage, r: amphibolite-facies retrograde mineral, l: low-grade origin mineral, u: cannot be texturally classified.

Sample	CM19R-11b							
Lithology	Calc-silicate							
Analysis	AM-25	AM-26	AM-27	AM-28	AM-29	AM-30	AM-31	AM-32
Textural position	m	m	m	m	m	r	r	m
SiO_2	50.41	44.20	50.32	49.20	47.38	60.19	58.66	45.45
TiO_2	-	0.17	-	-	-	-	-	-
Al_2O_3	8.81	16.75	9.85	10.85	14.41	-	0.65	15.05
FeO	0.95	1.38	1.13	1.16	0.95	-	-	1.32
Fe_2O_3	-	0.29	-	-	-	0.43	-	-
Cr_2O_3	-	-	-	-	-	-	-	-
MgO	22.33	19.09	22.14	22.01	20.59	25.22	24.88	19.93
MnO	-	-	-	-	-	-	-	-
CaO	12.99	12.50	12.59	12.91	12.56	13.75	13.42	12.97
Na_2O	2.19	2.92	2.34	2.78	3.30	0.34	0.56	3.00
K_2O	0.38	1.04	0.48	0.40	-	-	-	0.55
F*	0.42	0.37	-	-	-	-	-	-
Cl*	-	-	-	-	-	-	-	-
Total	98.50	98.34	98.85	99.31	99.19	99.93	98.18	98.27
Formula based on:	23.00 Oxygens							
Si	6.90	6.12	6.89	6.73	6.48	7.95	7.91	6.33
Ti	-	0.02	-	-	-	-	-	-
Al	1.42	2.73	1.59	1.75	2.34	-	0.12	2.47
Fe^{2+}	0.11	0.16	0.13	0.14	0.12	-	-	0.14
Fe^{3+}	-	0.03	-	-	-	0.05	-	-
Cr	-	-	-	-	-	-	-	-
Mg	4.55	3.94	4.52	4.49	4.18	4.97	5.00	4.14
Mn	-	-	-	-	-	-	-	-
Ca	1.90	1.85	1.85	1.90	1.84	1.94	1.93	1.93
Na	0.58	0.16	0.62	0.75	0.88	0.09	0.14	0.81
K	0.07	0.18	0.08	0.06	-	-	-	0.09
F**	0.18	0.16	-	-	-	-	-	-
Cl**	-	-	-	-	-	-	-	-
OH**	1.82	1.84	2.00	2.00	2.00	2.00	2.00	2.00
Total	17.53	17.80	17.67	17.81	17.83	17.00	17.09	17.90
#Mg	0.98	0.96	0.97	0.97	0.97	0.99	1.00	0.97
Name	F-bearing Edenite	F-bearing Pargasite	Edenite	Edenite	Pargasite	Tremolite	Tremolite	Pargasite

* Value is input as Wt%

**Calculated based on Locock, A. J., 2014.

Table 4. Scapolite. Scapolite is normalised in T= 12 a.p.f.u. (Teertstra and Sherriff, 1997). CO_3 (calculated) = 1.00 – (S+Cl), and Mei %= Ca / (Ca+Na). Textural positions: m: Main assemblage, r: amphibolite-facies retrograde mineral, l: low-grade origin mineral, u: cannot be texturally classified.

Sample	CM16R-09c							
Lithology	Marble							
Analysis	SCP-1	SCP-2	SCP-3	SCP-4	SCP-5	SCP-6	SCP-7	SCP-8
Textural position	m	m	m	m	m	m	m	m
SiO_2	44.78	45.95	43.76	44.34	44.06	44.51	45.19	45.54
TiO_2	-	-	0.16	-	-	-	-	-
Al_2O_3	28.13	28.65	29.18	29.34	28.40	28.55	28.08	27.97
FeO	0.49	0.47	0.42	0.45	0.43	0.49	0.32	0.46
MnO	-	-	-	-	-	-	-	-
MgO	-	-	0.08	0.19	0.08	-	0.08	-
CaO	18.82	19.53	19.51	19.91	18.95	19.25	18.85	18.81
Na_2O	2.22	2.62	2.09	2.19	2.16	2.39	2.40	2.44
K_2O	0.37	0.22	0.32	0.16	0.25	0.25	0.23	0.25
Cl*	0.11	-	-	0.07	0.07	0.18	0.14	0.14
SO_3	-	-	-	-	-	0.56	0.15	-
Total	94.93	97.45	95.52	96.65	94.38	96.20	95.45	95.63
Formula based on:	$Si + Al + (Ti + Fe^{3+}) = 12$ a.p.f.u.							
Si	6.90	6.90	6.70	6.73	6.82	6.83	6.93	6.96
Ti	-	-	0.02	-	-	-	-	-
Al	5.10	5.08	5.28	5.25	5.18	5.17	5.07	5.04
Fe^{3+}	-	0.02	-	0.02	-	-	-	-
Fe^{2+}	0.06	0.04	0.05	0.04	0.06	0.06	0.04	0.06
Mn	-	-	-	-	-	-	-	-
Mg	-	-	0.02	0.04	0.02	-	0.02	-
Ca	3.10	3.15	3.21	3.24	3.14	3.16	3.10	3.09
Na	0.67	0.76	0.62	0.65	0.65	0.71	0.71	0.72
K	0.07	0.04	0.06	0.03	0.05	0.05	0.05	0.05
S	-	-	-	-	-	0.06	0.02	-
Cl	0.03	-	-	0.02	0.02	0.05	0.04	0.04
CO_3 (calc)	0.97	1.00	1.00	0.98	0.98	0.89	0.94	0.96
Total	16.90	17.00	16.97	17.01	16.92	17.07	16.95	16.91
Mei%	82.23	80.56	83.81	83.25	82.85	81.72	81.32	81.05
Eq An %	70.14	69.31	75.93	74.99	72.67	72.21	69.08	67.98
Name	Meionite	Meionite	Meionite	Meionite	Meionite	Meionite	Meionite	Meionite

* Value is input as Wt%

Table 5. Epidote group minerals. Fe^{3+} has been calculated by the method of Droop (1987). Textural positions: m: Main assemblage, r: amphibolite-facies retrograde mineral, l: low-grade origin mineral, u: cannot be texturally classified.

Sample	CM16R-09c							
Lithology	Marble							
Analysis	EP-1	EP-2	EP-3	EP-4	EP-5	EP-6	CZO-1	ZO-1
Textural position	m	m	u	l	l	m	u	u
SiO_2	37.93	37.12	38.18	38.16	37.48	38.02	37.12	37.58
Al_2O_3	25.30	23.57	26.60	26.30	23.20	25.24	26.94	26.73
TiO_2	-	0.15	-	-	0.25	-	-	-
Fe_2O_3	9.90	11.88	9.76	9.90	13.01	10.80	4.05	1.82
FeO	0.68	0.15	0.30	0.15	0.15	0.46	-	-
Cr_2O_3	0.43	0.63	-	-	-	-	-	-
MnO	-	-	-	-	-	0.14	-	-
MgO	-	-	-	-	-	-	2.15	3.29
CaO	23.01	22.51	22.83	23.43	23.22	23.31	23.49	23.24
SrO	-	-	-	-	-	0.94	-	-
K_2O	-	-	0.06	-	-	-	-	0.11
Total	97.25	96.00	97.91	97.94	97.31	98.90	93.77	92.78
Formula based on:	12.50 Oxygens							
Si	3.01	3.00	2.99	3.00	3.00	2.98	2.95	2.99
Al	2.37	2.25	2.46	2.44	2.19	2.34	2.52	2.51
Ti	-	0.01	-	-	0.02	-	-	-
Fe^{3+}	0.61	0.73	0.58	0.58	0.79	0.64	0.26	0.12
Fe^{2+}	0.05	0.01	0.02	0.01	0.01	0.03	-	-
Cr	0.03	0.04	-	-	-	-	-	-
Mn	-	-	-	-	-	0.01	-	-
Mg	-	-	-	-	-	-	0.25	0.39
Ca	1.95	1.95	1.91	1.97	1.99	1.96	2.00	1.98
Sr	-	-	-	-	-	0.04	-	-
K	-	-	0.01	-	-	-	-	0.01
Total	8.01	8.00	8.00	8.00	7.99	8.00	8.00	8.00
Name	Epidote	Epidote	Epidote	Epidote	Epidote	Epidote	Clinozoisite	Zoisite

Table 5 (cont). Epidote group minerals. Fe^{3+} has been calculated by the method of Droop (1987). Textural positions: m: Main assemblage, r: amphibolite-facies retrograde mineral, l: low-grade origin mineral, u: cannot be texturally classified.

Sample	CM19R-11k							
Lithology	Mafic Granulite (meta-mafic rock)							
Analysis	ZO-1	ZO-2	ZO-3	ZO-4	ZO-5	ZO-6	CZO-1	CZO-2
Textural position	m	m	m	m	m	m	m	m
SiO_2	39.14	38.87	39.54	39.15	39.24	39.54	38.25	38.84
Al_2O_3	34.03	32.02	32.17	33.97	31.88	32.33	27.55	30.07
TiO_2	-	-	-	-	-	-	-	-
Fe_2O_3	-	2.22	1.10	-	2.13	2.02	7.79	5.16
FeO	-	-	1.66	0.49	0.41	0.71	1.07	0.35
Cr_2O_3	-	-	-	-	-	-	-	-
MnO	-	-	-	-	-	-	-	-
MgO	-	-	-	-	-	-	-	-
CaO	24.45	24.38	24.39	24.51	23.96	24.44	22.79	24.02
SrO	-	-	-	-	-	-	-	-
K_2O	-	-	-	-	-	-	-	-
Total	97.62	97.48	98.86	98.12	97.62	99.04	97.44	98.44
Formula based on:	12.50 Oxygens							
Si	2.98	2.97	2.99	2.96	3.01	2.99	3.01	2.98
Al	3.04	2.89	2.87	3.04	2.88	2.88	2.54	2.72
Ti	-	-	-	-	-	-	-	-
Fe^{3+}	-	0.14	0.06	-	0.12	0.12	0.46	0.31
Fe^{2+}	-	-	0.10	0.02	0.03	0.05	0.07	0.02
Cr	-	-	-	-	-	-	-	-
Mn	-	-	-	-	-	-	-	-
Mg	-	-	-	-	-	-	-	-
Ca	1.98	2.00	1.97	1.98	1.97	1.97	1.92	1.98
Sr	-	-	-	-	-	-	-	-
K	-	-	-	-	-	-	-	-
Total	8.00	8.00	8.00	8.00	8.00	8.01	7.99	8.01
Name	Zoisite	Zoisite	Zoisite	Zoisite	Zoisite	Zoisite	Clinozoisite	Clinozoisite

Table 6. Plagioclase. All Fe is considered as Fe^{3+}. Textural positions: m: Main assemblage, r: amphibolite-facies retrograde mineral, l: low-grade origin mineral, u: cannot be texturally classified.

Sample	CM16R-03e2							
Lithology	Mafic Granulite (meta-mafic rock)							
Analysis	PL-1	PL-2	PL-3	PL-4	PL-5	PL-6	PL-7	PL-8
Textural position	m	l	m	m	m	m	m	l
SiO_2	46.62	70.46	50.96	44.57	48.03	46.68	53.85	71.63
Al_2O_3	36.09	20.26	32,25	36.11	34.52	34.97	29.87	20.92
Fe_2O_3	-	-	-	-	-	0.60	-	-
CaO	18.31	-	13,99	18.97	16.79	17.30	11.27	-
Na_2O	1.26	11.97	3,43	0.73	2.08	1.61	4.86	11.33
K_2O	-	-	-	-	-	-	-	-
Total	102.29	102.69	100,64	100.38	101.42	101.15	100.15	103.87
Formula based on:	8.00 Oxygens							
Si	2.10	2.99	2,29	2.05	2.17	2.12	2.43	3.00
Al	1.91	1.01	1,72	1.96	1.84	1.88	1.59	1.03
Fe^{3+}	-	-	-	-	-	0.02	-	-
Ca	0.88	-	0,68	0.93	0.81	0.84	0.56	-
Na	0.11	0.99	0,31	0.07	0.18	0.14	0.42	0.92
K	-	-	-	-	-	-	-	-
Total	5.00	4.99	5,00	5.01	5.00	5.01	4.99	4.95
An %	88.89	-	68,92	93.31	81.82	85.71	57.14	-
Ab %	11.11	100.00	31,08	6.69	18.18	14.29	42.86	100.00
Kfs %	-	-	-	-	-	-	-	-
Name	Bytownite	Albite	Labradorite	Anorthite	Bytownite	Bytownite	Labradorite	Albite

Sample	CM16R-09c				CM19R-11k			
Lithology	Marble				Mafic Granulite (meta-mafic rock)			
Analysis	PL-9	PL-10	PL-11	PL-12	PL-13	PL-14	PL-15	PL-16
Textural position	l	l	l	l	m	m	m	m
SiO_2	67.87	68.78	68.52	68.10	43.10	43.42	44.49	43.09
Al_2O_3	20.40	20.26	20.04	20.01	36.64	36.47	37.13	36.04
Fe_2O_3	-	-	-	-	-	-	-	-
CaO	-	0.14	0.25	0.40	19.53	19.55	19.30	16.67
Na_2O	11.61	11.61	11.47	11.45	0.33	0.27	0.29	0.88
K_2O	-	-	0.10	-	-	-	-	0.87
Total	99.89	100.79	100.38	99.96	99.60	99.71	101.21	97.55
Formula based on:	8.00 Oxygens							
Si	2.97	2.98	2.98	2.98	2.00	2.01	2.03	2.04
Al	1.05	1.03	1.03	1.03	2.01	1.99	2.00	2.01
Fe^{3+}	-	-	-	-	-	-	-	-
Ca	-	0.01	0.01	0.02	0.97	0.97	0.95	0.84
Na	0.98	0.97	0.97	0.97	0.03	0.03	0.03	0.08
K	-	-	0.01	-	-	-	-	0.05
Total	5.00	4.99	4.99	4.99	5.01	5.00	5.00	5.03
An %	-	1.02	1.01	2.02	97.00	97.00	96.94	86.60
Ab %	100.00	98.98	97.98	97.98	3.00	3.00	3.06	8.25
Kfs %	-	-	1.01	-	-	-	-	5.15
Name	Albite	Albite	Albite	Albite	Anorthite	Anorthite	Anorthite	Bytownite

Table 6 (cont.). Plagioclase. All Fe is considered as Fe^{3+}. Textural positions: m: Main assemblage, r: amphibolite-facies retrograde mineral, l: low-grade origin mineral, u: cannot be texturally classified.

Sample	CM19R-11k							
Lithology	Mafic Granulite (meta-mafic rock)							
Analysis	PL-17	PL-18	PL-19	PL-20	PL-21	PL-22	PL-23	PL-24
Textural position	l	l	m	m	m	m	m	m
SiO_2	67.43	65.71	43.25	43.31	43.41	43.83	43.29	43.62
Al_2O_3	20.33	21.02	36.95	35.66	36.13	36.98	36.37	36.74
Fe_2O_3	-	-	-	-	-	0.48	-	-
CaO	0.79	1.95	19.93	19.93	19.03	19.18	19.34	19.50
Na_2O	11.16	10.67	0.30	0.40	0.47	0.36	0.33	0.21
K_2O	-	-	-	-	-	-	-	-
Total	99.71	99.35	100.43	99.29	99.05	100.83	99.33	100.08
Formula based on:	8.00 Oxygens							
Si	2.96	2.90	2.00	2.03	2.03	2.01	2.01	2.01
Al	1.05	1.10	2.01	1.96	1.99	2.00	2.00	2.00
Fe^{3+}	-	-	-	-	-	0.01	-	-
Ca	0.04	0.09	0.99	1.00	0.95	0.95	0.96	0.96
Na	0.95	0.91	0.03	0.04	0.04	0.03	0.03	0.01
K	-	-	-	-	-	-	-	-
Total	4.99	5.01	5.03	5.03	5.00	5.00	5.00	4.99
An %	4.04	9.00	97.06	96.15	95.96	96.94	96.97	98.97
Ab %	95.96	91.00	2.94	3.85	4.04	3.06	3.03	1.03
Kfs %	-	-	-	-	-	-	-	-
Name	Albite	Albite	Anorthite	Anorthite	Anorthite	Anorthite	Anorthite	Anorthite

Table 7. K-feldspar. Textural positions: m: Main assemblage, r: amphibolite-facies retrograde mineral, l: low-grade origin mineral, u: cannot be texturally classified.

Sample	CM16R-09c	
Lithology	Marble	
Analysis	KFS-1	KFS-2
Textural position	l	l
SiO_2	64.12	64.88
Al_2O_3	18.60	19.05
CaO	0.11	0.24
Na_2O	0.33	0.61
K_2O	16.27	15.61
Total	99.44	100.38
Formula based on:	8.00 Oxygens	
Si	2.98	2.98
Al	1.02	1.03
Ca	0.01	0.01
Na	0.03	0.05
K	0.97	0.91
Total	5.01	4.99
An %	0.99	1.03
Ab %	2.97	5.15
Kfs %	96.04	93.81
Name	K-feldspar	K-feldspar

Table 8. White micas. Fe^{3+} has been calculated by the method of Droop (1987). Textural positions: m: Main assemblage, r: amphibolite-facies retrograde mineral, l: low-grade origin mineral, u: cannot be texturally classified.

Sample	CM16R-09c							
Lithology	Marble							
Analysis	WMCA-1	WMCA-2	WMCA-3	WMCA-4	WMCA-5	WMCA-6	WMCA-7	WMCA-8
Textural position	m	m	m	l	u	l	m	u/l
SiO_2	45.42	46.29	45.74	45.36	47.87	45.77	48.51	38.42
Al_2O_3	32.55	31.82	33.53	38.23	36.14	36.71	28.31	27.99
Fe_2O_3	1.19	0.58	3.61	-	-	-	-	6.92
FeO	3.24	3.70	-	0.73	0.29	0.40	3.97	-
TiO_2	0.87	1.42	-	0.20	-	-	-	-
MgO	0.75	0.91	1.01	0.27	0.91	0.21	1.58	-
MnO	-	-	-	-	-	-	0.13	-
CaO	-	0.26	0.16	0.39	0.28	0.17	0.26	23.78
Na_2O	-	0.18	0.49	2.45	0.16	0.14	0.11	0.15
K_2O	10.89	10.54	10.7	7.53	11.07	10.61	10.12	-
F*	-	-	-	-	-	-	0.47	-
Cl*	-	-	-	-	-	-	-	-
Total	94.91	95.71	95.22	95.15	96.72	94.00	93.48	97.45
Formula based on:	11.00 Oxygens							
Si	3.08	3.12	3.06	2.98	3.12	3.07	3.31	2.60
Al (IV)	0.92	0.88	0.94	1.02	0.88	0.93	0.69	1.40
Fe^{3+}	0.06	0.03	0.21	-	-	-	-	0.39
Fe^{2+}	0.18	0.21	-	0.04	0.02	0.02	0.23	-
Ti	0.04	0.08	-	0.01	-	-	-	-
Al (VI)	1.69	1.65	1.69	1.94	1.89	1.96	1.59	0.84
Mg	0.08	0.02	0.10	0.03	0.09	0.02	0.16	-
Mn	-	-	-	-	-	-	0.01	-
Ca	-	0.02	0.01	0.03	0.02	0.01	0.02	1.73
Na	-	0.02	0.07	0.31	0.02	0.02	0.02	0.02
K	0.94	0.90	0.91	0.63	0.92	0.91	0.88	-
F**	-	-	-	-	-	-	0.10	-
Cl**	-	-	-	-	-	-	-	-
OH**	2.00	2.00	2.00	2.00	2.00	2.00	1.90	2.00
Total	9.00	9.00	8.99	9.00	8.96	8.95	8.90	8.98
Name***	Muscovite	Muscovite	Muscovite	White Mica	Muscovite	Muscovite	Muscovite	Margarite

* Value is input as Wt%

** Calculated based on Brady J. & Perkins D. (2007)

***The nomenclature has been based on Rieder et al (1998).

Table 8 (cont.). White micas. Fe^{3+} has been calculated by the method of Droop (1987). Textural positions: m: Main assemblage, r: amphibolite-facies retrograde mineral, l: low-grade origin mineral, u: cannot be texturally classified.

Sample	CM19R-11k							
Lithology	Mafic Granulite (meta-mafic rock)							
Analysis	WMCA-9	WMCA-10	WMCA-11	WMCA-12	WMCA-13	WMCA-14	WMCA-15	WMCA-16
Textural position	l	l	l	l	l	l	l	l
SiO_2	45.73	47.39	47.00	45.72	43.43	47.68	49.31	44.21
Al_2O_3	37.01	35.75	35.96	38.41	38.90	36.07	36.22	36.63
Fe_2O_3	-	-	-	-	-	-	-	-
FeO	-	-	0.43	-	0.48	0.64	-	-
TiO_2	-	-	-	-	-	-	-	-
MgO	0.34	1.02	0.63	0.53	0.39	0.52	2.68	-
MnO	-	-	-	-	-	-	-	-
CaO	-	-	-	0.90	1.82	-	1.32	-
Na_2O	-	-	-	0.32	0.61	-	0.55	-
K_2O	11.08	10.47	10.31	9.45	8.02	11.14	5.20	10.48
F*	-	-	-	-	-	-	-	-
Cl*	-	-	-	-	-	-	-	-
Total	94.16	94.62	94.33	95.33	93.66	96.05	95.29	91.33
Formula based on:	11.00 Oxygens							
Si	3.06	3.14	3.12	3.01	2.92	3.14	3.15	3.04
Al (IV)	0.94	0.86	0.88	0.99	1.08	0.86	0.85	0.96
Fe^{3+}	-	-	-	-	-	-	-	-
Fe^{2+}	-	-	0.02	-	0.02	0.04	-	-
Ti	-	-	-	-	-	-	-	-
Al (VI)	1.96	1.93	1.92	1.94	1.94	1.90	1.74	2.01
Mg	0.04	0.09	0.06	0.06	0.04	0.06	0.26	-
Mn	-	-	-	-	-	-	-	-
Ca	-	-	-	0.06	0.13	-	0.09	-
Na	-	-	-	0.04	0.07	-	0.07	-
K	0.95	0.88	0.88	0.79	0.68	0.94	0.42	0.92
F**	-	-	-	-	-	-	-	-
Cl**	-	-	-	-	-	-	-	-
OH**	2.00	2.00	2.00	2.00	2.00	2.00	2.00	2.00
Total	8.97	8.89	8.89	8.91	8.91	8.95	8.73	8.93
Name***	Sericite	Sericite	Sericite	Sericite	Sericite	Sericite	White Mica	Sericite

* Value is input as Wt%

** Calculated based on Brady J. & Perkins D. (2007)

***The nomenclature has been based on Rieder et al (1998).

Table 9. Biotite. Fe^{3+} has been calculated by the method of Droop (1987) and halogens by the method of Ketchum (2015). Textural positions: m: Main assemblage, r: amphibolite-facies retrograde mineral, l: low-grade origin mineral, u: cannot be texturally classified.

Sample	CM16R-09f1				CM19R-11b			
Lithology	Marble				Calc-Silicate			
Analysis	BT-1	BT-2	BT-3	BT-4	BT-5	BT-6	BT-7	BT-8
Textural position	m	m	m	m	m	m	m	m
SiO_2	42.04	42.75	42.05	42.48	41.33	42.65	41.25	41.64
Al_2O_3	14.46	14.56	14.28	14.49	15.79	15.59	17.78	17.56
Fe_2O_3	-	-	-	-	-	-	-	-
FeO	-	0.38	0.45	0.38	0.99	0.91	1.05	1.16
TiO_2	-	-	-	-	0.15	0.13	-	-
MgO	27.66	28.44	28.07	28.43	27.27	28.23	26.92	26.98
MnO	-	-	-	-	-	-	-	-
CaO	-	-	-	-	0.12	0.12	0.10	0.20
Na_2O	0.57	0.46	0.54	0.44	1.14	1.09	1.32	1.23
K_2O	9.88	9.80	9.94	10.48	8.95	9.07	8.83	8.70
F*	-	-	-	-	0.60	0.56	0.47	0.56
Cl*	-	-	-	-	-	-	-	-
Total	94.62	96.39	95.32	96.70	96.33	98.36	97.72	98.05
Formula based on:	11.00 Oxygens							
Si	2.93	2.93	2.92	2.91	2.82	2.85	2.81	2.82
Al (IV)	1.07	1.07	1.08	1.09	1.18	1.15	1.19	1.18
Fe^{3+}	-	-	-	-	-	-	-	-
Fe^{2+}	-	0.02	0.03	0.02	0.06	0.05	0.06	0.07
Ti	-	-		-	0.01	0.01	-	-
Al (VI)	0.12	0.10	0.09	0.08	0.09	0.08	0.23	0.23
Mg	2.88	2.90	2.91	2.91	2.78	2.81	2.72	2.72
Mn	-	-	-	-	-	-	-	-
Ca	-	-	-	-	0.01	0.01	0.01	0.01
Na	0.08	0.06	0.07	0.06	0.15	0.14	0.17	0.16
K	0.88	0.86	0.88	0.92	0.78	0.77	0.77	0.75
F**	-	-	-	-	0.13	0.12	0.10	0.12
Cl**	-	-	-	-	-	-	-	-
OH**	2.00	2.00	2.00	2.00	1.87	1.88	1.90	1.88
Total	9.95	9.94	9.97	9.99	9.88	9.87	9.96	9.94
Name***	Phlogopite	Phlogopite	Phlogopite	Phlogopite	F-bearing Phlogopite	F-bearing Phlogopite	F-bearing Phlogopite	F-bearing Phlogopite

* Value is input as Wt%

** Calculated by the method of Ketchum (2015).

*** The nomenclature has been based on Rieder et al (1998).

Table 9 (cont.). Biotite. Fe^{3+} has been calculated by the method of Droop (1987) and halogens by the method of Ketchum (2015). Textural positions: m: Main assemblage, r: amphibolite-facies retrograde mineral, l: low-grade origin mineral, u: cannot be texturally classified.

Sample	CM19R-11b							
Lithology	Calc-Silicate							
Analysis	BT-9	BT-10	BT-11	BT-12	BT-13	BT-14	BT-15	BT-16
Textural position	m	m	m	m	m	m	m	m
SiO_2	41.98	41.03	40.83	41.94	43.10	43.05	41.68	41.35
Al_2O_3	16.97	17.71	16.05	14.38	13.23	16.30	16.16	15.31
Fe_2O_3	-	-	-	-	-	-	-	-
FeO	1.14	1.32	1.18	1.01	0.89	0.91	1.04	0.93
TiO_2	0.15	0.25	0.30	0.16	0.19	0.21	-	0.27
MgO	27.30	26.78	27.68	29.01	30.43	28.62	26.86	27.76
MnO	-	-	-	-	-	-	-	-
CaO	0.11	0.08	-	0.17	0.17	0.10	0.45	0.12
Na_2O	1.42	1.08	-	0.65	1.09	1.31	0.68	1.24
K_2O	8.71	8.94	9.22	6.34	7.20	8.53	9.52	8.15
F*	0.54	0.52	-	0.42	0.39	-	0.51	0.46
Cl*	-	-	-	-	-	-	-	-
Total	98.32	97.71	95.27	94.08	96.70	99.03	96.89	95.60
Formula based on:	11.00 Oxygens							
Si	2.84	2.79	2.83	2.91	2.93	2.86	2.87	2.87
Al (IV)	1.16	1.21	1.17	1.18	1.06	1.14	1.13	1.13
Fe^{3+}	-	-	-	-	-	-	-	-
Fe^{2+}	0.06	0.07	0.07	1.01	0.05	0.05	0.06	0.05
Ti	0.01	0.01	0.02	0.16	0.01	0.01	-	0.01
Al (VI)	0.19	0.21	0.14	0.09	-	0.14	0.18	0.12
Mg	2.75	2.72	2.86	29.01	2.95	2.84	2.76	2.87
Mn	-	-	-	-	-	-	-	-
Ca	0.01	0.01	-	0.17	0.01	0.01	0.04	0.01
Na	0.18	0.14	-	0.65	0.14	0.17	0.09	0.17
K	0.75	0.78	0.82	6.34	0.62	0.72	0.83	0.72
F**	0.12	0.11	-	0.09	0.08	-	0.11	0.10
Cl**	-	-	-	-	-	-	-	-
OH**	1.88	1.89	2.00	1.91	1.92	2.00	1.89	1.90
Total	9.95	9.94	9.90	9.83	9.99	9.93	9.96	9.94
Name***	F-bearing Phlogopite	F-bearing Phlogopite	Phlogopite	F-bearing Phlogopite	F-bearing Phlogopite	Phlogopite	F-bearing Phlogopite	F-bearing Phlogopite

* Value is input as Wt%

** Calculated by the method of Ketchum (2015).

*** The nomenclature has been based on Rieder et al (1998).

Table 10. Carbonate minerals. The concentrations of the elements are given in percentage (%) per molecule. Textural positions: m: Main assemblage, r: amphibolite-facies retrograde mineral, l: low-grade origin mineral, u: cannot be texturally classified.

Sample	CM16R-03e2				CM16R-09c			
Lithology	Mafic Granulite (meta-mafic rock)				Marble			
Analysis	CB-1	CB-2	CB-3	CB-4	CB-5	CB-6	CB-7	CB-8
Textural position	u	u	u	u	m	m	m	m
$CaCO_3$	99.33	98.50	100.00	98.50	98.20	97.00	97.67	98.00
$MgCO_3$	-	0.50	-	0.50	0.60	1.00	1.33	1.13
$MnCO_3$	-	0.50	-	0.25	-	-	-	-
$FeCO_3$	0.67	0.50	-	0.75	1.20	2.00	1.00	0.87
$SrCO_3$	-	-	-	-	-	-	-	-
Total	100.00	100.00	100.00	100.00	100.00	100.00	100.00	100.00
Name	Calcite	Calcite	Calcite	Calcite	Calcite	Calcite	Calcite	Calcite

Sample	CM16R-09c					CM16R-09f1		
Lithology	Marble					Marble		
Analysis	CB-9	CB-10	CB-11	CB-12	CB-13	CB-14	CB-15	CB-16
Textural position	m	m	m	m	u	m	m	m
$CaCO_3$	97.50	98.00	98.13	100.00	98.13	93.83	92.83	94.00
$MgCO_3$	1.17	1.00	0.62	-	-	6.17	7.17	6.00
$MnCO_3$	-	-	0.12	-	-	-	-	-
$FeCO_3$	1.33	1.00	1.12	-	1.87	-	-	-
$SrCO_3$	-	-	-	-	-	-	-	-
Total	100.00	100.00	100.00	100.00	100.00	100.00	100.00	100.00
Name	Calcite	Calcite	Calcite	Calcite	Calcite	Calcite	Calcite	Calcite

Sample	CM16R-09f1				CM19R-11b			
Lithology	Marble				Calc-Silicate			
Analysis	CB-17	CB-18	CB-19	CB-20	CB-21	CB-22	CB-23	CB-24
Textural position	m	m	m	m	m	m	m	l
$CaCO_3$	93.50	51.50	51.67	51.50	97.13	92.87	51.18	95.67
$MgCO_3$	6.50	48.50	48.33	48.50	2.87	7.13	48.09	4.33
$MnCO_3$	-	-	-	-	-	-	-	-
$FeCO_3$	-	-	-	-	-	-	0.73	-
$SrCO_3$	-	-	-	-	-	-	-	-
Total	100.00	100.00	100.00	100.00	100.00	100.00	100.00	100.00
Name	Calcite	Dolomite	Dolomite	Dolomite	Calcite	Calcite	Dolomite	Calcite

Table 10 (cont.). Carbonate minerals. The concentrations of the elements are given in percentage (%) per molecule. Textural positions: m: Main assemblage, r: amphibolite-facies retrograde mineral, l: low-grade origin mineral, u: cannot be texturally classified.

Sample	CM19R-11b							
Lithology	Calc-Silicate							
Analysis	CB-25	CB-26	CB-27	CB-28	CB-29	CB-30	CB-31	CB-32
Textural position	m	m	m	m	m	m	m	l
$CaCO_3$	51.63	100.00	95.17	51.50	94.33	95.50	51.33	100.00
$MgCO_3$	48.38	-	4.83	48.00	5.67	4.50	47.83	-
$MnCO_3$	-	-	-	-	-	-	-	-
$FeCO_3$	-	-	-	0.50	-	-	0.83	-
$SrCO_3$	-	-	-	-	-	-	-	-
Total	100.00	100.00	100.00	100.00	100.00	100.00	100.00	100.00
Name	Dolomite	Calcite	Calcite	Dolomite	Calcite	Calcite	Dolomite	Calcite

Sample	CM19R-11k			
Lithology	Mafic Granulite (meta-mafic rock)			
Analysis	CB-33	CB-34	CB-35	CB-36
Textural position	m	m	m	m
$CaCO_3$	99.00	99.33	100.00	98.83
$MgCO_3$	0.50	-	-	0.67
$MnCO_3$	-	-	-	-
$FeCO_3$	0.50	0.67	-	0.50
$SrCO_3$	-	-	-	-
Total	100.00	100.00	100.00	100.00
Name	Calcite	Calcite	Calcite	Calcite

Table 11. Titanite. Textural positions: m: Main assemblage, r: amphibolite-facies retrograde mineral, l: low-grade origin mineral, u: cannot be texturally classified.

Sample	CM16R-03e2							
Lithology	Mafic Granulite (meta-mafic rock)							
Analysis	TTN-1	TTN-2	TTN-3	TTN-4	TTN-5	TTN-6	TTN-7	TTN-8
Textural position	m	m	m	m	m	m	m	m
SiO_2	31.17	31.01	30.75	30.68	31.80	30.74	30.58	31.34
TiO_2	37.40	36.34	37.49	36.63	37.70	36.54	35.83	37.07
Al_2O_3	2.61	2.96	2.11	2.70	2.76	2.79	3.22	3.74
FeO	-	-	-	0.39	-	0.41	0.67	-
CaO	28.99	28.45	28.36	28.23	29.33	28.21	27.88	28.62
F*	-	-	-	-	-	-	-	-
Total	100.17	98.77	98.71	98.64	101.59	98.68	98.17	100.78
Formula based on:	5.00 Oxygens							
Si	1.00	1.02	1.01	1.01	1.02	1.01	1.01	1.01
Ti	0.90	0.90	0.93	0.91	0.91	0.90	0.89	0.90
Al	0.10	0.11	0.08	0.10	0.10	0.11	0.13	0.14
Fe^{2+}	-	-	-	0.01	-	0.01	0.02	-
Ca	1.00	1.00	1.00	1.00	1.00	0.99	0.99	0.98
F	-	-	-	-	-	-	-	-
Total	3.00	3.03	3.02	3.03	3.03	3.02	3.03	3.03
Name	Titanite	Titanite	Titanite	Titanite	Titanite	Titanite	Titanite	Titanite

* Value is input as Wt%

Sample	CM16R-09c				CM16-09f1	CM19R-11k		
Lithology	Marble				Marble	Mafic Granulite (meta-mafic rock)		
Analysis	TTN-9	TTN-10	TTN-11	TTN-12	TTN-13	TTN-14	TTN-15	TTN-16
Textural position	m	m	m	m	m	m	m	m
SiO_2	30.42	30.67	30.58	30.93	30.07	30.34	30.63	30.34
TiO_2	36.24	37.24	37.42	37.34	35.02	35.23	35.57	36.05
Al_2O_3	2.26	2.12	1.61	1.87	4.10	3.28	1.71	2.78
V_2O_5	-	-	-	0.87	0.87	-	-	-
FeO	0.64	1.86	0.79	0.86	1.03	0.44	-	-
CaO	28.15	28.60	28.38	28.67	30.64	28.19	28.42	28.34
F*	-	-	-	-	-	0.68	0.74	-
Total	97.71	100.49	98.87	100.54	101.73	98.17	98.59	97.51
Formula based on:	5.00 Oxygens							
Si	1.01	1.00	1.01	1.00	0.97	1.02	1.02	1.01
Ti	0.91	0.91	0.93	0.91	0.85	0.88	0.89	0.90
Al	0.09	0.08	0.06	0.07	0.16	0.13	0.13	0.11
V	-	-	-	0.02	0.02	-	-	-
Fe^{2+}	0.02	0.05	0.02	0.03	0.03	0.01	-	-
Ca	1.01	1.00	1.00	0.99	1.06	1.01	1.01	1.01
F	-	-	-	-	-	0.08	0.08	-
Total	3.03	3.04	3.02	3.02	3.08	3.11	3.11	3.03
Name	Titanite	Titanite	Titanite	Titanite	Titanite	Titanite	Titanite	Titanite

* Value is input as Wt%

Table 12. Apatite. Textural positions: m: Main assemblage, r: amphibolite-facies retrograde mineral, l: low-grade origin mineral, u: cannot be texturally classified.

Sample	CM16R-03e2		CM16R-09c		CM16R-09f1		CM19R-11b	
Lithology	Mafic Granulite (meta-mafic rock)		Marble		Marble		Calc-Silicate	
Analysis	AP-1	AP-2	AP-3	AP-4	AP-5	AP-6	AP-7	AP-8
Textural position	m	m	m	m	m	m	m	m
CaO	56.19	54.73	54.62	55.85	56.88	57.05	55.70	55.76
P_2O_5	43.36	42.47	42.02	43.01	42.25	42.59	43.33	42.86
F*	2.73	2.89	2.91	3.84	0.71	0.73	2.42	2.14
Cl*	0.25	-	0.29	0.23	0.43	0.44	0.49	0.49
OH*	0.85	0.78	0.59	-	2.49	2.48	1.00	1.23
Total	102.17	99.64	99.14	101.13	102.37	102.88	101.81	101.46
Formula based on:				Full (F,Cl, OH) site				
Ca	9.90	9.87	9.92	9.92	10.13	10.10	9.86	9.93
P	6.04	6.05	6.03	6.03	5.95	5.96	6.06	6.03
F**	1.42	1.54	1.56	2.01	0.37	0.38	1.26	1.13
Cl**	0.07	-	0.08	0.06	0.12	0.12	0.14	0.14
OH**	0.51	0.46	0.36	-	1.51	1.50	0.60	0.74
Total	17.91	17.92	17.95	18.02	18.08	18.06	17.92	17.97
Name	Fluorapatite	Fluorapatite	Fluorapatite	Fluorapatite	Apatite	Apatite	Fluoroxy-apatite	Fluoroxy-apatite

Sample	CM19R-11b				CM19R-11k			
Lithology	Calc-Silicate				Mafic Granulite (meta mafic rock)			
Analysis	AP-9	AP-10	AP-11	AP-12	AP-13	AP-14	AP-15	AP-16
Textural position	m	m	m	m	m	m	m	m
CaO	55.86	56.19	54.87	55.66	54.50	54.73	55.27	54.64
P_2O_5	42.95	43.12	42.50	43.45	42.10	42.54	42.99	42.28
F*	2.54	2.35	2.54	1.96	3.22	3.04	2.93	3.02
Cl*	0.62	0.47	0.50	0.55	-	-	-	-
OH*	0.82	1.07	0.84	1.37	0.46	0.64	0.76	0.65
Total	101.58	102.10	100.07	102.04	98.92	99.67	100.72	99.31
Formula based on:				Full (F,Cl, OH) site				
Ca	9.93	9.94	9.88	9.84	9.90	9.86	9.86	9.89
P	6.03	6.03	6.05	6.07	6.04	6.06	6.06	6.05
F**	1.33	1.23	1.35	1.02	1.73	1.62	1.54	1.61
Cl**	0.17	0.13	0.14	0.15	-	-	-	-
OH**	0.50	0.64	0.51	0.82	0.27	0.38	0.46	0.39
Total	17.96	17.97	17.93	17.91	17.94	17.92	17.92	17.94
Name	Fluorapatite	Fluoroxy-apatite	Fluorapatite	Fluoroxy-apatite	Fluorapatite	Fluorapatite	Fluorapatite	Fluorapatite

* Value is input as Wt%

** Calculated by the method of Ketchum (2015).

Table 13. Zircon. Textural positions: m: Main assemblage, r: amphibolite-facies retrograde mineral, l: low-grade origin mineral, u: cannot be texturally classified.

Sample	CM16R-03e2			CM16R-09c	CM19R-11k			
Lithology	Mafic Granulite (meta-mafic rock)			Marble	Mafic Granulite (meta-mafic rock)			
Analysis	ZRN-1	ZRN-2	ZRN-3	ZRN-4	ZRN-5	ZRN-6	ZRN-7	ZRN-8
SiO_2	32.32	31.30	31.55	30.77	31.42	31.78	31.59	31.09
ZrO_2	69.45	68.70	69.03	66.54	68.34	68.94	67.52	67.53
FeO	-	-	-	-	0.62	-	-	-
CaO	-	-	-	0.37	-	-	-	-
HfO_2	1.64	-	-	-	1.36	1.46	1.27	1.19
Total	103.41	100.00	100.58	97.68	101.74	102.18	100.38	99.81
Formula based on:				4.00 oxygens				
Si	0.97	0.97	0.97	0.97	0.96	0.97	0.97	0.97
Zr	1.01	1.03	1.03	1.03	1.02	1.02	1.01	1.02
Fe	-	-	-	-	0.01	-	-	-
Ca	-	-	-	0.01	-	-	-	-
Hf	0.01	-	-	-	0.01	0.01	0.01	0.01
Total	1.99	2.00	2.00	2.01	2.01	2.00	2.00	2.00
Name	Zircon	Zircon	Zircon	Zircon	Zircon	Zircon	Zircon	Zircon

Table 14. Talc. Textural positions: m: Main assemblage, r: amphibolite-facies retrograde mineral, l: low-grade origin mineral, u: cannot be texturally classified.

Sample	CM16R-09f1				CM19R-11b	
Lithology	Marble				Calc-Silicate	
Analysis	TLC-1	TLC-2	TLC-3	TLC-4	TLC-6	TLC-7
Textural position	1	1	1	1	1	1
SiO_2	60.46	57.74	58.57	58.74	58.40	63.46
Al_2O_3	-	-	-	-	1.38	0.42
Fe_2O_3	-	-	-	-	0.59	0.67
FeO	0.38	0.27	-	0.43	-	-
MgO	29.30	27.72	27.19	27.50	29.65	32.16
CaO	-	-	0.28	0.21	1.32	0.10
Na_2O	0.34	-	-	-	0.13	0.21
K_2O	-	-	-	-	0.24	-
Total	90.48	85.81	86.04	86.88	91.72	97.02
Formula based on:	11.00 Oxygens					
Si	4.02	4.05	4.07	4.07	3.83	3.94
Al	-	-	-	-	0.11	0.03
Fe^{3+}	-	-	-	-	0.03	0.03
Fe^{2+}	0.02	0.02	-	0.02	-	-
Mg	2.91	2.90	2.82	2.84	2.89	2.97
Ca	-	-	0.02	0.02	0.09	0.01
Na	0.04	-	-	-	0.02	0.03
K	-	-	-	-	0.02	-
Total	6.99	6.97	6.91	6.95	6.99	7.01
Name	Talc	Talc	Talc	Talc	Talc	Talc

Table 15. Allanite. Textural positions: m: Main assemblage, r: amphibolite-facies retrograde mineral, l: low-grade origin mineral, u: cannot be texturally classified.

Sample	CM16R-03e2			
Lithology	Mafic Granulite (meta-mafic rock)			
Analysis	ALN-1	ALN-2	ALN-3	ALN-4
Textural position	m	m	m	m
SiO_2	35.47	35.32	35.66	35.49
Al_2O_3	22.38	22.42	22.58	24.33
Fe_2O_3	1.91	2.86	3.38	2.90
FeO	7.48	6.77	6.44	4.76
MgO	0.60	0.59	-	0.42
CaO	16.09	15.90	16.07	17.87
La_2O_3*	4.27	4.06	4.35	2.49
Ce_2O_3*	7.41	7.68	7.55	4.77
Nd_2O_3*	1.88	2.12	1.99	1.74
Pr_2O_3*	-	0.71	-	-
Total	97.29	98.09	98.02	94.77
Formula based on:	12.50 Oxygens			
Si	3.07	3.05	3.09	3.04
Al	2.28	2.28	2.30	2.45
Fe^{3+}	0.06	0.09	0.09	0.16
Fe	0.61	0.58	0.59	0.38
Mg	0.06	0.07	-	0.05
Ca	1.49	1.47	1.48	1.64
La	0.14	0.12	0.13	0.08
Ce	0.24	0.24	0.24	0.14
Nd	0.06	0.06	0.06	0.05
Pr	-	0.02	-	-
Total	8.00	8.00	8.00	8.00
Name	Allanite	Allanite	Allanite	Allanite

*Uncertain values due to peak overlap in the EDS spectra.

Table 16. Rutile. Textural positions: m: Main assemblage, r: amphibolite-facies retrograde mineral, l: low-grade origin mineral, u: cannot be texturally classified.

Sample	CM16R-09c			
Lithology	Marble			
Analysis	RT-1	RT-2	RT-3	RT-4
Textural position	m	m	m	m
TiO_2	98.72	95.70	98.75	98.65
V_2O_5	1.16	-	1.60	1.72
Fe_2O_3	-	3.68	0.56	0.62
CaO	0.37	0.30	-	-
Total	100.25	99.67	100.91	100.99
Formula based on:	2.00 Oxygens			
Ti	0.99	0.98	0.98	0.98
V	0.01	-	0.01	0.01
Fe^{3+}	-	0.04	0.01	0.01
Ca	0.01	<0.01	-	-
Total	1.01	1.02	1.00	1.00
Name	Rutile	Rutile	Rutile	Rutile

Table 17. Vesuvianite. Textural positions: m: Main assemblage, r: amphibolite-facies retrograde mineral, l: low-grade origin mineral, u: cannot be texturally classified.

Sample	CM16R-03e2
Lithology	Mafic Granulite (meta-mafic rock)
Analysis	VES-1
Textural position	l
SiO_2	33.98
Al_2O_3	15.59
TiO_2	8.48
FeO	3.83
CaO	36.52
F*	1.32
Total	99.72
Formula based on:	50-site cation normalization
Si	16.80
Al (IV)	1.20
Ti	3.15
Al (VI)	7.90
Fe	1.58
Ca	19.35
F	2.07
Total Cations	49.98
Total	52.05
Name	Vesuvianite

* Value is input as Wt%

Table 18. Prehnite. Textural positions: m: Main assemblage, r: amphibolite-facies retrograde mineral, l: low-grade origin mineral, u: cannot be texturally classified.

Sample	CM19R-11k				
Lithology	Mafic Granulite (meta-mafic rock)				
Analysis	PRH-1	PRH-2	PRH-3	PRH-4	PRH-5
Textural position	l	l	l	l	l
SiO_2	42.64	36.87	42.73	43.04	43.35
Al_2O_3	25.12	26.81	23.54	24.78	24.54
Fe_2O_3	-	2.41	-	-	-
FeO	-	-	0.64	-	0.48
MgO	-	1.43	-	-	-
CaO	26.21	22.7	25.76	26.58	26.40
Total	93.96	90.21	92.66	94.40	94.77
Formula based on:	11.00 Oxygens				
Si	2.97	2.66	3.03	2.99	3.01
Al (IV)	1.03	1.34	0.97	1.01	0.99
Fe^{3+}	-	0.14	-	-	-
Al (VI)	1.03	0.94	0.99	1.03	1.01
Fe	-	-	0.04	-	0.04
Mg	-	0.16	-	-	-
Ca	1.96	1.76	1.96	1.98	1.96
Total	6.99	7.00	6.99	7.01	7.01
Name	Prehnite	Prehnite	Prehnite	Prehnite	Prehnite

Tidigare skrifter i serien ”Examensarbeten i Geologi vid Lunds universitet”:

555. Stevic, Marijana, 2019: Stratigraphy and dating of a lake sediment record from Lyngsjön, eastern Scania - human impact and aeolian sand deposition during the last millennium. (45 hp)
556. Rabanser, Monika, 2019: Processes of Lateral Moraine Formation at a Debris-covered Glacier, Suldenferner (Vedretta di Solda), Italy. (45 hp)
557. Nilsson, Hanna, 2019: Records of environmental change and sedimentation processes over the last century in a Baltic coastal inlet. (45 hp)
558. Ingered, Mimmi, 2019: Zircon U-Pb constraints on the timing of Sveconorwegian migmatite formation in the Western and Median Segments of the Idefjorden terrane, SW Sweden. (45 hp)
559. Hjorth, Ingeborg, 2019: Paleomagnetisk undersökning av vulkanen Rangitoto, Nya Zeeland, för att bestämma dess utbrottshistoria. (15 hp)
560. Westberg, Märta, 2019: Enigmatic worm-like fossils from the Silurian Waukesha Lagerstätte, Wisconsin, USA. (15 hp)
561. Björn, Julia, 2019: Undersökning av påverkan på hydraulisk konduktivitet i förorenat område efter in situ-saneringsförsök. (15 hp)
562. Faraj, Haider, 2019: Tolkning av georadarprofiler över grundvattenmagasinet Verveln - Gullringen i Kalmar län. (15 hp)
563. Bjermo, Tim, 2019: Eoliska avlagringar och vindriktningar under holocen i och kring Store Mosse, södra Sverige. (15 hp)
564. Langkjaer, Henrik, 2019: Analys av Östergötlands kommande grundvattenresurser ur ett klimtperspektiv - med fokus på förstärkt grundvattenbildning. (15 hp)
565. Johansson, Marcus, 2019: Hur öppet var landskapet i södra Sverige under Atlantisk tid? (15 hp)
566. Molin, Emmy, 2019: Litologi, sedimentologi och kolisotopstratigrafi över krita–paleogen-gränsintervallet i borrningen Limhamn-2018. (15 hp)
567. Schroeder, Mimmi, 2019: The history of European hemp cultivation. (15 hp)
568. Damber, Maja, 2019: Granens invandring i sydvästa Sverige, belyst genom pollenanalys från Skottenesjön. (15 hp)
569. Lundgren Sassner, Lykke, 2019: Strandmorfologi, stranderosion och stranddeposition, med en fallstudie på Tylösand sandstrand, Halland. (15 hp)
570. Greiff, Johannes, 2019: Mesozoiska konglomerat och Skånes tektoniska utveckling. (15 hp)
571. Persson, Eric, 2019: An Enigmatic Cerapodian Dentary from the Cretaceous of southern Sweden. (15 hp)
572. Aldenius, Erik, 2019: Subsurface characterization of the Lund Sandstone – 3D model of the sandstone reservoir and evaluation of the geoenergy storage potential, SW Skåne, South Sweden. (45 hp)
573. Juliusson, Oscar, 2019: Impacts of subglacial processes on underlying bedrock. (15 hp)
574. Sartell, Anna, 2019: Metamorphic paragenesis and P-T conditions in garnet amphibolite from the Median Segment of the Idefjorden Terrane, Lilla Edet. (15 hp)
575. Végvári, Fanni, 2019: Vulkanisk inverkan på klimatet och atmorsfärcirkulationen: En litterarurstudie som jämför vulkanism på låg respektive hög latitud. (15 hp)
576. Gustafsson, Jon, 2019: Petrology of platinum-group element mineralization in the Koillismaa intrusion, Finland. (45 hp)
577. Wahlquist, Per, 2019: Undersökning av mindre förkastningar för vattenuttag i sedimentärt berg kring Kingelstad och Tjutebro. (15 hp)
578. Gaitan Valencia, Camilo Esteban, 2019: Unravelling the timing and distribution of Paleoproterozoic dyke swarms in the eastern Kaapvaal Craton, South Africa. (45 hp)
579. Eggert, David, 2019: Using Very-Low-Frequency Electromagnetics (VLF-EM) for geophysical exploration at the Albertine Graben, Uganda - A new CAD approach for 3D data blending. (45 hp)
580. Plan, Anders, 2020: Resolving temporal links between the Högberget granite and the Wigström tungsten skarn deposit in Bergslagen (Sweden) using trace elements and U-Pb LA-ICPMS on complex zircons. (45 hp)
581. Pilser, Hannes, 2020: A geophysical survey in the Chocaya Basin in the central Valley of Cochabamba, Bolivia, using ERT and TEM. (45 hp)
582. Leopardi, Dino, 2020: Temporal and genetical constraints of the Cu-Co Vena-Dampetorp deposit, Bergslagen, Sweden. (45 hp)
583. Lagerstam Lorien, Clarence, 2020: Neck mobility versus mode of locomotion – in what way did neck length affect swimming performance among Mesozoic plesiosaurs (Reptilia, Sauropterygia)? (45 hp)
584. Davies, James, 2020: Geochronology of gneisses adjacent to the Mylonite Zone in southwestern Sweden: evidence of a tec-

tonic window? (45 hp)

585. Foyn, Alex, 2020: Foreland evolution of Blåisen, Norway, over the course of an ablation season. (45 hp)
586. van Wees, Roos, 2020: Combining luminescence dating and sedimentary analysis to derive the landscape dynamics of the Velická Valley in the High Tatra Mountains, Slovakia. (45 hp)
587. Rettig, Lukas, 2020: Implications of a rapidly thinning ice-margin for annual moraine formation at Gornergletscher, Switzerland. (45 hp)
588. Bejarano Arias, Ingrid, 2020: Determination of depositional environment and luminescence dating of Pleistocene deposits in the Biely Váh valley, southern foothills of the Tatra Mountains, Slovakia. (45 hp)
589. Olla, Daniel, 2020: Petrografisk beskrivning av Prekambriska ortognejser i den undre delen av Särvskollan, mellersta delen av Skollenheten, Kaledonska orogenen. (15 hp)
590. Friberg, Nils, 2020: Är den sydatlantiska magnetiska anomalin ett återkommande fenomen? (15 hp)
591. Brakebusch, Linus, 2020: Klimat och väder i Nordatlanten-regionen under det senaste årtusendet. (15 hp)
592. Boestam, Max, 2020: Stränder med erosion och ackumulation längs kuststräckan Trelleborg - Abbekås under perioden 2007-2018. (15 hp)
593. Agudelo Motta, Laura Catalina, 2020: Methods for rockfall risk assessment and estimation of runout zones: A case study in Gothenburg, SW Sweden. (45 hp)
594. Johansson, Jonna, 2020: Potentiella nedslagskratrar i Sverige med fokus på Östersjön och östkusten. (15 hp)
595. Haag, Vendela, 2020: Studying magmatic systems through chemical analyses on clinopyroxene - a look into the history of the Teno ankaramites, Tenerife. (45 hp)
596. Kryffin, Isidora, 2020: Kan benceller bevaras över miljontals år? (15 hp)
597. Halvarsson, Ellinor, 2020: Sökande efter nedslagskratrar i Sverige, med fokus på avtryck i berggrunden. (15 hp)
598. Jirdén, Elin, 2020: Kustprocesser i Arktis – med en fallstudie på Prins Karls Forland, Svalbard. (15 hp)
599. Chonewicz, Julia, 2020: The Eemian Baltic Sea hydrography and paleoenvironment based on foraminiferal geochemistry. (45 hp)
600. Paradeisis-Stathis, Savvas, 2020: Holocene lake-level changes in the Siljan Lake District – Towards validation of von Post's drainage scenario. (45 hp)
601. Johansson, Adam, 2020: Groundwater flow modelling to address hydrogeological response of a contaminated site to remediation measures at Hjortsberga, southern Sweden. (15 hp)
602. Barrett, Aodhan, 2020: Major and trace element geochemical analysis of norites in the Hakefjorden Complex to constrain magma source and magma plumbing systems. (45 hp)
603. Lundqvist, Jennie, 2020: "Man fyller det med information helt enkelt": en fenomenografisk studie om studenters upplevelse av geologisk tid. (45 hp)
604. Zachén, Gabriel, 2020: Classification of four mesosiderites and implications for their formation. (45 hp)
605. Viðarsdóttir, Halla Margrét, 2020: Assessing the biodiversity crisis whitin the Triassic-Jurassic boundary interval using redox sensitive trace metals and stable carbon isotope geochemistry. (45 hp)
606. Tan, Brian, 2020: Nordvästra Skånes prekambriska geologiska utveckling. (15 hp)
607. Taxopoulou, Maria Eleni, 2020: Metamorphic micro-textures and mineral assemblages in orthogneisses in NW Skåne – how do they correlate with technical properties? (45 hp)
608. Damber, Maja, 2020: A palaeoecological study of the establishment of beech forest in Söderåsen National Park, southern Sweden. (45 hp)
609. Karastergios, Stylianos, 2020: Characterization of mineral parageneses and metamorphic textures in eclogite- to high-pressure granulite-facies marble at Allmenningen, Roan, western Norway. (45 hp)

LUNDS UNIVERSITET

Geologiska institutionen
Lunds universitet
Sölvegatan 12, 223 62 Lund